

**DOCTORAL THESIS**

# Surface Vessel Localization from Wake Measurements

Margus Rätsep

TALLINN UNIVERSITY OF TECHNOLOGY  
DOCTORAL THESIS  
7/2025

# Surface Vessel Localization from Wake Measurements

MARGUS RÄTSEP



TALLINN UNIVERSITY OF TECHNOLOGY

School of Science

Department of Cybernetics

This dissertation was accepted for the defence of the degree of Doctor of Philosophy (Applied Physics and Mathematics) 09/01/2025

**Supervisor:** Prof Tarmo Soomere  
Department of Cybernetics, School of Science  
Tallinn University of Technology  
Tallinn, Estonia

**Co-supervisor:** Prof Kevin E. Parnell  
Department of Cybernetics, School of Science  
Tallinn University of Technology  
Tallinn, Estonia

**Opponents:** Dr Luca Zaggia  
Institute of Geosciences and Earth Resources  
National Research Council of Italy  
Padova, Italy

Dr Hannes Tõnisson  
Institute of Ecology  
School of Natural Sciences and Health  
Tallinn University  
Tallinn, Estonia

**Defence of the thesis:** 28/01/2025, Tallinn

**Declaration:**

Hereby I declare that this doctoral thesis, my original investigation and achievement, submitted for the doctoral degree at Tallinn University of Technology has not been submitted for doctoral or equivalent academic degree.

Margus Rätsep

---

signature



European Union  
European Regional  
Development Fund



Investing  
in your future

Copyright: Margus Rätsep, 2025

ISSN 2585-6898 (publication)

ISBN 978-9916-80-252-6 (publication)

ISSN 2585-6901 (PDF)

ISBN 978-9916-80-253-3 (PDF)

DOI <https://doi.org/10.23658/taltech.7/2025>

Rätsep, M. (2025). *Surface Vessel Localization from Wake Measurements* [TalTech Press].  
<https://doi.org/10.23658/taltech.7/2025>

TALLINNA TEHNIKAÜLIKOOL  
DOKTORITÖÖ  
7/2025

# **Laevade asukohta ja liikumise parameetrite määramine laevalainete salvestustest**

MARGUS RÄTSEP





# Contents

List of publications .....	6
Author's contribution to the publications .....	7
Introduction .....	8
Monitoring vessel traffic .....	9
Vessel wakes .....	10
Spectrogram technique.....	12
Vessel detection using wake recordings in the littoral zone.....	13
The objective and outline of the thesis.....	15
1 Vessel wake detection .....	17
1.1 Selection of devices.....	17
1.2 Detection of a sequence of ship wakes.....	20
1.2.1 Software based approach .....	20
1.2.2 Hardware based approach .....	21
2 Vessel localization .....	25
2.1 Speed of the vessel .....	25
2.2 Vessel position and course.....	29
Conclusions .....	33
List of figures .....	35
References .....	37
Acknowledgements.....	43
Abstract.....	44
Lühikokkuvõte.....	45
Appendix: Publications constituting the thesis.....	47
Curriculum vitae.....	84
Elulookirjeldus.....	85

## List of publications

- I **Rätsep, M.**, Parnell, K.E., Soomere, T., 2020. Detecting ship wakes for the study of coastal processes. *Journal of Coastal Research*, Special Issue No. 95, 1258–1262. <https://doi.org/10.2112/SI95-243.1>
- II **Rätsep, M.**, Parnell, K.E., Soomere, T., Kruusmaa, M., Ristolainen, A., Tuhtan, J.A., 2020. Using spectrograms from underwater total pressure sensors to detect passing vessels in a coastal environment. *Journal of Atmospheric and Oceanic Technology*, 37(8), 1353–1363. <https://doi.org/10.1175/JTECH-D-19-0192.1>
- III **Rätsep, M.**, Parnell, K.E., Soomere, T., Kruusmaa, M., Ristolainen, A., Tuhtan, J.A., 2021. Surface vessel localization from wake measurements using an array of pressure sensors in the littoral zone. *Ocean Engineering*, 233, 109156. <https://doi.org/10.1016/j.oceaneng.2021.109156>

## **Author's contribution to the publications**

- I I prepared the figures, analyzed the data, wrote most of the paper and acted as the corresponding author.
- II I prepared the figures, analyzed the data, wrote most of the paper and acted as the corresponding author.
- III I prepared the figures, analyzed the data, wrote most of the paper and acted as the corresponding author.



## Introduction

Coastal zones have always been attractive because of their vast variety of resources, providing food and energy, enabling marine trade and transport, and as areas of recreational and cultural amenity (Neumann et al., 2015). For these reasons roughly one quarter of world's population lives in the area less than 100 km from coast (Reimann et al., 2023). This high concentration of people and activities creates many challenges when managing the common resource, known as the sea (Till, 2013). The situation is particularly complex in the contact zone between land and water where a delicate balance exists between different drivers and their impacts, and any change in the pressures, for example, general energy pollution (Kelpšaitė et al., 2009) or waves with unusual properties or propagation direction, may destroy this balance (Scarpa et al., 2019; Soomere, 2005).

One challenge is maintaining control and command of an adjacent state's territorial waters (Till, 2013). Other challenges include recognizing and stopping unlawful fishing (Kurekin et al., 2019), monitoring and preventing pollution (Landrigan et al., 2020), fighting piracy (Gong et al., 2023), regulating ship traffic to avoid navigational accidents (Chen et al., 2018), protecting underwater infrastructure (Gülcan and Erginer, 2023), and ensuring the security of various offshore and coastal facilities (Anupriya and Sasilatha, 2018; Dugad et al., 2017).

As world population increases so does the volume of both national and international marine trade. This process inherently leads to more ship traffic operating in the littoral zones and generally to a higher probability of accidents (Altan and Otay, 2018). The rising pressure on the coastal (Delpeche-Ellmann and Soomere, 2013) and marine (Claremar et al., 2017; Zanatta et al., 2020) environment calls for more advanced offshore and coastal sea management (van Westrenen and Baldauf, 2020).

With the rapid development of marine technology and increased interest in green energy, some new concerns have arisen. One example is the introduction of unmanned Marine Autonomous Surface Ships (MASSs) (Kim et al., 2022). These vessels operate in the same navigational environment (Kim et al., 2022) as ordinary manned vessels. Their introduction generates a need to investigate the ability to detect and classify medium size and small objects (e.g., leisure boats), to mitigate the risk of collisions. Such vessels often sail outside the traffic lanes and do not usually use self-reporting automatic ship identification systems.

It is also necessary to develop measures and protocols that ensure navigation safety in the case of technical malfunctions, unexpected behaviours due to storm conditions (Rødseth and Burmeister, 2015), and to ensure recovery capability (Thieme et al., 2018) in the case of failures. As there is usually no permanent crew on such ships, either losing contact with a ship or the malfunctioning of one or several sensors used for plotting and maintaining the course, can severely limit the options for maintaining control in critical situations.

Recent geopolitical developments suggest that in addition to challenges when operating in confined conditions with poor visibility and in areas with a high concentration of vessel traffic like inland rivers (Zhang et al., 2019), other situations need to be taken into account, e.g., hostile GPS signal disturbance. To cope with these risks, additional external devices located at critical locations (such as near harbours or offshore structures, or where lights at night interfere visually and tall buildings may damp radar sensing) are needed in order to detect, set and sustain the sailing characteristics.

A separate issue is that some operators do not want their vessels to be detected and identified, for military-driven reasons, because of illegal fishing or related to other malicious or illegal marine traffic (Reggiannini et al., 2024, 2019).

Another significant growing concern to navigational safety are offshore windfarms (Chang et al., 2014). These reduce the space available for shipping (Tsai and Lin, 2021) and thus increase the density of ships in other sea areas, which in turn increases the possibility of navigational accidents, both ship-to-facility (Chang et al., 2014) and ship-to-ship collisions (Tsai and Lin, 2021). The risk is greater due to the underperformance of radar systems when operating in their near vicinity (De la Vega et al., 2013), which emphasizes the need for additional vessel detection methods to mitigate the risks and assist nearby vessel navigation.

## **Monitoring vessel traffic**

There exists a vast variety of methods to detect and monitor movements of the vessels. Some of the best known long-range detecting and monitoring systems are based on various remote sensing technologies, from radar (Siegert et al., 2019) and radio surveillance (Ilčev, 2021) to satellite-based information, including synthetic aperture (SAR) technology (Gierull, 2019; Panico et al., 2017; Reggiannini et al., 2024; Zilman et al., 2004). More local options use airborne (Dahana and Gurning, 2020) and ground-based (both wide-spectrum visual and hyperspectral) optical techniques (Park et al., 2018) and various acoustic (sonar) technologies (Huang et al., 2017; Zhu et al., 2018). These methods can be complemented by visual observations from the coast or other vessels.

None of the methods is perfect for providing ship detection and surveillance in all situations. The additional complication is that these methods are well known, and measures exist to either intentionally (or even accidentally) reduce the rate of detection, or to completely avoid it. For example, self-reporting methods like Automatic Identification System (AIS) and Long-Range Identification Tracker (LRIT) (Dahana and Gurning, 2020) usually provide information about the vessel movements and intentions (name and destination), but these methods are reliant on whether devices are switched on (AIS) and are set to report (LRIT). As they rely on the operator's action, these devices can be used to provide false information about destination and purpose.

One of the most well-known ship detection methods, optical observations (visual and infrared) can be interfered with by using the appropriate paint coatings to conceal a vessel or to disguise its intentions (Aurdal et al., 2019; Casson, 1995). The common countermeasure to reduce the infrared signature is to put the exhaust outlets of the ship's engines in an area of the hull that is near the waterline.

The accuracy of a radar's readings about the ship depends on the vessel size, shape, and the weather conditions. Similarly to the above, as the radar technology developed, so did the countermeasures. The most common means to avoid accurate detection, known as stealth technology, is to use specific paint coatings, structure and hull materials that absorb and/or scatter the emissions. Another option is to reduce the size of the part of the vessel that is above the water, principally the superstructure. This tactic is used in smuggling narcotics from South America by building low-profile vessels (Ramirez and Bunker, 2015). These boats have small freeboard, which makes them difficult to detect using any of the methods described above.

Acoustic detection has so far been one of the most reliable methods for vessel detection. This technology also enables the monitoring of submersed vessels. However,

this method relies on the fact that ship has something that makes noise. The related challenges are gradually increasing with the arrival of green technologies like hydrogen cells or fully electric vessels that are conquering the market, pushing out internal combustion engines that have a well-known and recognized acoustic footprint. Related are methods that use wind and solar power (Nyanya et al., 2021) to help to propel the ship (e.g., during the transit in open ocean) and therefore reduce the time when the main engines and/or a propeller are used.

A further challenge is the limited amount of information the detection (sensor) system provides. Some of these techniques (e.g., several acoustic recognition systems) are only able to detect the presence of a ship in a certain region. Other technologies provide, similar to the AIS system, the location (or a sequence of locations) of vessels. However, reliable identification of the sailing parameters (speed and course of the vessel) from the provided information is not always possible (Fujino et al., 2019).

In order to address the gaps in both reliability and accuracy, additional means for the surveillance of sea areas should be researched. These efforts are in line with activities that move towards merging information from several sensor systems and techniques to detect and monitor vessel traffic with a high level of confidence. Navies and maritime security organisations refer to this process as creating a Recognized Maritime Picture (RMP) (Simard et al., 2000). Usually, a RMP provides information about each vessel in the region by determining its location and heading, also providing the possibility of follow-up actions based on the ship type and purpose (Simard et al., 2000).

## Vessel wakes

When considering the monitoring of vessel traffic, one approach would be to focus on the emissions created by the vessels themselves. While exhaust gas emissions as well as the radiation of noise and heat can be effectively eliminated by advanced technologies, there is an unavoidable emission for all items that move on the water surface. A vessel moving on the surface of body of the water leaves behind a trace known as wake (Newman, 1977; Wehausen, 1973). This trace consists of several different linear (Kuznetsov et al., 2002) and often nonlinear components (Fang et al., 2011; Soomere, 2007; Sorensen, 1973). The most well-known, classic representation is the triangular wave pattern known as the Kelvin wake (Figure 1) (Newman, 1977) which obtains its textbook shape about three-vessel lengths behind the ship.

A Kelvin wake and its variations for subcritical speeds are composed of two sets of waves: transverse and divergent waves. They both exist if the vessel speed does not reach or exceed the so-called critical speed  $U = \sqrt{gh}$ , where  $g$  is acceleration due to gravity and  $h$  is water depth (Sorensen, 1973). These wave systems are traditionally treated as linear waves (Liang et al., 2024) even though for larger speeds they exhibit nonlinear properties (Soomere, 2007; Sorensen, 1973).

Transverse waves propagate in the same direction as the vessel heading. Therefore, their crests are perpendicular to the sailing line. Divergent waves move away from the sailing line and their crests form a smaller angle with the vessel's path (Newman, 1977).

A set of so-called cusp waves is formed by interactions of transverse and divergent waves, along the borders of the ship wake (Kuznetsov et al., 2002). Cusp waves are usually the most observable part of the wake because their amplitude decays slowly (as  $r^{-1/3}$ ) with the distance  $r$  from the vessel (Kuznetsov et al., 2002).

The wave pattern, in general, depends on the vessel properties, water depth and the sailing speed. On many occasions the vessel's stern and bow produce their own wake systems with the height depending on the vessel geometry and sailing regime. The basic geometric properties of the Kelvin wake produced by a single moving point are still universal and can be described in terms of a depth Froude number  $F_h$  (Newman, 1977):

$$F_h = \frac{U}{\sqrt{gh}}. \quad (1)$$

In deep water or when sailing at low speed ( $F_h < 1$ ), the divergent and transverse waves fill a triangular area (Kelvin wedge) with half apex angle of  $\arcsin(1/3) \approx 19.47^\circ$  (Figure 1) (Newman, 1977). When the speed increases or water depth decreases so that  $F_h$  has values 0.5–0.7, the Kelvin wedge starts to widen, energy starts to concentrate to a few divergent components, and transverse waves become weaker. At  $F_h \rightarrow 1$ , the wave system becomes highly nonlinear (Soomere, 2007; Sorensen, 1973) and cannot be described in terms of a Kelvin wedge. In the supercritical speed range  $F_h > 1$  the apex angle starts to decrease, and most of the wave energy is concentrated in a few long-crested divergent waves which dominate the wave pattern (Pethiyagoda et al., 2014; Soomere, 2007). The wave system may contain several types of solitons at  $F_h \rightarrow 1$  and  $F_h > 1$  (Soomere, 2007). On many occasions it may resemble a Mach-type wave system (Rabaud and Moisy, 2013).

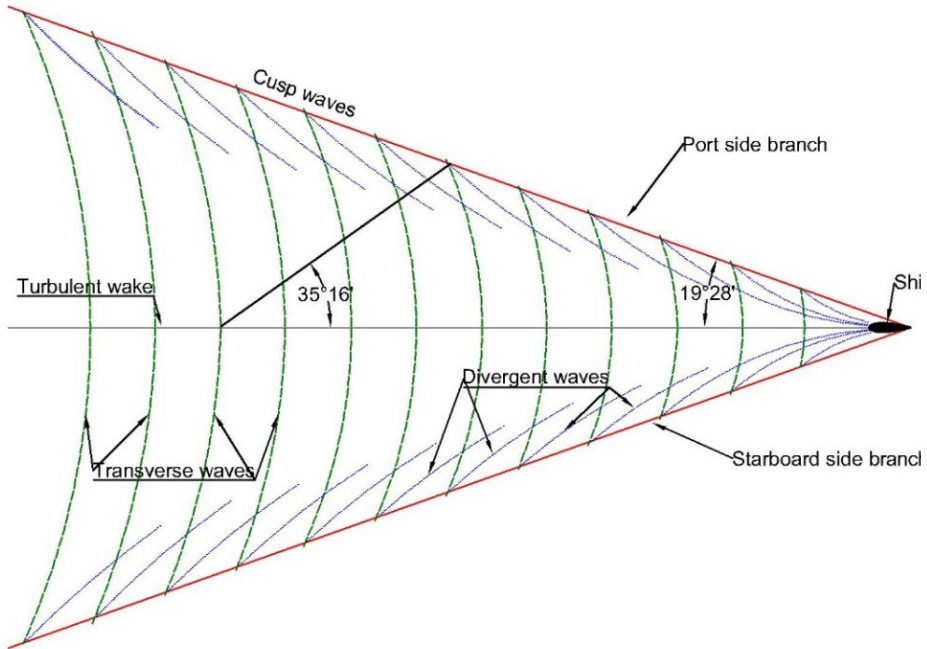


Figure 1. A scheme of the linear Kelvin wake generated by a ship sailing in deep water ( $h = \infty$ ) to the right. The half-angle of the Kelvin wake is  $19^\circ 28'$  and the propagation direction of cusp waves forms an angle of  $\arccos(\sqrt{2}/3) \approx 35^\circ 16'$  with the sailing line (Newman, 1977; Torsvik et al., 2015b). From Paper III.

## Spectrogram technique

Vessel wakes have been used extensively for detecting and characterizing vessels and their movement using various kinds of two-dimensional (2D) data from, e.g., synthetic aperture radars (SAR) (Zilman et al., 2004) and satellite photos (Rabaud and Moisy, 2013). The benefit of this method is that it is applicable to vessels of different size as their Kelvin wake always has the same geometry, and its “arms” (cusp lines) have the same length (as the wave height decays according to the same law) and varies only in amplitude (Zilman et al., 2004). A natural limitation of this method is the signal to noise ratio that can be low when extracting the properties of Kelvin wakes due to the high sea clutter, which requires additional algorithms for filtering (Kuo and Chen, 2003).

The ideal Kelvin wedge is stationary in the coordinate system attached to the moving ship. This perspective is convenient for several theoretical considerations, but it is not straightforward to use for practical applications. Most observing systems of ship wakes are anchored at some location or mounted on the shore. On such occasions the ship wake is recorded as a complex system of water surface undulations or pressure variations. It is notably unsteady and short crested, despite appearing stationary to an observer on the generating vessel (Liang et al., 2024).

Therefore, another approach is to use wakes for ship detection and specification of sailing properties from the water elevation or pressure data, from the perspective of an Earth-fixed observer. While transverse waves are represented as signals with an almost constant frequency, the signal of divergent waves is chirp-like and has a gradually increasing frequency. The properties of these signals carry information about the speed and location of the vessel. Wu (1991) was the first to show that the sailing speed can be estimated from the minimum frequency of divergent waves  $f_{min}$  as

$$U = \frac{g}{2\pi f_{min}}. \quad (2)$$

This frequency was evaluated from the 2D wake spectrum. This technique applied by Wu (1991) to estimate the ship speed and direction had problems with the evaluation of the exact location of the locus of the wake signature. It was further elaborated by Arnold-Bos et al. (2007) who used the generalized Radon Transform and Stochastic Matched Filtering to detect the locus of the wake signature in the 2D spectrum wave recordings. Finally, Torsvik et al. (2015b) derived expressions for the ship’s distance to the measurement location based on this information.

Another more promising approach using a windowed Fourier transform (so-called spectrogram) to study the nonlinear components of wakes was first employed by Wyatt and Hall (1988). The method was expanded by Sheremet et al. (2012) for a broader selection of vessels. A more elaborate description of different components was performed by Torsvik et al. (2015b). A systematic analysis of the nonlinear components based on dispersion curves of ship wake components was presented by Pethiyagoda et al. (2017), with a description of the effects of different sailing regimes (turning, accelerating) on the properties of the wake.

The major benefit of an application of a windowed Fourier transform (or Short Time Fourier Transform, STFT) to water surface elevation data is that a vessel wake has a distinct L-like shape (Figure 2). This shape appears for data gathered directly from (above) the water level as well as for data converted from seabed pressure readings (Paper II), The upper, inclined part (also called a chirp signal (Sheremet et al., 2012)) of this signature corresponds to divergent waves. The frequency of these waves increases

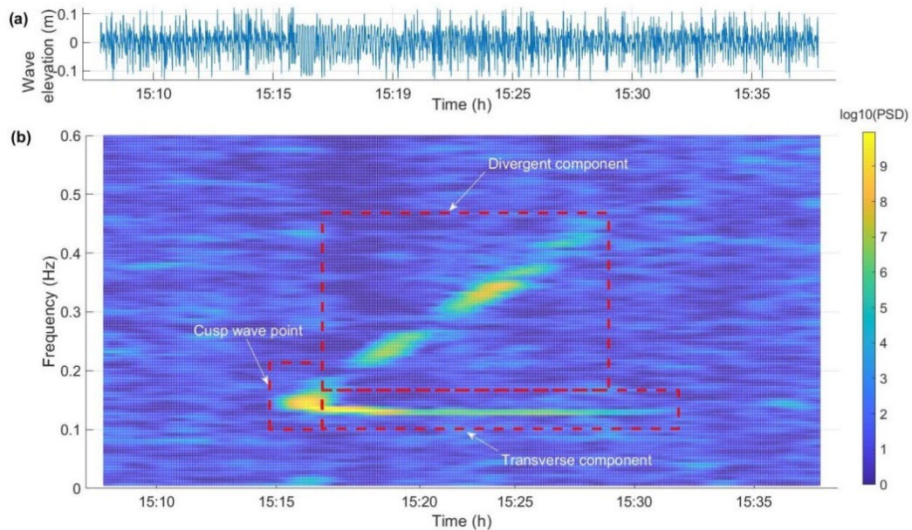


Figure 2. (a) An example of pressure time series of a vessel wake that is converted to water elevation data. (b) Short-time Fourier transform (spectrogram) of the corresponding series (note that the spectrograms are represented in normalized way). Wake elements are marked with red dashed rectangles. From Paper II.

over time at each Earth-fixed location. This feature is commonly observed at a fixed location in the nearshore, at the seashore or on the bottom after the passage of a steadily sailing ship (Sheremet et al., 2012). The lower, mostly horizontal part of this signature represents transverse waves. They have a constant frequency for a fixed observer who records the wake of a steadily sailing ship. The cusp waves are represented by the common point of these two parts of the signature.

Both windowed Fourier transform, and wavelet transform can be used to derive a time-frequency representation of the wake data (Sheremet et al., 2012). Testing has shown that wavelet transform usually has a higher signal-to-noise ratio than Fourier transform, however, Fourier transform provides the results on a uniform frequency scale compared to the logarithmic scale obtained from wavelet analysis (Torsvik et al., 2015b). This in turn simplifies the extraction and analysis of useful information (which is, in general, determination of the frequencies of the ship wake structure) to such an extent that the loss in signal-to-noise ratio was acceptable for this study, and wavelet analysis was not pursued here.

## Vessel detection using wake recordings in the littoral zone

Areas near the ports tend to have more vessel traffic than other shipping zones (Li et al., 2023) and therefore there is a greater emphasis on managing the traffic. One such location is Tallinn Bay. It is a semi-enclosed bay approximately  $10 \times 20$  km in size situated on the north coast of Estonia (Figure 3). The two entrances to the bay (from the north and west) are regulated by a local vessel traffic separation scheme (Figure 3).

As this study tried to evaluate the prospect of using wake recordings as the basis of a vessel detection system, for simplicity, only steady wake signatures, which would not be affected by the speed and course alternations, were used. In other words, course and speed alternations (Pethiyagoda et al., 2021) which are a crucial part of every vessel's sailing trajectory in coastal zones and should also be counted by the vessel detection

system, are not studied. The focus was on the vessels approaching the Port of Tallinn from the north-north-west (NNW). Wakes from ships departing the port had a wake signature typical of an accelerating vessel and vessels heading to or coming from the west had elements indicating the turn in their wake signatures (Pethiyagoda et al., 2021).

An optimal location for retrieving wakes from incoming vessels, that met the criteria, is near the eastern shore of the Paljassaare Peninsula where the Pikakari Beach has been formed over the last century (Figure 3). Katariina Jetty to the south-east and the tip of this peninsula to the north-west shelter the measurement location from waves generated by predominant winds from west and south. Also, due to these natural obstacles, the wakes from the departing vessels (sailing at course 339° clockwise from north) are negligible at the sensor location.

The sailing direction of vessels that approach the Port of Tallinn from NNW was approximately 159° (clockwise from north). The deviation of courses of single ships from this, estimated from ship self-reporting systems, was typically less than  $\pm 10^\circ$ . The water depth in the part of the traffic separation scheme where the wakes of the approaching vessels could have originated (Figure 3) ranges from 40 to 70 m. Passenger

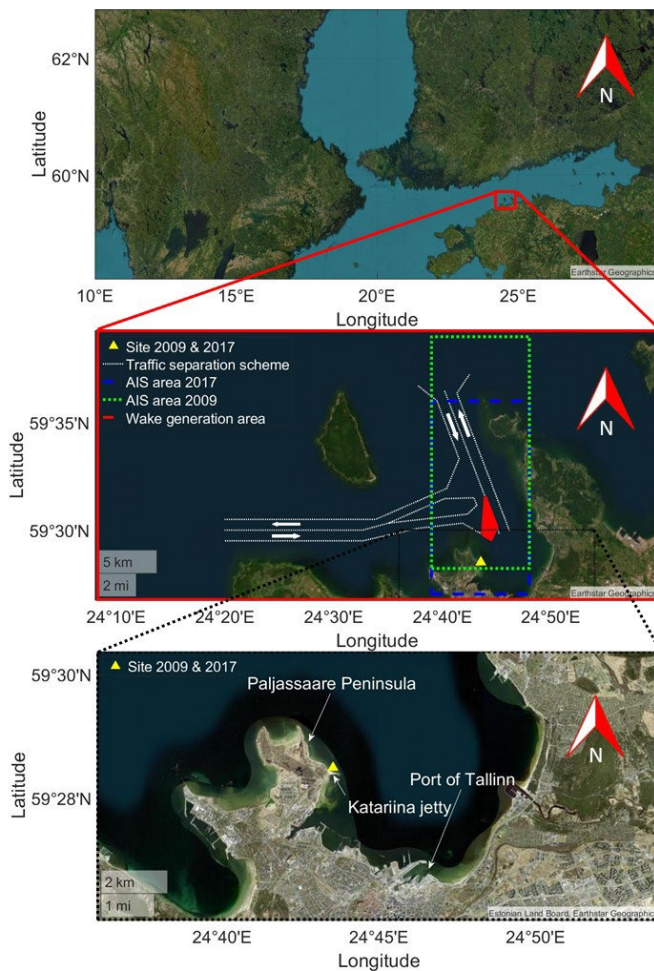


Figure 3. The study area in Tallinn Bay on the north coast of Estonia. The traffic separation scheme allows two approaches to the Port of Tallinn: from the north and west. Adapted from Paper II.

vessels entering to the port were travelling at 15 to 30 knots<sup>1</sup>, and therefore they were sailing at subcritical speeds. Even though the depth Froude number for such speeds may reach values about 0.7, on average it was below 0.5. Thus, the deviation of the geometry of the Kelvin wedge from the deep-water geometry was insignificant

This study uses two datasets of wave measurements obtained from this location. As the author was not involved in either of the field experiments the following is based on datasets collected by others, references and other indirect sources.

The first dataset was gathered in 2009 by the Wave Engineering Laboratory. This dataset was used in a number of studies of natural and ship-generated waves (Didenkulova and Rodin, 2013; Kurennoy et al., 2011; Soomere et al., 2011). Measurements were taken with a “LOG\_alevel” echosounder mounted on a tripod in 2.6–2.7 m deep water. Data were collected at a frequency of 5 Hz and divided into 24-h blocks starting at 04:00 (prior to the first ferry wake of the day) local time. Field experiments were conducted on 24.–25.06.2009 and 27.–30.06.2009. The properties of the study site, measurement location, devices deployed, procedures and preprocessing details are described in these studies.

The second dataset was gathered by the Centre for Biorobotics at the same location on 10.–14.07.2017 and 16.–21.07.2017. They deployed nine devices called hydromasts (Ristolainen et al., 2019) in a regularly spaced rectangular array on a 5 × 5 m aluminum frame at a depth of 3 m. The frame was anchored using 8 mm metal bars and additional weights at the corners of the frame. The frame was oriented towards NNE (22.5°) to face the traffic separation scheme. Measurements (pressure) were taken at a height of 0.2 m from the seabed with a frequency of 100 Hz.

## **The objective and outline of the thesis**

The main goal of this thesis is to evaluate the prospect of using the spectrogram technique as a vessel traffic monitoring system. As these techniques are applicable for any kind of wave recordings, including time series of water surface elevation data measured from above the water surface and time series of wave-induced pressure or velocity fluctuations measured in the water column, they provide a vast variety of opportunities for choosing equipment and deploying location. Several sets of wave elevation data and pressure recordings from the Tallinn Bay are acquired. The results are compared with “ground truth” – in this case, derived from the AIS data covering the same period and area.

The evaluation is viewed in the context of the previously mentioned ‘Recognized Maritime Picture’ which usually consists of five steps: a) detection, b) localization, c) recognition, d) identification and e) dissemination, from which the first three (detection, localization and recognition) are sensor based (NATO Standardization Agency, 2015). As the possibility of achieving recognition (determining the characteristics of a contact) from wake measurements is still unclear, and it is based on the success of previous steps, the focus of this work was to evaluate the method for detection and for localization of the vessels (NATO Standardization Agency, 2015).

The evaluation process for vessel detection, that is whether a vessel is in the survey area or not, requires collecting a time series of water surface elevation from either above the water surface or from within the water column or on the seabed), and determining its quality and the level of noise. Secondly, the process is used to investigate means by

---

<sup>1</sup> 1 knot is 1.852 km per hour



which wakes can be detected automatically. This process should answer questions relating to the circumstances under which vessels can be identified from the wake spectrogram (speed, size and distance) These questions are not specifically addressed here as all the tests were conducted at the same location and are based on the same types of vessels sailing at same speed.

Vessel localization involves finding the exact location of the vessel and its sailing characteristics (speed and course). Here the main questions are whether the speed based on the wake measurements (Torsvik et al., 2015b; Wu and Meadows, 1991) relate to the actual ship's movement. Also, is there a possibility to determine the direction of the incoming wake, which, when combined with the distance travelled by the wake calculated using the previously determined speed, could be used to estimate the vessel location? Finally, does the direction of wake propagation and its propagation angle correspond to the actual course of a ship?

The thesis is organized according to these questions. Chapter 1 focuses on investigating sensor-specific methods for wake detection and extraction. It follows Papers I and II. Paper I reviews the author's master thesis which was completed in early 2018 and is presented here as a reference due to low resolution of reference AIS data. It expands the model derived by Torsvik et al. (2015b) by adding automated vessel detection abilities. The focus of this paper is on the dataset measured by Laboratory of Wave Engineering in 2009 (Kurennoy et al., 2011). Chapter 2 investigates different methods of evaluation of the speed of the vessel and the distance of the location from where the wake was generated. It is based on the findings from Paper I but it is illustrated using the data from Paper III. Also, it tests the ability to determine the direction of the wake at its original location and thus the course of the vessel.

As papers 2 and 3 focus on the same dataset measured by the Centre for Biorobotics then they should be considered together because they represent a single pipeline from receiving input data to providing the vessel position and sailing parameters. Secondly, model development was done mostly in 2018. This means that improvements, findings from other authors from that period onwards on the same topic are not considered here.

# 1 Vessel wake detection

In general, there are two main methods for retrieving water wave data on-site for the analysis of ship wakes (if not including wake studies based on the far field readings like SAR radars, satellite images etc.). A widely applied approach is recording the fluctuations of the water surface using either buoys (Metters et al., 2021) or devices that can read the water level from within the water column or from the seabed or from above the water surface, e.g. echo sounders (Parnell et al., 2008) or lasers. The use of pressure sensors mounted in the water column (Soomere and Rannat, 2003) or near the seabed (Sheremet et al., 2012) is also common. Both methods have positive and negative aspects, as discussed below, leaving the final decision dependent on the available hardware and the deployment location.

Another issue relating to vessel detection is the scale (size of area, number of the ships and sensors, frequency at which data is gathered). When the dataset is small (short time periods and/or low intensity traffic), manual detection is likely to be sufficient. However, it can get labor intensive quite quickly near busy ship lanes. This is often the case and creates a need for additional means to automate the detection process.

This problem was examined in Papers I and II from both software and hardware perspectives. The software development in Paper I relies on a straightforward algorithm utilizing Gabor multipliers (Dörfler and Matusiak, 2013). A major development towards more advanced hardware is the use of a new type of sensors to describe the wake characteristics, both with respect to measuring pressure and with respect to water velocity. These devices, called 'hydromasts' are multimodal sensor systems developed by the Centre for Biorobotics, Tallinn University of Technology (Egerer et al., 2024; Ristolainen et al., 2019), discussed in Paper II. The results of both previously mentioned approaches were compared with visual findings and results obtained from convolutional neural networks.

## 1.1 Selection of devices

A straightforward and often preferred approach for recording water level elevation data in ship wakes, without any kind of conversion loss (as is the case with pressure-based methods) is to use a sensor system that can take readings from above the water surface. There are several different types of devices available (Metters et al., 2021; Parnell et al., 2008). The core data set used for this chapter was recorded in Tallinn Bay in 2009 using a downward looking echo sounder mounted on a stable tripod. The tripod was deployed in 2.6 m deep water, with the sensor mounted about 2.5 m above the typical water level during the measurement campaign (Kurennoy et al., 2011; Torsvik et al., 2015b).

Two examples of wake spectrograms<sup>2</sup> are shown in Figure 4, where the motor vessel (M/V) Star is approaching the port of Tallinn with a speed of 24 knots. Panel a) shows the situation on a windy day (wind ~4.0 m/s from NE) while panel b) shows the recording made on a calm day (wind ~1 m/s from SW). A comparison of the upper parts of these spectrograms firstly signals that the presence of a mild background wave field does not significantly change or blur the geometry of the patterns that reflect the components of

---

<sup>2</sup> All the development processes were conducted using a mathematical package Matlab with the addition of 'The Large Time-Frequency Analysis Toolbox' (Průša et al., 2014; Søndergaard et al., 2012) and OCEANLYZ toolbox (Karimpour and Chen, 2017).

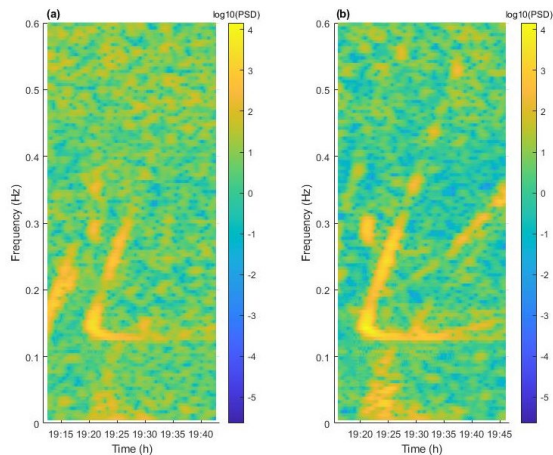


Figure 4. The signature of passenger ferry Tallink Star approaching the Port of Tallinn on a) relatively windy day 27.06.2009 and on b) a relatively calm day 28.06.2009. In both cases data is recorded from the above the water surface.

the wakes. It also shows that even relatively weak winds can generate waves with periods of 2–3 s (frequency about 0.3–0.5 Hz) with relatively wide spectrum in semi-closed areas like Tallinn Bay, and appear as noise in the upper higher-frequency parts of the spectrogram. These short period waves can mask the upper parts of the signal of divergent waves (Figure 4a).

Open ocean swells usually have a narrow frequency spectrum and periods commonly longer than components of ship wakes (Soomere, 2005). Therefore, they can be removed using spectral filters. However, short and young waves of the Baltic Sea (Björkqvist et al., 2018) often have a wide spectrum that overlaps with the frequencies of wake components.

This feature renders the process of filtering out noise from wave recordings quite difficult, especially if the goal is to avoid a significant loss in information about the vessel wakes. Further processing spectrograms that contain a high level of noise can increase error and add uncertainties during the following steps of wake analysis, for example when finding the vessel speed and distance to the wake origin point (Torsvik et al., 2015a).

The use of data collected from above the water surface, despite being noisy (Kurennyy et al., 2011), is better than other methods with respect to establishing accurate water surface elevation measurements, especially for investigations that examine the high frequency and/or low energy components. Other survey methods, such as near-bottom pressure recordings, either tend to mask or attenuate such components, sometimes to the level of being unusable.

It is common to use pressure sensors positioned either somewhere in the water column or on the seabed to record wake signals. In this case the high-frequency part of the surface wave field is attenuated because the pressure signal decreases in the water column, most rapidly for shorter waves (Dean and Dalrymple, 1991). This feature also suppresses the previously mentioned noise produced by wind waves. The near-bed pressure signal frequently contains a sufficient level of lower-frequency components to evaluate the properties of transverse waves and the longest fraction of divergent waves. On some occasions pressure oscillations with periods >10 s can mask the longer

components of the wake such as transverse waves or precursor solitons (e.g. near-horizontal higher energy lines up to 0.2 Hz in Figure 5b compared to Figure 5a).

This shortcoming was addressed by using time series from several temporally synchronized pressure sensors that were close to each other (Paper II). The idea is that different from short and short-crested wind waves, single wave components of the wake (possibly except for cusp wakes, (Liang et al., 2024)) are, ideally, long-crested (Soomere, 2007; Sorensen, 1973). It is therefore natural that wake components produce a coherent signal at closely located sensors whereas the signal from wind waves is random and varies much more from sensor to sensor. In other words, if the background noise (either low-frequency or high-frequency) is not coherent over the distance between the instruments, it could be suppressed by merging several synchronized spectrogram snapshots of coherent waves into one picture. To make use of this idea, is it necessary to consider small delays in the arrival of long-crested wake components to different sensors.

Time series from a set of 9 devices was available at nodes of a regular rectangular  $5 \times 5$  m rack with a step of 2.5 m in the relevant experiments (Paper II). The best result was achieved using five sensors (four in the corners and one in the center). The results were optimal for the further steps of the vessel wake analysis. The wake-to-background spectrum noise ratio (Figure 5c) was greatly improved. The result significantly simplified the wake detection process, eliminated most false detection decisions, and made it possible to extract and analyze vessel wake components and evaluate properties of ship motion (Paper II).

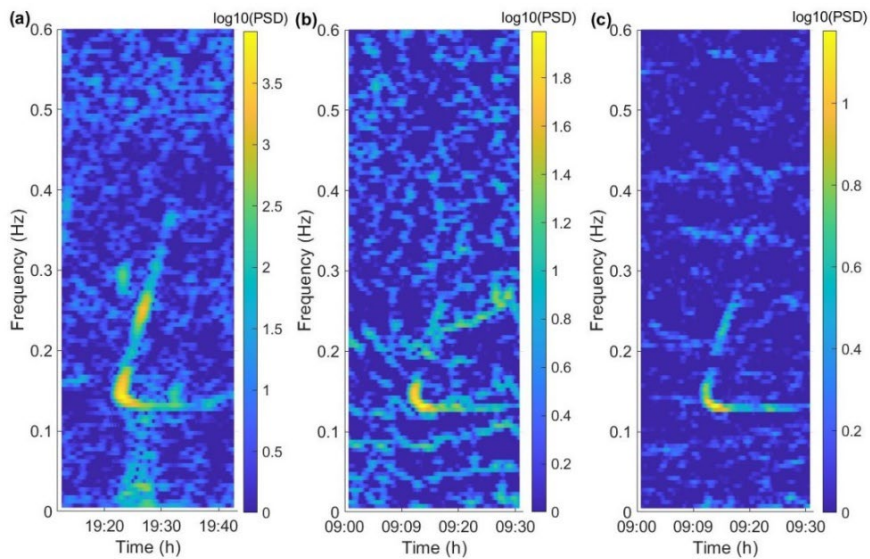


*Figure 5. The signature of passenger ferry Tallink Star approaching the Port of Tallinn on 25.06.2009 with a wind-generated sea with typical periods of 2–2.5 s (Torsvik et al., 2015b). The wake is measured using a one-point measurement device (a downward-looking echosounder mounted on a tripod) from above the water surface. (b) The signature of the same vessel approaching the Port of Tallinn on 17.07.2017 under similar weather conditions. The wake is detected using a single pressure sensor mounted at the seabed at a depth of 3 m. The pressure sensor is mounted at a height of 0.2 m from the seabed. (c) The same event as observed in (b) but visualized using five sensors located in the center and the corners of a frame of  $5 \times 5$  m. The spectrograms are normalized by frequency spectrum and overlapped. From Paper II.*

## 1.2 Detection of a sequence of ship wakes

If ship traffic is light, the dataset of wake-representing spectrograms is small and probably the best way for wake detection is visually picking the exact time moments from the spectrogram. Doing so would also make it possible to recognize complicated “portrayals” of high-speed vessels (Torsvik et al., 2015b). When there are many wake events, an automated wake detection method must be considered. A feasible option may be to apply convolutional neural networks, which have already been successfully used in similar studies for vessel wake detection from synthetic aperture radar and satellite images (Kang and Kim, 2019). Downsides to this method are the quantity of necessary data (including data collected under different weather conditions) and the time needed to train the model to detect the wakes to reach an acceptable level of detection. Another disadvantage is that this method is a supervised learning method: after deployment, the operator must go through the data meant for learning and classify the wakes by hand.

### 1.2.1 Software based approach

For real applications, methods that can start to detect the wakes without intervention are clearly preferred, especially those methods that do not need a long period to adapt to the data. Here, an example of such a method from the signal analysis is applied, namely, the technique to detect irregularities from the incoming signal by using so-called Gabor multipliers, as proposed by Dörfler and Matusiak (2013) (Paper I). Gabor multipliers are, in essence, composite operators, in other words, sequences of operations. The first operation is a short-time Fourier transform, like the one used to produce a spectrogram. This is followed by a pointwise multiplication with a distribution on phase space (called the Gabor symbol). The last step applied is an inverse short-time Fourier transform. This sequence helps map the input signal to its analyzed-synthesized (reconstructed) form (Feichtinger and Nowak, 2003). Manipulations based on Gabor multipliers are based on ‘The Large Time-Frequency Analysis Toolbox’ (Průša et al., 2014; Søndergaard et al., 2012).

The Gabor multipliers are not uniquely defined. They are usually chosen so that the information loss between the original and reconstructed representations is reduced to a minimum level. A compelling argument for using this multi-step technique is that the method suppresses (in the sense that it does not carry over) the irregularities of the original signal to its reconstructed version. Therefore, a comparison of these representations often reveals anomalies and objects in the input signal (Dörfler and Matusiak, 2013) and thus makes it possible to remove doubtful situations and avoid false detections (Paper I).

The method described is cost-effective in terms of computing power and does not require an additional learning period. However, it may be prone to continuously changing external forces like weather conditions. An example of the results is given in Figure 6. The vessel wakes were counted for one 24-hour cycle from 04:00 on 24.06.2009 to 04:00 on 25.06.2009. This period contained both calm times and events with notable wind wave activity. As discussed above, wind waves can distort the ability of the technology to separate the wake components from other fluctuations of the sea surface. During the calm periods (from 04:00 to 12:00 and from 21:00 to 01:00), the method using the Gabor multipliers has significant outcome only when ship wakes are present and thus leads to efficient detection of wakes. However, during the windy period (wind speed 5 m/s from the north-east from 12:00 to 21:00) the significantly higher wind wave driven noise level in the spectrograms required additional steps for wake detection.

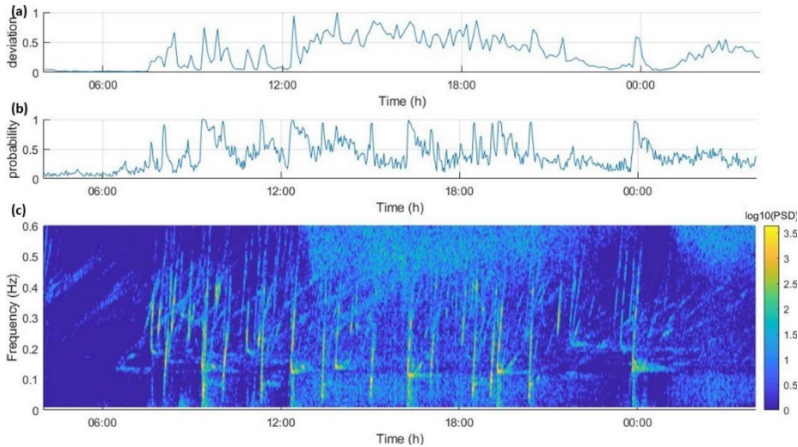


Figure 6. Wake detection with different methods: (a) using Gabor multipliers, (b) using shallow convolutional neural network. (c) A spectrogram depicting a measurement period from 04:00 24.06.2009 to 04:00 25.06.2009. Based on the results of Paper I.

For comparison, vessel wakes were also detected using a shallow convolutional neural network (CNN). It consisted of a CNN layer of ten 0.25 Hz by 100 s elements, a rectifier layer, a fully connected layer and a softmax layer. This system was trained with 15 epochs and with 16 iterations in each epoch. The results are shown in Figure 6b. The accuracy (ratio of the number of detected cases over the total number of events) was 0.44. Of 36 visually detected wakes, CNN detected 24, missed 12 and gave 19 false positive signals. The method using the Gabor multipliers gave an accuracy of 0.47: 27 detected, 9 missed and 21 false positive signals. The wake events listed here were counted as peaks from the outputs.

The presented comparison indicates that both methods have comparable detection power. They miss around one third of the wakes due to the windy (low signal-to-noise ratio) periods during the daytime. They also produce a comparable number of false positive signals, due to the same reason. A major difference is that the method using the Gabor multipliers was applied to the dataset with no previous knowledge. It used only the first couple of iterations (10–15 minutes of data) to adapt to the environment. The method based on the convolutional neural networks was trained on data that was selected from different days that experienced both calm and windy conditions and already had wakes detected and classified by the (human) operator. For these reasons, Gabor multipliers were used as a primary method for detecting wakes from the dataset measured by the Wave Engineering Laboratory in 2009 (Paper I).

### 1.2.2 Hardware based approach

An alternative approach would be to solve the wake detection problem by using advanced devices that can sense the wake events in the water column. Ideally, the approach would describe the water flow itself. A step in this direction was taken when recording a dataset, using devices made by the Centre for Biorobotics, Tallinn University of Technology, in 2017.

This measurement campaign used devices called ‘hydromasts’ (Egerer et al., 2024; Ristolainen et al., 2019). Each hydromast had a pressure sensor for collecting the water level data, and a vibrating vertical stem with a length of 100 mm, 15 mm in diameter and with a density close to water density. The movement of this stem was measured by a

micromechanical inertial measurement unit (IMU) (Ristolainen et al., 2019). Another, stationary (reference) IMU was mounted in the housing of the device (Ristolainen et al., 2019). The inertial measurements were registered along three perpendicular axes (Ristolainen et al., 2019). The idea was that any water flow passing the device would be registered as movements of the stem that acts like the lateral line of a fish (Ristolainen et al., 2019). The movements of the stem were used as the proxy of the water's velocity passing the sensor.

For wake detection, the data from the IMU connected to the vibrating stem was corrected by the data from the stationary IMU. The resulting values were viewed as linear acceleration and gravity vector (Figure 7). For the comparison, wakes were detected by the methods described previously: by convolutional neural networks (Figure 7c) and using Gabor multipliers (Figure 7d). The corresponding spectrogram (Figure 7e) highlights ship wakes as L-shaped features as discussed above. As the (horizontal) time scale is strongly compressed, horizontal branches of these items are short, and the features are mostly represented by more-or-less vertical bright lines.

The detection and training processes for the Gabor multipliers and convolutional neural networks were conducted mostly as described in the previous section. As Gabor multipliers rely on the combination of a direct and a reverse transformation of the input signal, the technique was applied to the pressure data of each sensor separately. The results were afterwards summed and normalized with the assumption that the outcome converges sufficiently to be regarded as a wake event. Convolutional neural networks are meant for feature detection from the images, therefore firstly the spectrograms from the sensors were merged (as seen in Figure 7e), and afterwards the CNN technique was applied. This sequence of operations is the reason, in the current example, that the CNN-based detection leads to better results than the use of Gabor multipliers: the CNN was applied to the cleaned input data.

The example in Figure 7 covers the time frame from 15:00 to 24:00 on the evening of 10 July 2017. During that time, 12 wake events were visually counted from the spectrogram (Figure 7e). There were 14 peaks in both the linear vibration data and in the gravity vector that could indicate a wake. From these, 10 events were detected as wakes (true positives), 2 events were missed, and 2 false positives were generated giving an accuracy rate of 0.63. The use of the CNN methods leads to the same results (10 detected, 2 missed, 2 false positives). The performance of the method based on Gabor multipliers was slightly worse. The total number of registered events was 18, from which 9 were actual wakes, 3 wakes were missed and 9 were false positives giving a total accuracy rate as 0.4. Both methods using the water flow data missed the events at the end of the data stream (at 22:40 and 23:50) Figure 7a and Figure 7b) while the CNN application missed events at 19:10 and 23:50 (Figure 7c). The method based on Gabor multipliers failed to detect cases at 19:10, 22:40 and 23:50 (Figure 7d).

From those three wake events, the event at 23:50 was missed due to proximity to the end of the data series so that only the high peak is present in the spectrogram. Only the CNN technique was able to detect it as it relied on the contrast of the input (spectrogram) image rather than on raw input data. This shortcoming could be easily removed by overlapping data subsets or keeping the data in a continuous stream. The sensors measured the data continuously and the data was divided into days to simplify the analysis. Wakes at 19:10 and 22:40 were missed due to the low signal-to-noise ratio. In both cases only the chirp part of the wake representing divergent waves is present at high frequencies compared to the rest of the wakes.

This feature leads to one of the key issues of this analysis. Namely, wakes from the vessels sailing at 15 knots (approximately 28 km/h) or below were seldom visible in spectrograms. Even if they were, their properties often had too large uncertainty so that the rest of the analysis struggled to determine the sailing characteristics.

The results imply that regardless of which of the methods was selected (either relying on hardware, applying general feature detection methods from images, or using signal analysis) the overall result of the automated process has adequate accuracy compared to the case when wake events were counted on spectrograms manually. Also, for all the methods described, the final selection of the events to be identified as a ship wake was done by counting the peaks over a certain threshold. This means that for the methods based on hardware (Figure 7a, Figure 7b), the gravity vector data (Figure 7b) is usable immediately whereas the linear acceleration data (Figure 7a) requires additional low-pass filtering.

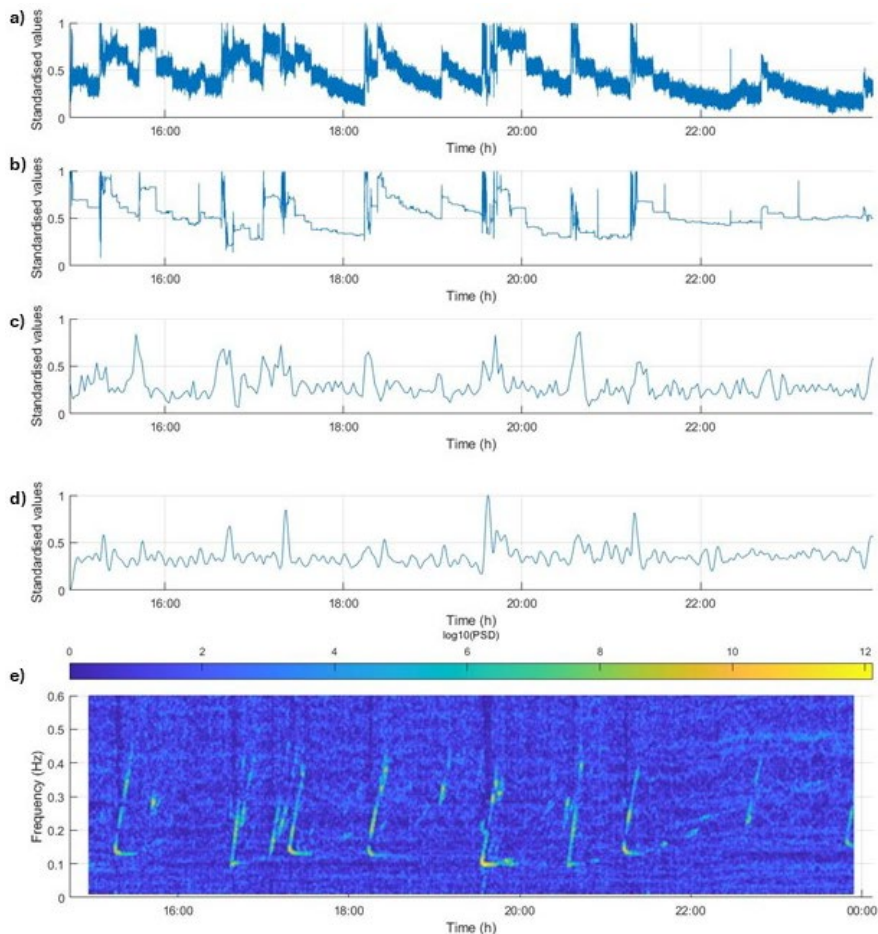


Figure 7. The comparison of the detection results on 10 July 2017. (a) Time series of the linear acceleration, (b) time series of the gravity vector, (c) the probability for detection found using convolutional neural networks, (d) the combined probability for vessel wakes calculated with Gabor multipliers, (e) the spectrogram based on the pressure data where ship wakes are portrayed as yellow structures. Amended from Paper II.



To sum up, all the different methods that are reported and used for gathering and analysis of the vessel wake data are suitable for detection of the presence of ships via their wakes. A natural limiting factor is the water depth because for pressure sensors from some point wave attenuation would be too great, and it is difficult to install and retrieve the sensors in deeper areas. For above-surface sensors, deployment requires shallow water depths. The preferable way forward is to move from single sensor systems to sensor arrays and grids. Doing so will 1) improve the overall data quality by suppressing the signal of random wave fields (Figure 5); and 2) provide additional information about the vessel itself, as will be discussed in the next chapter. A broad range of methods can be effectively used for signal analysis, automatic wake detection, and feature detection, from the (spectrogram) images to hardware-based approaches. The performance of all developed and employed methods is comparable to the accuracy achieved by visually picking the events on spectrograms.

There are also obvious limitations for the detection and analysis of vessel wakes in such a way. The first limitation is the vessel speed. Equally important is the actual location of the measurement device(s). Both datasets used in this thesis were collected in the same location which had natural obstacles to shelter the waves and wakes from the south-east and north-west. Therefore, the focus was on the vessels approaching port from the north. However, the records contain wakes that have arrived from the south-east due to diffraction or refraction. For example, wakes from some fast vessels that travelled out of the port to the north are seen with the cases at 19:10 and 22:40 (the high frequency divergent components). Thirdly, as the wake events may last several tens of minutes (Soomere, 2007), traffic density could be a problem. For example, if several vessels pass the sensor(s) within, say, 30 minutes, the spectrogram will have several overlapping wake traces. This pattern may be interpreted as a single wake event by the automated detection methods described above.

## 2 Vessel localization

After wake detection, the second step in the process is to determine the vessel position and its sailing parameters. This step can be regarded as vessel localization. Combined, the two steps provide sufficient information about a ship's presence and its movement. Along with vessel recognition, that is determination of its type and/or purpose, they form the backbone of the vessel traffic monitoring system. The data provided by these systems allows real-time continuous vessel tracking. However, usually with the ship wake events are single point recordings in time and space, and they are usually recorded with a significant time delay that is the result of the time taken for the wake to travel from the point of generation to the measurement devices. Therefore, at best, this method only allows one historical snapshot per vessel as it passes the sensor system.

Continuous vessel monitoring systems use consecutive timestamps to determine to where and how the ship is moving. Wake events, despite being single events, contain enough information, which, if measured by the right equipment and interpreted adequately, may give the same result. The goal is to determine the following four parameters: speed, distance, bearing and the course of the ship from a single measurement for each passing vessel. Speed and distance can be obtained directly from the spectrogram of the wake itself, while the bearing and course can be estimated by using a grid of closely positioned sensors. In this chapter the findings are presented using the data from Paper III, as the results of Paper I use AIS data provided with very coarse time resolution and thus cannot be regarded to be reliable for estimating actual vessel sailing parameters.

### 2.1 Speed of the vessel

In general, the basic idea for determining the speed of the vessel and the distance of the wake-generation location from the sensors relies on the understanding that this information is hidden in the frequency of cusp waves, that is, in the frequency of waves that arrive first to the observer or sensor (Wu, 1991). This frequency can be found using the spectral representation of the wake by determining the frequency of waves at the point of the Kelvin wedge that reaches the sensors.

Recent developments in the understanding of the structure of ship wakes have provided further options to solve this problem. Pethiyagoda et al. (2017) showed that most of the wake energy is concentrated on the linear dispersion curve (Figure 8) in the spectrogram. This curve can be described in time-frequency coordinates as:

$$2\sqrt{2}\omega_{\pm} = \sqrt{T^2 + 4 \pm T\sqrt{T^2 - 8}}, \quad (3)$$

where  $\omega_{\pm}$  is the dimensionless angular frequency of the waves and  $T = t/y$  corresponds to dimensionless time of propagation of the wake over distance  $y$ . This curve has two branches. The plus sign '+' represents the frequency range of divergent waves and the minus sign '-' the frequency range of transverse waves. These two branches interact at the point where  $T = \sqrt{8}$ ,  $\omega = \sqrt{3/2}$  (point "A" in Figure 8). This point represents the edge of the Kelvin wakes for the observer or sensor. This edge is usually represented by cusp waves, that is, the strongest wake components. Even though their arrival would be the easiest to detect, identification of their common frequency is a nontrivial problem as waves with this frequency exist during a short time interval and the signal is rapidly split into two components. This complexity is reflected in Figure 8. The cusp waves are

represented as the vertical location of the dispersion curve. This means that, technically, it is necessary to identify the frequency of a signal that changes infinitely fast. This situation can lead to a misinterpreted frequency value.

A solution to this problem can be found from the properties of the two branches of the linear dispersion curve. Namely, the branches of this curve for the divergent and transverse waves have asymptotes for large values of  $T$ . In other words, for large values of  $T$  both branches can be approximated by a straight line. These lines are represented as  $\omega = T/2$  for the divergent components and a horizontal line  $\omega = 1$  for the transverse components. The crossing point of these asymptotes (point “B” in Figure 8) at  $T = 2$ ,  $\omega = 1$  (in nondimensional coordinates) can be interpreted as a first (linear) approximation of the arrival time instant of the Kelvin wedge. It is invariant with respect to the ship’s speed and to the depth Froude number at subcritical speeds (Pethiyagoda et al., 2017). The relevant frequency is the long-term average value of transverse waves. This feature immediately signals that this approximation is applicable only if the vessel sails at a subcritical speed. In critical and supercritical speed regimes, when the divergent component becomes the dominant feature and transverse waves disappear, this method does not work.

Torsvik et al. (2015b) applied two methods to identify and make use of the frequency of Kelvin wake components to find the speed  $U$  of the vessel and the distance of the wake generation location to the sensor. First, he noted that the vessel’s speed can be estimated as (Torsvik et al., 2015b):

$$U = \frac{g}{2\pi f_{t\infty}}, \quad (4)$$

where  $f_{t\infty}$  denotes the limiting frequency of transverse waves if  $T \rightarrow \infty$ , that is, the frequency at point “B” in Figure 8. This frequency can be evaluated as the average frequency of the transverse components after some time of the passage of the cusp waves. This approach is a variation of the method expressed by Eq. (2) and proposed by

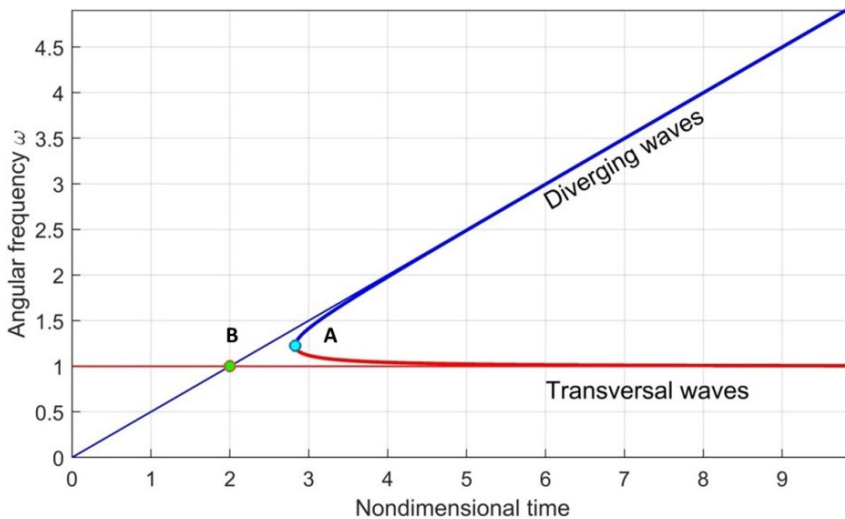


Figure 8. Representation of the nondimensional linear dispersion curve of ship waves (Pethiyagoda et al., 2017). Point “A” is the edge point of Kelvin wedge, point “B”, the crossing point of the asymptotes of the linear and transverse component, represents the linear approximation of the edge of the Kelvin wedge (of point “A”). From Paper III.

Wu (1991). Second, Torsvik et al. (2015b) demonstrated that the speed of the ship can be calculated as:

$$U = \sqrt{\frac{3}{2} \frac{g}{2\pi f_{cusp}}}. \quad (5)$$

where  $f_{cusp}$  is the frequency of the waves at the edge of the Kelvin wake, that is, corresponding to the location of point “A” in Figure 8. These two approaches are equivalent because  $f_{cusp}/f_{t\infty} = \sqrt{3/2}$  (Pethiyagoda et al., 2017). Therefore, it is enough to correctly evaluate  $f_{t\infty}$  to specify the frequency of the cusp waves.

This aspect was discussed in Paper I in the context of the reliability of estimates based on Eqs. (4) and (5). As the frequency of cusp speed corresponds to the vertical section of the linear dispersion curve (Pethiyagoda et al., 2017), even small errors in the estimates of cusp wave timing may lead to large errors in  $f_{cusp}$ . The estimates of  $f_{t\infty}$  are much more stable. Consistent with the described features, the approach based on the signature of the transverse component leads to a better match of the estimates of the speed of the vessels compared to the AIS information (Paper I).

If the speed  $U$  of the vessel is calculated, the distance travelled by the wake can be determined from the properties of the divergent waves. It is sufficient to determine the time interval  $\Delta t$  during which the frequency of the divergent component increases from the maximum frequency  $f_{cusp}$  (frequency of cusp waves) to a  $\sqrt{2}$  times higher value (Torsvik et al., 2015b). The distance  $L$  travelled from the wake generation location to the observer or the measurement site can be estimated as (Torsvik et al., 2015b):

$$L = \sqrt{6}U\Delta t. \quad (6)$$

Three applications were used to evaluate the ship speed and distance: 1) direct evaluation the frequency  $f_{cusp}$  of cusp waves from the record of the highest wave components at the arrival of the wake, 2) evaluation of this frequency using the shape of the branch for divergent waves in Figure 8, 3) relying on the properties of the asymptote of the branch for transverse waves, equivalently, Eq. (4).

In ideal conditions all three methods should provide adequate and matching estimates of the actual sailing speed of the passing ship (Figure 9). Theoretically, the estimate that relies on properties of transverse components is expected to be closest to actual values because it uses in the best way possible the properties of the Kelvin wake. A comparison of the data from monitoring the actual vessel traffic and the three applications shows that the results are different, but the above hypothesis concerning their performance is correct (Figure 9). A comparison of the performance of the three methods was reported in Papers I and III. In both cases the same conclusion was reached even though the temporal resolution of the AIS data was different, with the 2017 reference AIS information about the passing vessels being available at much finer resolution (5 minute compared to 1 hour in 2009) (Mitev, 2018; “VesselFinder,” 2020).

The attempts to directly evaluate the cusp wave frequency (Figure 9a) led to systematic overestimation of ship speed and therefore underestimation of this frequency. Similarly, the use of properties of divergent waves (Figure 9b) usually led to overestimation of ship speed. The approximation of the cusp frequency using the limiting frequency of the transverse components (Figure 9c) has succeeded in providing values close to actual reference data.

In addition to the theoretical arguments, this method has several significant practical advantages. Firstly, the transverse part of the wake in the spectrograms is tightly

confined on the frequency scale. As a result, the errors of estimates are small (Figure 9c). Secondly, it occurs in a region on the time-frequency scale with a small number of interfering factors in the study area, therefore enabling a lossless extraction and analysis. Thirdly, if present, it is well defined over the entire duration of the wake. This increases the level of confidence of the frequency estimates.

A disadvantage is that it is prone to external influencing factors, such as the ship moving at a very high speed, equivalently, at large depth Froude numbers. As a result, this component is not always present or is masked by noise or by other wakes. These features limit the use of this method: even if it works adequately in good conditions, it has the lowest application rate among the three.

Therefore, methods for directly determining the frequency of cusp waves at the edge of the Kelvin wedge should also, at times, rely on the properties of wake components which are more frequently present or more pronounced than the transverse component. The approach based on the direct evaluation of the cusp wave properties (Figure 9a) has an advantage over similar estimates that make use of properties of the divergent component (Figure 9b) due to the simplicity of the analysis. The disadvantage is that it is based on one single highest energy value at the intersection of the two branches. Therefore, one should not be overconfident of the values found. This feature is illustrated by large error bars in the relevant values (Figure 9a) compared with other methods. The results found from the properties of divergent waves rely on the part of the wake in the spectrogram that is often affected by high noise caused by wind waves. Along with the wide range of frequencies and energy covered by this branch, the estimates contain high uncertainty levels (Figure 9b). As this step is a crucial part in the process of determining the distance between the vessel (wake generation location) and sensor system and it relies on more data than the method of cusp waves, it should be considered as a fallback method if the transverse component is absent, or the calculation based on it fails.

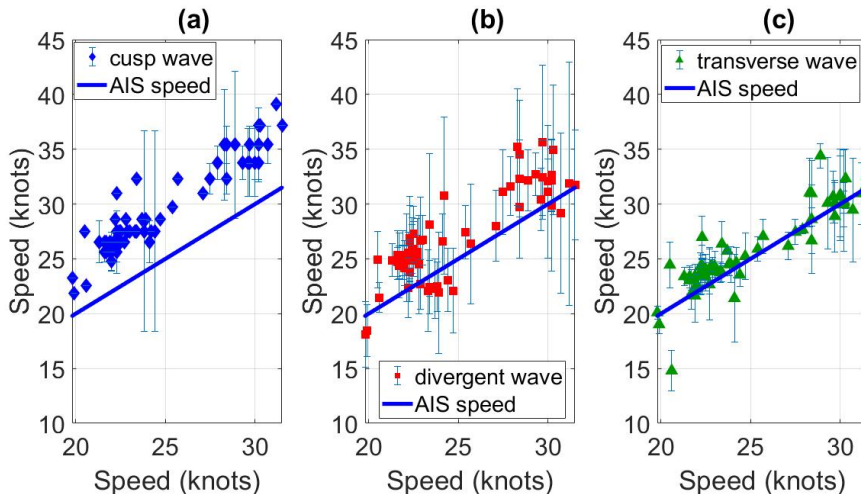


Figure 9. A comparison between the actual vessel traveling speed (blue line) and estimates found using the properties of (a) cusp waves, (b) divergent waves, and (c) transverse waves (c). Error bars represent the 95% confidence level of the calculated values. Recalculated based on results presented in Paper I and Paper III. Note that Paper I originally compared the estimates with the average distance to the centerline of traffic separation scheme, which was a guess at best and for this reason they are recalculated here.

The presented description demonstrates that the accuracy of estimates of the distance travelled by the wake depends on the quality of the extraction of the starting point of the divergent component. In most cases, the divergent component is quite reliable when it comes to extraction and analysis. However, one should note the mentioned uncertainty levels and their influence when calculating the actual distance between the vessel and the sensor system.

## 2.2 Vessel position and course

The AIS data from 2017 enabled a vessel's actual position close to the point where the wake was generated to be determined. The use of several sensors made it possible to evaluate the direction of the incoming wake, which was combined with the distance calculation, as discussed before, based on the transverse component of the wake. The following discussion is based on Paper III.

The background assumption is that most wake components are long-crested waves with locally straight crests. This assumption is not correct for cusp waves (Liang et al., 2024) but acceptable for the rest of the wake. The general idea was that if sensors are close enough together to record simultaneously the same wave crest or trough passing, such as during one wave period, then the direction from which the wake is propagating can be calculated based on the time differences of the passing of the trough or crest at different sensors. It is therefore crucial to follow wave crests that move at phase speed. Considering a 7 s period for a transverse wake component, the depth of instruments being 3 m which results in a phase speed of 4.3 m/s, then the maximum allowed gap between the sensors to register the same wave crest or trough would be around 30 m. As described above, we used an array of 9 sensors mounted on a regular rectangular frame of 5 × 5 m. Therefore, the largest distance between a pair of sensors was 7 m.

This method is an implementation of the widely used phase-shift technique used in many fields, including *estimates* of the directional spectra of ocean waves (e.g., Dean and Dalrymple, 1991). For an ideal regular long-crested wave pattern with straight wave crests an estimate of delay (phase shift) between the arrival of wave crests to the location of any two devices represents two propagation directions of the wave pattern. Therefore, for establishing a reliable estimate, several sensor pairs are needed to build statistics of directions.

The data used in Paper III for this purpose was measured with 9 devices. This gives 36 different sensor pairs and 72 wave propagation directions (dashed lines in Figure 10). This number of pairs provided in most cases an approximation for the approach direction for the incoming wake that correlated well with the direction prescribed by the traffic separation scheme (within  $\pm 10^\circ$  around  $14.3^\circ$ , area with dashed red lines in Figure 3). The means to reduce the number of instruments (currently 9) needed to find the necessary direction and their arrangements are not viewed here.

The estimates of wave propagation direction using the phase shift method were based on the pressure data used for calculating the spectrograms. Getting the time delays from the evaluation of the proxy of water velocities (speed and direction) that were used for wake event detection in the previous chapter was also considered. Due to the high level of noise and sensitivity of the calculation process to small deviations, the retrieved values were not consistent enough to be considered as reliable results.

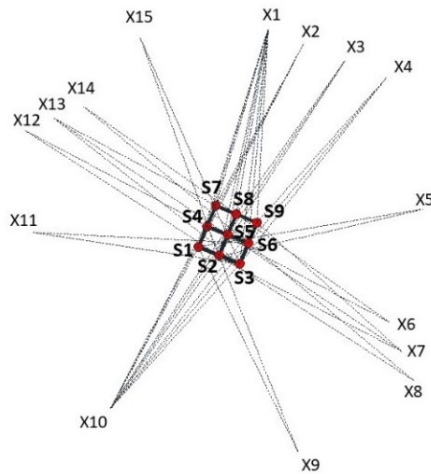


Figure 10. Distribution of 72 potential wave propagation directions (dashed straight lines) from 36 sensor pairs (all pairs from sensors S1 to S9). One direction from every sensor pair (in total 36) leads to the expected (most probable) direction X1 while the second possible direction contributes to the set of misleading directions X2 to X15. From Paper III.

Combining the determined direction of the incoming wave with the distance travelled by the wake leads to the estimation of the vessel position at the time moment when the wake was generated. One such example is shown in Figure 11 that presents the vessel position on its movement track around the time the wake was generated. The uncertainty area is large because, due to the low AIS resolution of 5 minutes, the vessel's exact location had to be interpolated. Figure 11 also depicts the calculated position using the

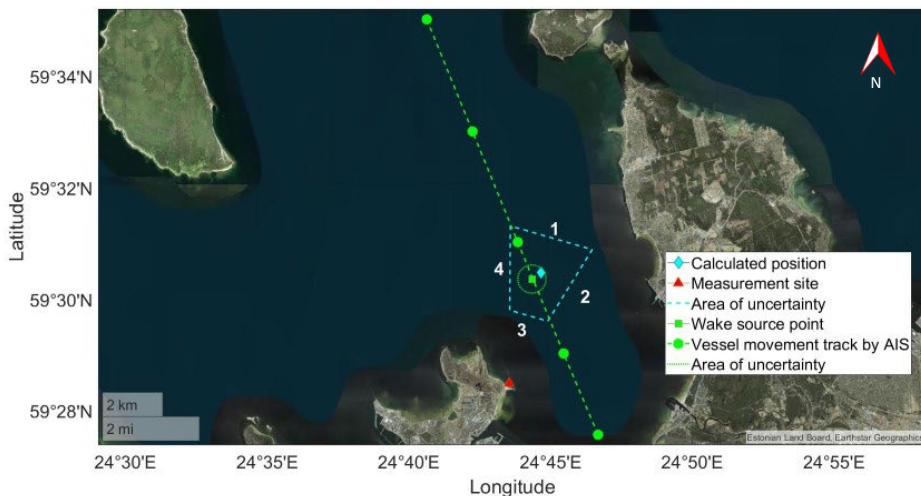


Figure 11. An example of the results of an evaluation of the position and sailing line of M/S Megastar approaching the Port of Tallinn (marked as a 'Vessel movement track by AIS', green dots indicate the vessel AIS locations) on 13.07.2017. The wake source point was calculated using the AIS positions. The green rectangle with a green dotted circle around it indicates possible course ( $\pm 5^\circ$ ) and speed ( $\pm 2$  knots) alterations. The vessel location at this instant found from the wake readings is indicated by the 'Calculated position'. The area of uncertainty (error estimations for the distance and direction) is shown as the cyan polygon within 95% error bars. From Paper III.

distance travelled by the wake and its direction along its area of uncertainty (from distance and direction evaluation).

The calculated position is close to the position estimated from the AIS data. The difference is around 400 m for example in Figure 11, and for majority of the cases the estimate falls into a 0.5 km circle around the actual position (Figure 12). However, the area of uncertainty is quite big: about 2 km wide (from line 2 to line 4 in Figure 11) and 2.8 km long (between lines 1 and 3 in Figure 11). As discussed previously, the uncertainty first stems from errors in calculating the distance. This step often contains substantial inaccuracies when extracting the properties of divergent components from the spectrogram. The resulting high level of uncertainty (see error bars on Figure 9b) translates further into calculating the distance to the location of the wave generation based on the estimates of vessel speed. Another dimension of inaccuracies stems from estimates of the wave propagation direction. This component of uncertainty becomes evident as the width of the area of uncertainty despite showing the general direction very well.

The likely main reasons for this large uncertainty are the short distance between the sensors and high level of the background noise. Together they result in quite a large (approximately 30°) uncertainty in the wave propagation direction and thus the sailing direction. A feasible way to reduce this kind of uncertainty is to increase the distance between the sensors. This has a natural limit as the quality of the spectrogram should not diminish even if the overlapping procedure described earlier is used. However, as no actual measurements were conducted, then this solution has not been checked.

From Figure 12 another interesting phenomenon arises. There is a correlation between the estimates of the distance and the direction of the incoming wake. In cases when the calculated distance was shorter compared to the actual value, the evaluated sailing direction was shifted towards the north. When the calculated distance exceeded the actual distance, the direction was shifted towards the east compared to the actual direction.

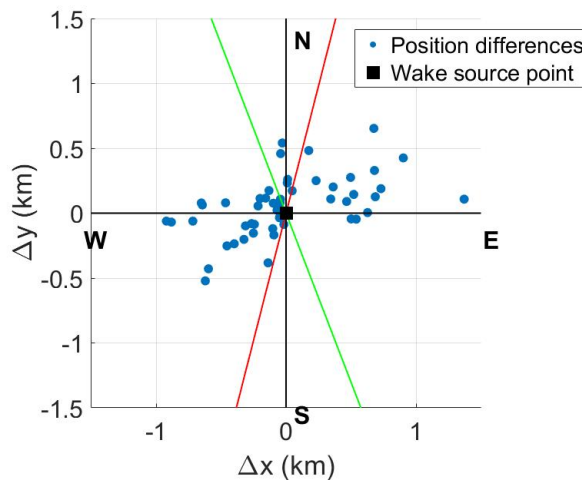


Figure 12. Differences between wake origin points found from the AIS data (the black rectangle in the center) and calculated wake origin points from pressure data plotted in cardinal directions (N: North, E: East, S: South, W: West). The measurement site is in the SW corner. Red line: the direction of the incoming wake. Green line: the course to port. From Paper III.



Vessel courses were calculated by applying the angle of cusp waves ( $35^{\circ}16'$ ) to the calculated directions of propagation of wake wave crests. This approach leads to two courses of the vessel. There is no way to determine which of them is correct based solely on the wake data. Therefore, the final estimate of the vessel course should be determined using additional information. One solution is to use the local sailing conditions (Engen and Johnsen, 1995). This approach was used in these estimates. The possible course (around  $230^{\circ}$ ) was dismissed as it was directing ships directly to the land (Figure 11). These left values of the realistic courses which coincided with the orientation of the traffic separation corridor ( $159^{\circ}$ ).

An approach to resolve this issue would be to use two sets of sensors, analogous to using two subsequent synthetic aperture radar images to determine the wave propagation direction (Ouchi et al., 1999). As the course calculation was a linear manipulation of the direction of the incoming wake, the same outcomes were inherited: calculated results matched well with actual courses of the vessels sailing to port (within  $\pm 10^{\circ}$  of  $159^{\circ}$ ), but the uncertainty, was kept also in a range of  $30^{\circ}$ .

To sum up, methods for determining the vessel location and its sailing parameters at the time instant when the wake was generated can produce results that are comparable to actual data. However, the biggest problem is the ambient noise, mostly due to wind waves. Its presence significantly increased the level of uncertainty of the estimates. Another big issue was the high traffic intensity in the study area. For this reason, only the cases when a single vessel was approaching the port were used. The presence of wakes from multiple vessels within the same time window (15 minutes) complicated the analysis process from the extraction of the wake structure from the spectrogram to finding the direction of the incoming wake. Lastly, these methods are only appropriate if the ship sails steadily along a fixed course. As shown by Pethiyagoda et al. (2017), violations of these assumptions can produce spectrogram images where several shapes of wake components are overlapping, and the proposed analysis becomes unreliable.

## Conclusions

Despite the absence of a well-established method for vessel traffic monitoring, there are a vast variety of tools and instruments available to gather, detect and analyze information about ship wakes from water elevation data, applicable to different environments. The main purpose of the work was to investigate whether it is feasible to use spectral images of wakes of passing vessels as a component of a vessel traffic monitoring system. The analysis addresses the first two major steps – vessel detection and localization – out of five stages of creating a Recognized Maritime Picture (NATO Standardization Agency, 2015). The third step, recognition, which characterizes the vessel and therefore is also heavily dependent on the data collected by the sensors, is not considered here.

Ship detection provides information as to whether the trace of the ship is present in the input data (Papers I and II). This aspect was investigated in terms of choice of environment, signal quality and prospects for automation of the detection. Vessel localization means identification of its location and where it is heading (Papers I and III). This was addressed by calculating the speed of the detected ship and the distance from the measurement location to the point where the detected wake was generated from wake spectrograms. Further, the propagation direction of the incoming wake was estimated and incorporated to determine the location of a ship at a time moment when the wake was generated, and the course it was heading.

The key findings of the analysis of options relating to the use of ship wake spectrograms for vessel detection and location are as follows:

- Wind-wave noise can be reduced by using pressure sensors placed on the seabed in a shallow area. The quality of the spectrogram can be improved by overlapping results from multiple closely positioned devices (Paper II and Chapter 1.1)
- Ship wakes can be detected by evaluating water flow data from near the sensor (Paper II and Chapter 1.2). They can be detected by single-step detection algorithms based on signal transformation (Paper I and Chapter 1.2)
- Vessel speed estimated based on the structure of a wake in the spectrogram corresponds well with the actual speeds. Approximation using the asymptotic properties of transverse components provides the best results in terms of accuracy and the level of the uncertainty (Paper I and Chapter 2.1).
- Using several sensors positioned appropriately close together enables the determination of the propagation direction of the incoming wake. This, along with the distance to the location of wake generation derived from the wake structure from the spectrogram, can be used to find the location where the wake was generated (Paper III and Chapter 2.2).
- If the direction of the wake is known, the course of the ship can be estimated with the addition of external information (Paper III and Chapter 2.2)

The general conclusion is that the developed method of spectral analysis of ship wakes as part of vessel traffic monitoring system has limited applicability if a single sensor is used. It provides a single snapshot of the location and the sailing parameters of the passing vessel. The outcome of the method is only reliable if the ship sails on a steady course and at a steady speed in subcritical regime but faster than ~15 knots. The method is trustworthy if only one ship wake is present at the same time. Lastly, all the information is retrieved with a delay that reflects the propagation time of the wake from the generation location to the measurement devices. The advantage of the

described approach is that the required equipment and its deployment are cost-effective requiring only pressure sensors that can be deployed in 2–3 m deep water from the land or by small boat.

Some further considerations relate to the ship types, their sizes, and the maximum distance at which the wakes are detectable. These issues were not considered as all the measurements were taken at one location, near the Pikakari Beach facing the approach lane of the marine traffic separation scheme. Thus, all detected wakes were generated approximately 3.2 km away. All the ships in this study were ferries approximately equal in size. Further research and measurements could be designed and implemented to address these questions. Potential locations include areas near ports (like the Pikakari Beach) with more varied traffic (for example the Hel Peninsula in Poland), or areas that could test detectability of vessels sailing at larger distances from the measurement location (for example the Kõpu Peninsula on the island of Hiiumaa).

## List of figures

- Figure 1. A scheme of the linear Kelvin wake generated by a ship sailing in deep water  $h = \infty$  to the right. The half-angle of the Kelvin wake is  $19^{\circ}28'$  and the propagation direction of cusp waves forms an angle of  $\arccos(\sqrt{2/3}) \approx 35^{\circ}16'$  with the sailing line (Newman, 1977; Torsvik et al., 2015b). From Paper III. .... 11
- Figure 2. (a) An example of pressure time series of a vessel wake that is converted to water elevation data. (b) Short-time Fourier transform (spectrogram) of the corresponding series (note that the spectrograms are represented in normalized way). Wake elements are marked with red dashed rectangles. From Paper II. .... 13
- Figure 3. The study area in Tallinn Bay on the north coast of Estonia. The traffic separation scheme allows two approaches to the Port of Tallinn: from the north and west. Adapted from Paper II. .... 14
- Figure 4. The signature of passenger ferry Tallink Star approaching the Port of Tallinn on a) relatively windy day 27.06.2009 and on b) a relatively calm day 28.06.2009. In both cases data is recorded from the above the water surface. .... 18
- Figure 5. The signature of passenger ferry Tallink Star approaching the Port of Tallinn on 25.06.2009 with a wind-generated sea with typical periods of 2–2.5 s (Torsvik et al., 2015b). The wake is measured using a one-point measurement device (a downward-looking echosounder mounted on a tripod) from above the water surface. (b) The signature of the same vessel approaching the Port of Tallinn on 17.07.2017 under similar weather conditions. The wake is detected using a single pressure sensor mounted at the seabed at a depth of 3 m. The pressure sensor is mounted at a height of 0.2 m from the seabed. (c) The same event as observed in (b) but visualized using five sensors located in the center and the corners of a frame of  $5 \times 5$  m. The spectrograms are normalized by frequency spectrum and overlapped. From Paper II. .... 19
- Figure 6. Wake detection with different methods: (a) using Gabor multipliers, (b) using shallow convolutional neural network. (c) A spectrogram depicting a measurement period from 04:00 24.06.2009 to 04:00 25.06.2009. Based on the results of Paper I... 21
- Figure 7. The comparison of the detection results on 10 July 2017. (a) Time series of the linear acceleration, (b) time series of the gravity vector, (c) the probability for detection found using convolutional neural networks, (d) the combined probability for vessel wakes calculated with Gabor multipliers, (e) the spectrogram based on the pressure data where ship wakes are portrayed as yellow structures. Amended from Paper II..... 23
- Figure 8. Representation of the nondimensional linear dispersion curve of ship waves (Pethiyagoda et al., 2017). Point “A” is the edge point of Kelvin wedge, point “B”, the crossing point of the asymptotes of the linear and transverse component, represents the linear approximation of the edge of the Kelvin wedge (of point “A”). From Paper III. .... 26
- Figure 9. A comparison between the actual vessel traveling speed (blue line) and estimates found using the properties of (a) cusp waves, (b) divergent waves, and (c) transverse waves (c). Error bars represent the 95% confidence level of the calculated values. Recalculated based on results presented in Paper I and Paper III. Note that Paper I originally compared the estimates with the average distance to the centerline of traffic separation scheme, which was a guess at best and for this reason they are recalculated here..... 28

Figure 10. Distribution of 72 potential wave propagation directions (dashed straight lines) from 36 sensor pairs (all pairs from sensors S1 to S9). One direction from every sensor pair (in total 36) leads to the expected (most probable) direction X1 while the second possible direction contributes to the set of misleading directions X2 to X15. From Paper III. .... 30

Figure 11. An example of the results of an evaluation of the position and sailing line of M/S Megastar approaching the Port of Tallinn (marked as a 'Vessel movement track by AIS', green dots indicate the vessel AIS locations) on 13.07.2017. The wake source point was calculated using the AIS positions. The green rectangle with a green dotted circle around it indicates possible course ( $\pm 5^\circ$ ) and speed ( $\pm 2$  knots) alterations. The vessel location at this instant found from the wake readings is indicated by the 'Calculated position'. The area of uncertainty (error estimations) for the distance and direction) is shown as the cyan polygon within 95% error bars. From Paper III. .... 30

Figure 12. Differences between wake origin points found from the AIS data (the black rectangle in the centre) and calculated wake origin points from pressure data plotted in cardinal directions (N: North, E: East, S: South, W: West). The measurement site is in the SW corner. Red line: the direction of the incoming wake. Green line: the course to port. From Paper III. .... 31

## References

- Altan, Y.C., Otay, E.N., 2018. Spatial mapping of encounter probability in congested waterways using AIS. *Ocean Eng.* 164, 263–271. <https://doi.org/10.1016/j.oceaneng.2018.06.049>
- Anupriya, K.R., Sasilatha, T., 2018. Ship intrusion detection system – A review of the state of the art, in: Zelinka, I., Senkerik, R., Panda, G., Lekshmi Kanthan, P.S. (Eds.), *Soft Computing Systems*. Springer Singapore, Singapore, pp. 147–154.
- Aurdal, L., Løkken, K.H., Klausen, R.A., Brattli, A., Palm, H.C., 2019. Adversarial camouflage for naval vessels, in: Dijk, J. (Ed.), *Artificial Intelligence and Machine Learning in Defense Applications*. SPIE, 111690K. <https://doi.org/10.1117/12.2532756>
- Björkqvist, J.-V., Lukas, I., Alari, V., van Vledder, G.P., Hulst, S., Pettersson, H., Behrens, A., Männik, A., 2018. Comparing a 41-year model hindcast with decades of wave measurements from the Baltic Sea. *Ocean Eng.* 152, 57–71. <https://doi.org/https://doi.org/10.1016/j.oceaneng.2018.01.048>
- Casson, L., 1995. *Ships and Seamanship in the Ancient World*. JHU Press.
- Chang, S.-J., Tseng, K.-C., Chang, S.-M., 2014. Assessing navigational risk of offshore wind farm development — with and without ship’s routing, in: *OCEANS 2014 – TAIPEI*. <https://doi.org/10.1109/OCEANS-TAIPEI.2014.6964565>
- Chen, P., Huang, Y., Mou, J., van Gelder, P.H.A.J.M., 2018. Ship collision candidate detection method: A velocity obstacle approach. *Ocean Eng.* 170, 186–198. <https://doi.org/10.1016/j.oceaneng.2018.10.023>
- Claremar, B., Haglund, K., Rutgersson, A., 2017. Ship emissions and the use of current air cleaning technology: Contributions to air pollution and acidification in the Baltic Sea. *Earth Syst. Dyn.* 8, 901–919. <https://doi.org/10.5194/esd-8-901-2017>
- Dahana, U., Gurning, R.O.S., 2020. Maritime aerial surveillance: Integration manual identification system to Automatic Identification System. *IOP Conf. Ser. Earth Environ. Sci.* 557, 12014. <https://doi.org/10.1088/1755-1315/557/1/012014>
- De la Vega, D., Matthews, J.C.G., Norin, L., Angulo, I., 2013. Mitigation Techniques to Reduce the Impact of Wind Turbines on Radar Services. *Energies*, 6(6), 2859–2873. <https://doi.org/10.3390/en6062859>
- Dean, R.G., Dalrymple, R.A., 1991. *Water Wave Mechanics for Engineers and Scientists*. World Scientific.
- Delpeche-Ellmann, N.C., Soomere, T., 2013. Investigating the Marine Protected Areas most at risk of current-driven pollution in the Gulf of Finland, the Baltic Sea, using a Lagrangian transport model. *Mar. Pollut. Bull.* 67, 121–129. <https://doi.org/10.1016/j.marpolbul.2012.11.025>
- Didenkulova, I., Rodin, A., 2013. A typical wave wake from high-speed vessels: Its group structure and run-up. *Nonlin. Process. Geophys.* 20(1), 179–188. <https://doi.org/10.5194/npg-20-179-2013>
- Dörfler, M., Matusiak, E., 2013. Tracing sound objects in audio textures, in: *10th Int. Conf. Sampl. Theory Appl. (SampTA 2013)*, pp. 408–411.
- Dugad, S., Puliyadi, V., Palod, H., Johnson, N., Rajput, S., Johnny, S., 2017. Ship intrusion detection security system using image processing & SVM, in: *2017 Int. Conf. Nascent Technol. Eng. ICNTE 2017*. <https://doi.org/10.1109/ICNTE.2017.7947948>

- Egerer, M., Ristolainen, A., Piho, L., Vihman, L., Kruusmaa, M., 2024. Hall effect sensor-based low-cost flow monitoring device: Design and validation. *IEEE Sens. J.* 24(5), 5986–5997. <https://doi.org/10.1109/JSEN.2024.3354194>
- Engen, G., Johnsen, H., 1995. SAR-ocean wave inversion using image cross spectra. *IEEE Trans. Geosci. Remote Sens.* 33, 1047–1056. <https://doi.org/10.1109/36.406690>
- Fang, M.C., Yang, R.Y., Shugan, I. V., 2011. Kelvin ship wake in the wind waves field and on the finite sea depth. *J. Mech.* 27, 71–77. <https://doi.org/10.1017/jmech.2011.9>
- Feichtinger, H.G., Nowak, K., 2003. A first survey of Gabor multipliers, in: Feichtinger, H.G., Strohmer, T. (Eds.), *Advances in Gabor Analysis*. Birkhäuser Boston, Boston, MA, pp. 99–128. [https://doi.org/10.1007/978-1-4612-0133-5\\_5](https://doi.org/10.1007/978-1-4612-0133-5_5)
- Fujino, I., Claramunt, C., Boudraa, A.-O., 2019. Extracting courses of vessels from AIS data and real-time warning against off-Course, in: *ICBDR '18: Proc. 2nd Int. Conf. Big Data Research*, pp. 62–69. <https://doi.org/10.1145/3291801.3291823>
- Gierull, C.H., 2019. Demystifying the capability of sublook correlation techniques for vessel detection in SAR Imagery. *IEEE Trans. Geosci. Remote Sens.* 57, 2031–2042. <https://doi.org/10.1109/TGRS.2018.2870716>
- Gong, X., Jiang, H., Yang, D., 2023. Maritime piracy risk assessment and policy implications: A two-step approach. *Mar. Policy* 150, 105547. <https://doi.org/10.1016/j.marpol.2023.105547>
- Huang, W., Wang, D., Garcia, H., Godø, O.R., Ratilal, P., 2017. Continental shelf-scale passive acoustic detection and characterization of diesel-electric ships using a coherent hydrophone array. *Remote Sens.* 9(8), 772. <https://doi.org/10.3390/rs9080772>
- Ilčev, D.S., 2021. New aspects of progress in the modernization of the maritime radio direction finders (RDF). *Trans. Marit. Sci.* 10(1), 68–83. <https://doi.org/10.7225/toms.v10.n01.005>
- Kang, K., Kim, D., 2019. Ship velocity estimation from ship wakes detected using convolutional neural networks. *IEEE J. Sel. Top. Appl. Earth Obs. Remote Sens.* 12, 4379–4388. <https://doi.org/10.1109/JSTARS.2019.2949006>
- Karimpour, A., Chen, Q., 2017. Wind wave analysis in depth limited water using OCEANLYZ, A MATLAB toolbox. *Comput. Geosci.* 106, 181–189. <https://doi.org/10.1016/j.cageo.2017.06.010>
- Kelpšaitė, L., Parnell, K.E., Soomere, T., 2009. Energy pollution: the relative influence of wind-wave and vessel-wake energy in Tallinn Bay, the Baltic Sea. *J. Coast. Res. Special Issue* 56, 812–816.
- Kim, T., Perera, L.P., Sollid, M.-P., Batalden, B.-M., Sydnes, A.K., 2022. Safety challenges related to autonomous ships in mixed navigational environments. *WMU J. Marit. Aff.* 21, 141–159. <https://doi.org/10.1007/s13437-022-00277-z>
- Kuo, J.M., Chen, K.S., 2003. The application of wavelets correlator for ship wake detection in SAR images. *IEEE Trans. Geosci. Remote Sens.* 41, 1506–1511. <https://doi.org/10.1109/TGRS.2003.811998>
- Kurekin, A.A., Loveday, B.R., Clements, O., Quartly, G.D., Miller, P.I., Wiafe, G., Agyekum, K.A., 2019. Operational monitoring of illegal fishing in Ghana through exploitation of satellite earth observation and AIS data. *Remote Sens.* 11(3), 293. <https://doi.org/10.3390/rs11030293>
- Kurennoy, D., Parnell, K.E., Soomere, T., 2011. Fast-ferry generated waves in south-west Tallinn Bay. *J. Coast. Res. Special Issue* 64, 165–169.

- Kuznetsov, N.G., Maz'ya, V.G., Vainberg, B., 2002. *Linear Water Waves: A Mathematical Approach*. Cambridge University Press, Cambridge, UK.
- Landrigan, P.J., Stegeman, J.J., Fleming, L.E., Allemand, D., Anderson, D.M., Backer, L.C., Brucker-Davis, F., Chevalier, N., Corra, L., Czerucka, D., Bottein, M.-Y, D., Demeneix, B., Depledge, M., Deheyn, D.D., Dorman, C.J., Fénichel, P., Fisher, S., Gaill, F., Galgani, F., Gaze, W.H., Giuliano, L., Grandjean, P., Hahn, M.E., Hamdoun, A., Hess, P., Judson, B., Laborde, A., McGlade, J., Mu, J., Mustapha, A., Neira, M., Noble, R.T., Pedrotti, M.L., Reddy, C., Rocklöv, J., Scharler, U.M., Shanmugam, H., Taghian, G., van de Water, J.A.J.M., Vezzulli, L., Weihe, P., Zeka, A., Raps, H., Rampal, P., 2020. Human health and ocean pollution. *Ann. Glob. Heal.* 86(1), 151. <https://doi.org/10.5334/aogh.2831>
- Li, M., Mou, J., Chen, P., Chen, L., van Gelder, P.H.A.J.M., 2023. Real-time collision risk based safety management for vessel traffic in busy ports and waterways. *Ocean Coast. Manag.* 234, 106471. <https://doi.org/https://doi.org/10.1016/j.ocecoaman.2022.106471>
- Liang, H., Li, Y., Chen, X., 2024. An Earth-fixed observer to ship waves. *J. Fluid Mech.* 984, A14. <https://doi.org/10.1017/jfm.2024.167>
- Metters, D., Waldron, J., Ryan, J., 2021. Extraction of ship wake information from wave buoy records., in: *Coasts and Ports 2021*. Christchurch. [https://www.coastsandports.org/papers/2021/067\\_metters\\_finalpaper.pdf](https://www.coastsandports.org/papers/2021/067_metters_finalpaper.pdf)
- Mitev, M., 2018. VT Explorer Historical Data Request [WWW Document]. URL sent to [margus.ratsep@ttu.ee](mailto:margus.ratsep@ttu.ee) (accessed 4.16.18).
- NATO Standardization Agency, 2015. Mtp-01, Volume I: Multinational Maritime Tactical Instructions and Procedures.
- Neumann, B., Vafeidis, A.T., Zimmermann, J., Nicholls, R.J., 2015. Future coastal population growth and exposure to sea-level rise and coastal flooding - A global assessment. *PLoS One* 10, e0118571.
- Newman, J.N., 1977. *Marine Hydrodynamics*. Massachusetts Institute of Technology, Cambridge, Massachusetts.
- Nyanya, M.N., Vu, H.B., Schönborn, A., Ölçer, A.I., 2021. Wind and solar assisted ship propulsion optimisation and its application to a bulk carrier. *Sustain. Energy Technol. Assessments* 47, 101397. <https://doi.org/https://doi.org/10.1016/j.seta.2021.101397>
- Ouchi, K., Maedoi, S., Mitsuyasu, H., 1999. Determination of ocean wave propagation direction by split-look processing using JERS-1 SAR data. *IEEE Trans. Geosci. Remote Sens.* 37, 849–855. <https://doi.org/10.1109/36.752202>
- Panico, A., Graziano, M.D., Renga, A., 2017. SAR-based vessel velocity estimation from partially imaged Kelvin pattern. *IEEE Geosci. Remote Sens. Lett.* 14, 2067–2071. <https://doi.org/10.1109/LGRS.2017.2751083>
- Park, J.-J., Oh, S., Park, K.-A., Foucher, P.-Y., Jang, J.-C., Lee, M., Kim, T.-S., Kang, W.-S., 2018. The ship detection using airborne and in-situ measurements based on hyperspectral remote sensing. *J. Korean Earth Sci. Soc.* 38, 535–545. <https://doi.org/10.5467/jkess.2017.38.7.535>
- Parnell, K.E., Delpêche-Ellmann, N.C., Didenkulova, I., Dolphin, T., Erm, A., Kask, A., Kelpšaitė, L., Kurennoy, D., Quak, E., Räämet, A., Soomere, T., Terentjeva, A., Torsvik, T., Zaitseva-Pärnaste, I., 2008. Far-field vessel wakes in Tallinn Bay. *Est. J. Eng.* 14(4), 273–302. <https://doi.org/10.3176/eng.2008.4.01>



- Pethiyagoda, R., McCue, S.W., Moroney, T.J., 2017. Spectrograms of ship wakes: Identifying linear and nonlinear wave signals. *J. Fluid Mech.* 811, 189–209. <https://doi.org/10.1017/jfm.2016.753>
- Pethiyagoda, R., McCue, S.W., Moroney, T.J., 2014. What is the apparent angle of a Kelvin ship wave pattern? *J. Fluid Mech.* 758, 468–485. <https://doi.org/10.1017/jfm.2014.530>
- Pethiyagoda, R., Moroney, T.J., Macfarlane, G.J., McCue, S.W., 2021. Spectrogram analysis of surface elevation signals due to accelerating ships. *Phys. Rev. Fluids* 6, 104803. <https://doi.org/10.1103/PhysRevFluids.6.104803>
- Průša, Z., Søndergaard, P.L., Holighaus, N., Wiesmeyr, C., Balazs, P., 2014. The large time-frequency analysis toolbox 2.0, in: *Sound, Music, and Motion*, LNCS. Springer International Publishing, pp. 419–442. [https://doi.org/10.1007/978-3-319-12976-1\\_25](https://doi.org/10.1007/978-3-319-12976-1_25)
- Rabaud, M., Moisy, F., 2013. Ship wakes: Kelvin or mach angle? *Phys. Rev. Lett.* 110, 214503. <https://doi.org/10.1103/PhysRevLett.110.214503>
- Ramirez, B., Bunker, R.J., 2015. *Narco-Submarines. Specially Fabricated Vessels Used for Drug Smuggling Purposes*. Leavenworth, KS: Foreign Military Studies Office.
- Reggiannini, M., Righi, M., Tampucci, M., Lo Duca, A., Bacciu, C., Bedini, L., D'Errico, A., Di Paola, C., Marchetti, A., Martinelli, M., Mercurio, C., Salerno, E., Zizi, B., 2019. Remote sensing for maritime prompt monitoring. *J. Mar. Sci. Eng.* 7(7), 202. <https://doi.org/10.3390/jmse7070202>
- Reggiannini, M., Salerno, E., Bacciu, C., D'Errico, A., Lo Duca, A., Marchetti, A., Martinelli, M., Mercurio, C., Mistretta, A., Righi, M., Tampucci, M., Di Paola, C., 2024. Remote sensing for maritime traffic understanding. *Remote Sens.* 16(3), 557. <https://doi.org/10.3390/rs16030557>
- Reimann, L., Vafeidis, A.T., Honsel, L.E., 2023. Population development as a driver of coastal risk: Current trends and future pathways. *Cambridge Prism. Coast. Futur.* 1, e14. <https://doi.org/DOI: 10.1017/cft.2023.3>
- Ristolainen, A., Tuhtan, J.A., Kruusmaa, M., 2019. Continuous, near-bed current velocity estimation using pressure and inertial sensing. *IEEE Sens. J.* 19, 12398–12406. <https://doi.org/10.1109/JSEN.2019.2937954>
- Rødseth, Ø.J., Burmeister, H.-C., 2015. Risk assessment for an unmanned merchant ship. *TransNav Int. J. Mar. Navig. Saf. Sea Transp.* 9(3), 357–364. <https://doi.org/10.12716/1001.09.03.08>
- Scarpa, G.M., Zaggia, L., Manfè, G., Lorenzetti, G., Parnell, K., Soomere, T., Rapaglia, J., Molinaroli, E., 2019. The effects of ship wakes in the Venice Lagoon and implications for the sustainability of shipping in coastal waters. *Sci. Rep.* 9, 19014. <https://doi.org/10.1038/s41598-019-55238-z>
- Sheremet, A., Gravois, U., Tian, M., 2012. Boat-Wake Statistics at Jensen Beach, Florida. *J. Waterw. Port, Coastal, Ocean Eng.* 139, 286–294. [https://doi.org/10.1061/\(asce\)ww.1943-5460.0000182](https://doi.org/10.1061/(asce)ww.1943-5460.0000182)
- Siebert, G., Hoth, J., Banyś, P., Heymann, F., 2019. Generic framework for vessel detection and tracking based on distributed marine radar image data. *CEAS Sp. J.* 11, 65–79. <https://doi.org/10.1007/s12567-018-0208-6>
- Simard, M.-A., Lefebvre, E., Helleur, C., 2000. Multisource information fusion applied to ship identification for the recognized maritime picture. *Sens. Fusion Archit. Algorithms, Appl.* IV 4051, 67–78. <https://doi.org/10.1117/12.381666>

- Søndergaard, P.L., Torr sani, B., Balazs, P., 2012. The Linear Time Frequency Analysis Toolbox. *Int. J. Wavelets, Multiresolution Anal. Inf. Process.* 10. <https://doi.org/10.1142/S0219691312500324>
- Soomere, T., 2007. Nonlinear components of ship wake waves. *Appl. Mech. Rev.* 60(3), 120–138. <https://doi.org/10.1115/1.2730847>
- Soomere, T., 2005. Fast ferry traffic as a qualitatively new forcing factor of environmental processes in non-tidal sea areas: A case study in Tallinn Bay, Baltic Sea, *Environmental Fluid Mechanics* 5(4), 293–323. <https://doi.org/10.1007/s10652-005-5226-1>
- Soomere, T., Parnell, K.E., Didenkulova, I., 2011. Water transport in wake waves from high-speed vessels. *J. Mar. Syst.* 88, 74–81. <https://doi.org/10.1016/j.jmarsys.2011.02.011>
- Soomere, T., Rannat, K., 2003. An experimental study of wind waves and ship wakes in Tallinn Bay. *Proc. Estonian Acad. Sci. Eng.* 9(3), 157–184. <https://doi.org/10.3176/eng.2003.3.02>
- Sorensen, R.M., 1973. Ship-generated waves. *Adv. Hydrosci.* 9, 49–83.
- Thieme, C.A., Utne, I.B., Haugen, S., 2018. Assessing ship risk model applicability to Marine Autonomous Surface Ships. *Ocean Eng.* 165, 140–154. <https://doi.org/10.1016/j.oceaneng.2018.07.040>
- Till, G., 2013. *Seapower: a Guide for the Twenty-First Century*. Hoboken, Taylor and Francis, London, United Kingdom.
- Torsvik, T., Herrmann, H., Didenkulova, I., Rodin, A., 2015a. Analysis of ship wake transformation in the coastal zone using time–frequency methods. *Proc. Est. Acad. Sci.* 64(3S), 379–388. <https://doi.org/10.3176/proc.2015.3s.08>
- Torsvik, T., Soomere, T., Didenkulova, I., Sheremet, A., 2015b. Identification of ship wake structures by a time-frequency method. *J. Fluid Mech.* 765, 229–251. <https://doi.org/10.1017/jfm.2014.734>
- Tsai, Y.-M., Lin, C.-Y., 2021. Investigation on Improving Strategies for Navigation Safety in the Offshore Wind Farm in Taiwan Strait. *J. Mar. Sci. Eng.* <https://doi.org/10.3390/jmse9121448>
- van Westrenen, F., Baldauf, M., 2020. Improving conflicts detection in maritime traffic: Case studies on the effect of traffic complexity on ship collisions. *Proc. Inst. Mech. Eng. Part M J. Eng. Marit. Environ.* 234, 209–222. <https://doi.org/10.1177/1475090219845975>
- VesselFinder [WWW Document], 2020. URL <https://www.vesselfinder.com/> (accessed 9.14.20).
- Wehausen, J. V., 1973. The wave resistance of ships. *Adv. Appl. Mech.* 13, 93–245.
- Wu, Z., 1991. On the Estimation of a Moving Ship’s Velocity and Hull Geometry Information from its Wave Spectra. Technical Report No. 91. Department of Atmospheric, Oceanic and Space Sciences
- Wu, Z., Meadows, G.A., 1991. A remote sensing technique for the estimation of a moving ship’s velocity and length from its wave spectra. *Ocean 91 Conf.* (Honolulu HI 1991-10-01).
- Wyatt, D.C., Hall, R.E., 1988. Analysis of ship-generated surface waves using a method based upon the local Fourier transform. *J. Geophys. Res.-Oceans*, 93(C11), 14133–14164. <https://doi.org/10.1029/JC093iC11p14133>

- Zanatta, M., Bozem, H., Köllner, F., Schneider, J., Kunkel, D., Hoor, P., de Faria, J., Petzold, A., Bundke, U., Hayden, K., Staebler, R.M., Schulz, H., Herber, A.B., 2020. Airborne survey of trace gases and aerosols over the Southern Baltic Sea: from clean marine boundary layer to shipping corridor effect. *Tellus, Ser. B Chem. Phys. Meteorol.* 72, 1–24. <https://doi.org/10.1080/16000889.2019.1695349>
- Zhang, X., Zhang, Q., Yang, J., Cong, Z., Luo, J., Chen, H., 2019. Safety risk analysis of unmanned ships in inland rivers based on a Fuzzy Bayesian Network. *J. Adv. Transp.* 2019, 4057195. <https://doi.org/10.1155/2019/4057195>
- Zhu, C., Garcia, H., Kaplan, A., Schinault, M., Handegard, N.O., Godø, O.R., Huang, W., Ratilal, P., 2018. Detection, localization and classification of multiple mechanized ocean vessels over continental-shelf scale regions with Passive Ocean Acoustic Waveguide Remote Sensing. *Remote Sens.* 10, 1–26. <https://doi.org/10.3390/rs10111699>
- Zilman, G., Zapolski, A., Marom, M., 2004. The speed and beam of a ship from its wake's SAR images. *IEEE Trans. Geosci. Remote Sens.* 42, 2335–2343.

## **Acknowledgements**

This research has been supported by the Estonian Ministry of Education and Research and Estonian Research Council via institutional support IUT33-3 and grants PUT1990 and PRG1129, the European Regional Development Fund program Mobilitas+, project MOBTT72, reg. nr 2014-2020.4.01.16-0024, the Flag-ERA project FuturiCT2.0, Estonian Center of Excellence EXCITE, the Estonian Research Infrastructures Roadmap object Infotechnological Mobility Observatory (IMO), and EEA Financial Mechanisms 2014–2021 Baltic Research Programme project “Solutions to current and future problems on natural and constructed shorelines, eastern Baltic Sea” (SolidShore, EMP480). Part of the underlying experiments has been done in the frame of the European Union’s Horizon 2020 research and innovation program project LAKsMI under Grant Agreement 635568.

## **Abstract**

### **Surface vessel localization from wake measurements in the littoral zone**

There are numerous different vessel detection systems available, but they can be deceived or have limitations in certain situations. This thesis examines the possibility of using spectral representations of ship wakes to fill the knowledge gaps in this area. The main purpose was to test the feasibility of the idea that the spectral representation of vessel wakes that are recognized from far-field water surface elevation, water velocity or pressure data at one or at a few points, could be used to fill the knowledge gaps.

The work focused on two steps: ship detection, to determine whether there are indications that a ship was present in the region in the input data, and ship localization, to determine the location of the vessel and its speed and course. The focus was on simple implementation and the possibility of automation. Two datasets were used: one measured in 2009 and the second measured in 2017. Both sets were collected at the same location, near Pikakari Beach, gathering information on ships approaching the port in Tallinn Bay, on the southern side of the Gulf of Finland in the Baltic Sea.

From the results it was concluded that pressure sensors located on the seabed were able to filter out shorter wind waves. The attenuation of the ship wake data was reduced by overlapping spectrograms from several sensors. Wake detection was achieved by using specific algorithms for signal analysis and by monitoring the corresponding water movements. Both developed algorithms are capable of working without supervision after being set up. Vessel speed calculated from the spectrogram by using different parts of wake was in accord with actual speeds measured using an automatic identification system (AIS). The use of transverse components of the wake provided the most accurate results with the lowest level of uncertainty. The distance travelled by the wake and the vessel speed were derived from the divergent component of the wake signature. The direction of the incoming wake was calculated using an array of closely positioned sensors. These parameters gave a vessel location comparable to actual position at the time the wake was generated as measured by AIS. Combining some additional information made it possible to establish the ship's course from the propagation direction of the incoming wake.

From the results it was seen that this method provided a single snapshot of the vessel movement during the period when the ship passed the sensor. This information was received with significant time delay. Also, the signal analysis had some restrictions. Accurate determinations required that no more than one vessel wake was present in the record simultaneously; the vessel had to sail on steady course and at a steady speed in the subcritical range and at a speed greater than 15 knots. Ship identification (characteristics such as type, hull shape etc.) and the maximum distance between the ship and the measurement site were not considered in this work. It was concluded that this method provided limited information about the presence of the ships and their sailing parameters, but at this stage it is not a standalone system for vessel traffic monitoring and must be complemented by other methods.

## Lühikokkuvõte

### Laevade asukohta ja liikumise parameetrite määramine laevalainete salvestustest

Analüüsitakse võimalusi kasutada laeva käigulainete salvestuste spektraalset esitust laevaliikluse jälgimiseks. Peamiseks eesmärgiks oli katsetada, kas ühes punktis tehtud veepinna asendi muutumise salvestusest või vähestes lähestikku asuvates punktides madal mere põhja lähedale paigutatud rõhuandurite signaalidest tuletatud informatsiooni saab kasutada täiendava vahendina möödivate aluste tuvastamiseks ja nende liikumise parameetrite hindamiseks.

Käigulainete analüüs toimus kahe sammuna. Esimese sammuna (avastamine) tehti kindlaks, kas laev paiknes vaadeldavas alas. Teise sammuna (lokaliseerimine) määratleti laeva asukoht ja liikumisandmed. Vastava tehnoloogia loomisel seati eesmärgiks lihtsus ja võimalus seda kasutada automaatrežiimis. Kasutati kaht salvestatud andmestikku. Üks neist oli mõõdetud 2009. ja teine 2017. aastal. Mõlemad salvestati Pikakari ranna lähisel Paljassaare poolsaare rannavetes. Mõõtekoht on avatud Tallinna sadama poolde suunduvate laevade lainetele.

On näidatud, et ranniku lähedal madalas vees merepõhjas paiknevate rõhuandurite signaalis on tuulelainetest tingitud müra suhteliselt nõrk. Ka laeva käigulainete signaal on osaliselt sumbunud võrreldes veepinna asendi muutumisega. Kuna käigulained on pikaharjalised, on neid võimalik eristada lähestikku paiknevates andurites registreeritud signaalide spektraalkujutiste kombineerimise teel. On näidatud, et käigulaineid on võimalik tuvastada automaatselt, kasutades nii signaalitöötuse algoritme kui ka hinnates lainete tekitatud vee liikumise kiirust. Kumbki meetod ei vaja spetsiaalset seadistamist enne andmete kogumist.

Laeva kiirust hinnati kahel erineva meetodiga, kasutades käigulaine struktuuri eri osasid. Saadud hinnangud langesid hästi kokku laevade automaatpositsioneerimise infost (AIS) leitud väärtustega. Käigulainete ristkomponendi asümptoodi omaduste alusel arvutatud hinnangud olid täpsemad. Koha kaugus, kus lained olid tekitatud, leiti laeva kiiruse hinnangu ja käigulainete kaldkomponendi sageduse muutumise tempo kaudu. Käigulaine harjade orientatsioon ja sellele vastav lainete leviku suund arutati lähestikku paiknevate sensorite salvestatud signaali ajanihke alusel. Selle suuna ja kauguse põhjal määratleti laeva asukoht käigulaine tekkimise hetkel. Nõnda leitud asukohad kattusid hästi AIS andmetega laeva tegeliku asukoha kohta. Laeva kurss ei ole kõnesolevatest andmetest üheselt leitav. Näidati, et kursi saab enamikel juhtudel leida käigulaine levimise suuna ja kohalike navigatsioonioluside võrdlemise alusel.

Töö keskse tulemusena näidati, et kirjeldatud tehnoloogia võimaldab leida laeva positsiooni ja liikumisandmed (kiirus ja kurss) hetkel, mil laev tekitab salvestatud käigulaine esimese osa, teisisõnu, vaid ühel ajamomendil. Meetodi kasutamist piirab asjaolu, et käigulaine jõuab mõõtepunkti arvestatava viiteajaga; enamasti mõnikümmend minutit. Signaalitöötlust saab automatiseerida vaid siis, kui analüüsiks kasutatavas ajaaknas on vaid ühe laeva signaal. Meetod annab adekvaatse tulemuse, kui laev liigub fikseeritud kursil kindla kiirusega vähemalt 15 sõlme. Laeva identifitseerimist (kere kuju, otstarve jne) ja maksimaalset kaugust mõõtepunktist käesolevas töös ei vaadatud.

Tulemustest selgub, et käigulainete analüüs võimaldab saada ajas ja ruumis võrdlemisi piiratud informatsiooni laeva asukoha ja liikumise kohta. Seetõttu sobib kirjeldatud meetod täienduseks teistele laevaliikluse jälgimise süsteemidele.



## Appendix: Publications constituting the thesis



### Publication I

Rätsep, M., Parnell, K.E., Soomere, T., 2020. Detecting ship wakes for the study of coastal processes. *Journal of Coastal Research*, Special Issue No. 95, 1258–1262. <https://doi.org/10.2112/SI95-243.1>





## Detecting Ship Wakes for the Study of Coastal Processes

Margus Rätsep\*, Kevin E. Parnell, and Tarmo Soomere

Department of Cybernetics  
School of Science  
Tallinn University of Technology  
Tallinn, Estonia



www.cerf-jcr.org



www.JCRonline.org

### ABSTRACT

Rätsep, M.; Parnell, K.E., and Soomere, T., 2020. Detecting ship wakes for the study of coastal processes. In: Malvárez, G. and Navas, F. (eds.), *Global Coastal Issues of 2020. Journal of Coastal Research*, Special Issue No. 95, pp. 1258–1262. Coconut Creek (Florida), ISSN 0749-0208.

Wakes from contemporary vessels may affect, and in some places dominate, coastal processes in the vicinity of major shipping lanes. The analysis of the properties and impact of wakes has generally been restricted to wakes that can be visually observed in raw data. In this work, spectral analysis of the time series of single-point measurements of water surface elevation from Tallinn Bay is used to highlight the structure of ship wakes using a Short Time Fourier Transform. This method makes it possible to determine the speed and distance of a vessel from the measurement site. Wakes are detected using an algorithm based on Gabor multipliers. The results are compared with vessel passages retrieved from the Automatic Identification System (AIS) data. The algorithm detects the majority of ship wakes that can be visually recognized in spectrograms and misses only those with low signal to noise ratio or those in close proximity to another vessel wake. The calculated speed and distance are consistent with the AIS data except for high-speed vessels sailing at  $\geq 30$  knots. The results indicate that by using these techniques the detection of vessel wakes from a single-point wave record is achievable under favorable weather conditions. The methods provide an option for mitigation of the impact of ship wakes in semi-enclosed water bodies.

**ADDITIONAL INDEX WORDS:** AIS data, windowed Fourier transform, Gabor multipliers.

### INTRODUCTION

Wakes of vessels may have a significant negative impact on shorelines and waterways (Parnell, McDonald, and Burke, 2007). Their strong influence in places has resulted in regulation that uses the limitation of vessel speed or wave height to mitigate damage (Croad and Parnell, 2002). With an increase in the size and speed of ships and the intensity of ship traffic, the need to effectively protect the coastal environment motivates further research on vessel wake detection and analysis aimed at linking ship and wave properties with coastal processes, impacts and management.

Vessel wakes consist of several different components (Fang, Yang, and Shugan, 2011; Soomere, 2007). Its wavelike features form a characteristic wave pattern about three-vessel lengths behind the ship, called a Kelvin wake (Figure 1) (e.g., Newman, 1977). This is usually composed of transverse and divergent waves. The crests of transverse waves are almost perpendicular to the vessel's track and they propagate in the same direction as the sailing line. The crests of divergent waves make a larger angle to the vessel's path and move outward from the sailing line (Newman, 1977). A combination of transverse and divergent waves forms a set of cusp waves along the borders of the ship wake (the so-called cusp lines). In deep water, the Kelvin wake fills a triangular area (Kelvin wedge) with half angle of  $19.5^\circ$  from the sailing line (Newman, 1977). The wave pattern in shallow waters depends on

the vessel, water depth and the sailing speed. Its basic properties can be described in terms of a depth Froude number  $F_h$ :

$$F_h = \frac{U}{\sqrt{gh}}, \quad (1)$$

where  $U$  is the speed of the vessel through the water,  $g$  is gravity acceleration and  $h$  is the water depth (Newman, 1977). If  $F_h = 1$ , then the speed is called the critical speed. When the speed increases, the Kelvin wedge widens. If  $F_h \rightarrow 1$ , its half-angle increases up to  $90^\circ$  and the ship wake, ideally, covers the entire half plane aft from the ship (Sorensen, 1973). In the supercritical speed range ( $F_h > 1$ ) the angle starts to decrease and the wave pattern is composed of only divergent waves (Pethiyagoda, McCue, and Moroney, 2015; Soomere, 2007).



Figure 1. Examples of a Kelvin wake.

DOI: 10.2112/SI95-243.1 received 31 March 2019; accepted in revision 13 February 2020.

\*Corresponding author: margus.ratsep@ttu.ee

©Coastal Education and Research Foundation, Inc. 2020

Ship wakes created at moderate and high Froude numbers contain a large number of linear and nonlinear components with a multitude of constituents with different heights, periods, propagation directions, and timings. In recent years, spectral analysis of wake wave data has revealed further information about the internal structure of vessel wake, and its characteristics (Pethiyagoda, McCue, and Moroney, 2017; Sheremet, Gravois, and Tian, 2012; Torsvik *et al.*, 2015;). An application of a Short Time Fourier Transform (STFT) to water surface elevation data reveals that a vessel wake contains a distinct sliding frequency signal (chirp) (Figure 2b) in the corresponding spectrogram (Sheremet, Gravois, and Tian, 2012). This internal structure makes it possible to reliably extract the wake from the background and to separate it into components with a different period, height and timing (Pethiyagoda, McCue, and Moroney, 2017; Torsvik *et al.*, 2015). It was demonstrated that each type of vessel has a specific signature. Moreover, this kind of separation of components not only enables the estimation of the energy levels of different parts of the wake but also makes it possible to retrieve several sailing parameters of the vessel.

This type of spectral analysis also opens new ways for (semi) automatic ship wake detection using either a single-point water level time series or a pressure time series. This challenge, however, requires further refinement of the method, particularly a thorough analysis of the applicability of the approach using a larger number of vessels.

The aim of this research is to extend the work undertaken by Sheremet, Gravois, and Tian (2012) and Torsvik *et al.* (2015) towards the use of the spectral methods of wake analysis for vessel detection and management. This paper focuses on the possibilities

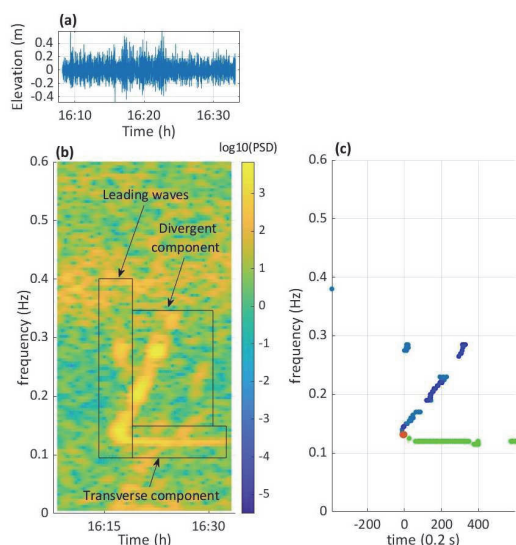


Figure 2. (a) Wave elevation recordings of the wake of the MV Superstar entering Tallinn port on 27 June 2009. (b) Example of the outcome of an STFT applied to the wake data. The boxes indicate different parts of the ship wake. (c) The peaks of the same wake extracted from the background noise (cusp wave: red, transverse waves: green, divergent waves: blue).

of remote, passive detection of ship wakes and specification of several sailing parameters from water surface elevation data. The outcome of this approach is compared with similar data retrieved from the output of the vessel's self-reporting systems (AIS).

### METHODS

The analysis is based on the data from Tallinn Bay, an almost tideless area in the north-eastern Baltic Sea, approximately 10 km by 20 km in size. The bay opens to the Gulf of Finland to the north and northeast. The city of Tallinn is located at the southern end of the bay (Torsvik *et al.*, 2015) (Figure 3). Measurements used in this study were performed in June 2009 at Pikakari Beach on Paljassaare Peninsula, (red dot in Figure 3) (Kurennoy, Parnell, and Soomere, 2011).

The position of water surface elevation was measured using a "LOG\_alevel" echosounder mounted on a tripod in 2.6–2.7 m deep water. For a more detailed description of the field measurements, see Torsvik *et al.* (2015). Data were collected continuously at a frequency of 5 Hz. The data stream was subsequently divided into 24-h blocks starting at 04:00. Each block represents one calendar day of Tallinn to Helsinki ferry traffic. In total, six days of data from Pikakari in 2009 were available for the analysis.

A reference dataset containing AIS information was retrieved from vtexplorer.com (Mitev, 2018). This dataset listed vessels with a gross tonnage of 100 and more. The area of interest (green box in Figure 3) covered the approaches to the Port of Tallinn. The total number of passages of ships of this size was 158. The number of ships per day was 25 to 30. From these data, the estimated time when the ship was passing the measurement site was calculated and single vessels were matched with wakes.

Ship wakes were detected from the surface elevation signal using an algorithm developed by Dörfler and Matusiak (2013) and based on Gabor multipliers. This algorithm is preferred over other possibilities (*e.g.*, convolutional neural networks) as it depends on the STFT and thus its outcome is consistent with the results obtained by Torsvik *et al.* (2015). Also in this case, it was able to be implemented without using additional learning phase before applying the algorithm to the data set.

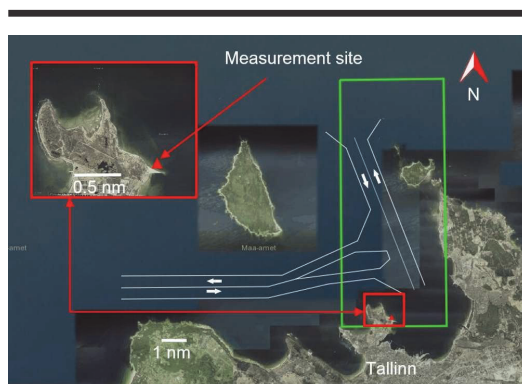


Figure 3. The traffic separation scheme of Tallinn Bay (white lines) and the directions of sailing (white arrows). The area from which reference AIS data was obtained is marked with a green box (SW corner 59.47°N 24.65°E; NE corner 59.65°N, 24.80°E) and the measurement site with a red triangle (here 1 nm = 1852 m). The background is from Estonian Maritime Administration (2017).

Gabor multipliers are composite operators (sequences of operations) that consist of a short-time Fourier transform similar to STFT, a subsequent multiplication by a distribution on phase space (called the Gabor symbol) and, finally, an inverse short-time Fourier transform. By combining analysis (short-time Fourier transform) and synthesis windows (of the inverse transform) with a sequence of complex coefficients over a time-frequency lattice, they help to map a signal to its analyzed-synthesized (reconstructed) form (Feichtinger and Nowak, 2003). In order to prevent data loss, the sequence of coefficients is chosen so it minimizes the difference between the original and reconstructed signals, however, differences that remain can reveal objects in the signal (Dörfler and Matusiak, 2013).

For the analysis, STFT with a Gaussian window function of 4096 data points, an overlap of 1024 data points and in 120 channels was used. For synthesis, an inverse STFT was used. Calculations were undertaken with a toolbox developed by Søndergaard, Torrèsani, and Balazs (2012). The results were filtered to allow one wake in a 6-minute interval in order to reduce multiple detections of the same wake. Each wake lasted on average 10–15 minutes.

The STFT was implemented on the detected events. The ship wakes were extracted from the background noise and separated into different elements using the classification proposed in, and experimental procedure introduced in Torsvik *et al.* (2015). For filtering, the initial signal was first de-measured. Low-frequency water-level fluctuations were removed by means of subtraction of the 2-minute running average from the time series. This procedure may eliminate precursor solitons from the analysis; however, they are not always present in ship wakes in Tallinn Bay and their amplitude is usually very small in such environments (Soomere, 2007). For the analysis, a 900 data point Hamming window was used. The overlap of subsequent windows was 178 s with a 0.5 s step. The range of resolved frequencies was from 0.005 to 0.6 Hz.

Wakes were extracted from the background by identification of peaks in the signal (Figure 2c). From the group of recognized peaks, the components of the wake were reconstructed and used in the detection of wakes (Figure 2b). Cusp waves are often the highest and arrive first. The transverse component is represented by the nearly horizontal sequence of peaks from the cusp wave peak. The divergent component has a variable frequency and is represented by the inclined set of peaks in Figure 2b.

The calculation of speed relied on the frequency  $f$  of cusp waves. Three methods were used. Methods 1 and 2 used the following relationship between the frequency of cusp waves and sailing speed  $U$  in deep water (Torsvik *et al.*, 2015):

$$U = \sqrt{\frac{3}{2}} \frac{g}{2\pi f}. \quad (2)$$

The cusp wave frequency was derived either from the frequency from the highest energy peak in the leading waves (Didenkulova and Rodin, 2013) (Method 1) or using the lowest frequency of the divergent component at the beginning of its signal (Method 2). Method 3 applied a linear fit to the extracted transverse component of the ship wake to find frequency  $f$ . The ship's speed was calculated using the approximated relation (Torsvik *et al.*, 2015)

$$U = \frac{1}{0.9826} \frac{g}{2\pi f}. \quad (3)$$

The closest distance  $Y$  between the vessel and the measurement site was estimated by using the ship's speed  $U$  and the time difference  $\Delta t$  between frequencies of the cusp wave point ( $f$ ) and  $\sqrt{2}$  times the higher value on the divergent (chirp) component (Torsvik *et al.*, 2015). The least-squares fit was used for the chirp (divergent) line data and the shortest distance  $Y$  to the measurement site from the shipping line was calculated as

$$Y = \sqrt{2} U \Delta t. \quad (4)$$

## RESULTS

In total, 190 structures that resembled ship wakes were identified in the spectrograms. The detection algorithm provided 277 instances of possible wakes, of which 164 were confirmed to be ship wakes, 113 were false positive cases (that is, the signal was not a wake) and 26 wakes were missed by the algorithm. A large number of the false positives were due to the short time window (6 min) which was used to filter the results. Due to the high traffic intensity near the port, the subsequent wakes arrived shortly after each other within a shorter time than the typical duration of a wake (10 to 15 minutes). Still the short time window for filtering the results was a trade-off between the detection rate and the number of false positives. Another reason for the missed contacts was a changing signal to background spectrum noise ratio due to the presence of wind waves, which masked some low energy ship wakes.

Wakes detected by the algorithm were matched with corresponding vessels by using the time, speed and the course obtained from the AIS data. The total number of matched cases was 83 (out of 164 wakes seen visually and detected by model). For the reference, AIS information provided 158 events for the given time period and study area (the green box in Figure 3). In most of the matched events ships were sailing at a speed of 15 knots and higher and thus producing a clear wake.

A large part of the difference between observed wakes and actual passing vessels stems from the particular location of the measurement site. The site was sheltered for the wakes from vessels departing from Port of Tallinn by Katariina jetty (in Figure 3 to the south-east of the site). Secondly, the AIS data had a time resolution of 1 h. Consequently, vessels that travelled at higher speeds (30 knots and more) were able to pass the traffic separation scheme without a single AIS contact. Thirdly, AIS covered vessels with IMO numbers only, which limited the number of different ships under observation significantly.

A reasonable estimate of the ship's speed was calculated in 126 cases out of 164 wakes detected by the model. From this set, 58 cases had AIS references. These vessels were divided into three groups according to the AIS information about their sailing speed. Group 1 was vessels with speed of 15–20 knots, group 2 vessels sailing at 23–28 knots, and group 3 faster vessels that sailed at 30–37 knots (Note that 1 knot = 1.852 km/h  $\approx$  0.51 m/s). Methods for finding the speed and distance were evaluated by the number of the cases when the corresponding component (cusp wave point, divergent or transverse branch) was presented and extracted from the spectrogram. Method 1 was applicable to 49 events ( $R^2=0.51$ ), method 2 to 47 ( $R^2=0.29$ ) and method 3 to 44 cases ( $R^2=0.31$ ) out of 58 matched pairs. The comparison with the reference AIS data is shown in Figure 4. Method 1 provided slightly larger estimates of speed for vessels in groups 1 (15 to 20 knots) and 2 (23 to 28 knots) than methods 2 and 3. The outliers

for speed in groups 1 and 2 occurred due to the limitation of the processing of sequences of several wakes from different vessels in close proximity. Vessels in group 3 sail at 30–38 knots, that is, in high-speed subcritical regime with depth Froude numbers  $F_h$  close to 1. The wakes produced at such speeds differ from the classic Kelvin wake. They are often composed of one branch that represents waves with very high energy throughout the structure. As a consequence, the identification of the exact location of the cusp wave frequency is complicated. This resulted in large differences in the estimates of speed using different methods, and when compared to AIS data (Figure 4).

A sensible estimate of the minimum distance from the measurement site to the sailing line (Figure 5) was produced in 52 cases out of 58 previously matched pairs. The procedure was applicable for both departing and approaching vessels. The reference distances were based on the local traffic separation scheme (Figure 3). The departing vessels were approximately 0.2 nm (nautical mile 1 nm = 1852 m) further away than approaching vessels. The relevant average difference was practically the same for all methods (0.25 nm, 0.27 nm and 0.22 nm for methods 1, 2 and 3, respectively). Even though spectrograms of vessels from group 3 (speed >30 knots) did not contain distinct traces of transverse and divergent components, estimates of the distance in question had the same accuracy as for other vessels.

**DISCUSSION**

The aim of this research was to explore the applicability of the spectrogram technique for vessel detection and management systems. The wake detection was done by using an algorithm proposed by Dörfler and Matusiak (2013). This was combined with methods developed by Torsvik *et al.* (2015) for the identification of sailing characteristics. The results were compared with the estimates received from AIS data.

The algorithm for detecting peaks and changes in a signal (Dörfler and Matusiak, 2013) was able to detect a majority of the ship wakes for vessels sailing at  $\geq 15$  knots and passing the measurement site closer than 2 nm. Wakes were missed mostly due to the low the signal-to-noise ratio. The method also failed to separate and detect wakes that arrived at the detection site soon after an earlier wake. The methods provided by Torsvik *et al.* (2015) generally led to estimates for vessel speed and distance which were comparable with the actual values. The method encountered problems for wakes generated by high speed ( $\geq 30$  knots) vessels which did not have clearly distinguishable divergent and transverse components. These ships were sailing at close to the critical speed determined from the depth-based Froude number. These results suggest that the development of a ship wake detection and analysis system based on these methods to assist in ship traffic and environmental management is achievable.

However, there remain several problems that need to be considered. Firstly, when wind waves were significant, the detection was not always reliable. Secondly, if used for enforcement, as is needed for regulation in such cases (Croad and Parnell, 2002), having the measurement device located above the water level may be problematic. Thirdly, the method had difficulty in analyzing wakes of faster ( $\geq 30$  knots) vessels, travelling in the high-speed subcritical regime at depth Froude numbers close to 1. Further developments need to include improvements of the spectrogram technique to cover situations of high Froude number (Pethiyagoda, McCue, and Moroney, 2017), and concealed wake measurement devices (Ristolainen, Tuhtan, and Krusmaa, 2019).

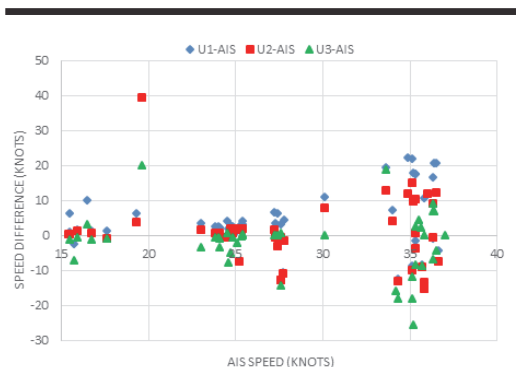


Figure 4. Variation in the estimates of sailing speed using the AIS data (horizontal axis), method 1 (cusp wave point, blue rhombi), method 2 (the leftmost peak of the divergent component, red rectangles) and method 3 (estimated from the transverse component, green triangles).

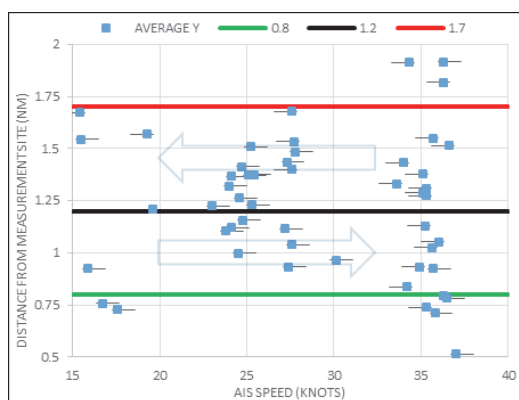


Figure 5. Calculated average of the minimum distance (based on three methods) of vessels from the measurement site. Horizontal lines show the location of the traffic lanes and arrows illustrate the sailing direction. The lane for entering to port is located 0.8 to 1.2 nm from the site and departing lane is 1.2 to 1.7 nm from the site. The horizontal bars at symbols and indicate the vessel's sailing direction (right side for entering the port, left side for departing).

**CONCLUSIONS**

The goal of this paper was to test the methods of determining the sailing properties of vessels from one-point recordings of their wakes, developed by Torsvik *et al.* (2015), for a larger group of vessels sailing at different regimes in the open sea. The aim was to determine whether these methods could be used in multi-purpose vessel wake detection and analysis systems. The measurements were taken with a single point down-looking echosounder. The wakes in the water elevation data were found using the algorithm of Dörfler and Matusiak (2013). A Short Time Fourier Transform was used to extract the wake structure and to identify its components. The vessel speed and her minimum distance from the measurement device were calculated using the methods of Torsvik *et al.* (2015). The results were compared with AIS data.

The majority of wakes were detected by the algorithm. Some events were missed due to the low signal to noise ratio, or wakes were closely following each other. The speed and distance obtained from the wake spectrograms had a reasonable match with AIS data. The largest mismatch occurred for vessels that sailed at  $\geq 30$  knots at depth Froude numbers close to 1, where the wakes did not have the classic Kelvin wake structure. The results suggest that an automatic ship wake detection and analysis system based on spectrograms technique is achievable for the majority of ships sail in the range of up to 4 km from the measurement site under relatively calm conditions.

#### ACKNOWLEDGEMENTS

This research was co-supported by the Estonian Ministry of Education and Research (Estonian Research Council, institutional support IUT33-3), the European Regional Development Fund program Mobilitas+ MOBTT72, No 2014-2020.4.01.16-0024, and the EEA project "Solutions to current and future problems on natural and constructed shorelines, eastern Baltic Sea (EMP480).

#### LITERATURE CITED

- Croad, R. and Parnell, K.E., 2002. *Proposed Controls On Shipping Activity in the Marlborough Sounds. A Review Under s. 32 of the Resource Management Act*. Report to the Marlborough District Council, New Zealand. Opus International Consultants Ltd., Auckland Uniservices Ltd, 53p.
- Didenkulova, I. and Rodin, A., 2013. A typical wave wake from high-speed vessels: Its group structure and run-up. *Nonlinear Processes in Geophysics*, 20(1), 179-188.
- Dörfler, M. and Matusiak, E., 2013. Tracing sound objects in audio textures. *10th International Conference on Sampling Theory and Applications*, (Bremen, Germany), pp. 408-411.
- Estonian Maritime Administration, 2017. *Nutimeri*. Available at: <https://gis.vta.ee/nutimeri/> (Accessed: 24 September 2019).
- Fang, M.C.; Yang, R.Y., and Shugan, I.V., 2011. Kelvin ship wake in the wind waves field and on the finite sea depth. *Journal of Mechanics*, 27(1), 71-77.
- Feichtinger, H.G. and Nowak, K., 2003. A first survey of Gabor multipliers. In Feichtinger, H.G. and Strohmer, T. (eds) *Advances in Gabor Analysis*. Boston, MA: Birkhäuser Boston, pp. 99-128.
- Kurennoy, D.; Parnell, K.E., and Soomere, T., 2011. Fast-ferry Generated Waves in South-West Tallinn Bay. *Journal of Coastal Research*, (S64), 165-169.
- Mitev, M., 2018. *VT Explorer Historical Data Request*. Available at: sent to margus.ratsep@ttu.ee (Accessed: 16 April 2018).
- Newman, J.N., 1977. *Marine Hydrodynamics*. Cambridge, MA, Massachusetts Institute of Technology, 402 p.
- Parnell, K.E.; McDonald, S.C., and Burke, A.E., 2007. Shoreline effects of vessel wakes, Marlborough Sounds, New Zealand. *Journal of Coastal Research*, (S50), 502-506.
- Pethiyagoda, R.; McCue, S.W., and Moroney, T.J., 2015. Wake angle for surface gravity waves on a finite depth fluid. *Physics of Fluids*, 27(6), 061701.
- Pethiyagoda, R.; McCue, S.W., and Moroney, T.J., 2017. Spectrograms of ship wakes: Identifying linear and nonlinear wave signals. *Journal of Fluid Mechanics*, 811, 189-209.
- Ristolainen, A.; Tuhtan, J.A., and Kruusmaa, M., 2019. Continuous, near-bed current velocity estimation using pressure and inertial sensing. *IEEE Sensors Journal*.
- Sheremet, A.; Gravois, U., and Tian, M., 2012. Boat-wake statistics at Jensen Beach, Florida. *Journal of Waterway, Port, Coastal, and Ocean Engineering*, 139(4), 286-294.
- Søndergaard, P.L.; Torrèsani, B., and Balazs, P., 2012. The linear time frequency analysis toolbox. *International Journal of Wavelets, Multiresolution Analysis and Information Processing*, 10(4), 1250032.
- Soomere, T., 2007. Nonlinear components of ship wake waves. *Applied Mechanics Reviews*, 60(3), 120-138.
- Sorensen, R.M., 1973. Ship-generated waves. *Advances in Hydrosciences*, 9, 49-83.
- Torsvik, T.; Soomere, T.; Didenkulova, I., and Sheremet, A., 2015. Identification of ship wake structures by a time-frequency method. *Journal of Fluid Mechanics*, 765, 229-251.

Copyright of Journal of Coastal Research is the property of Allen Press Publishing Services Inc. and its content may not be copied or emailed to multiple sites or posted to a listserv without the copyright holder's express written permission. However, users may print, download, or email articles for individual use.



**Publication II**

Rätsep, M., Parnell, K.E., Soomere, T., Kruusmaa, M., Ristolainen, A., Tuhtan, J.A., 2020. Using spectrograms from underwater total pressure sensors to detect passing vessels in a coastal environment. *Journal of Atmospheric and Oceanic Technology*, 37(8), 1353–1363. <https://doi.org/10.1175/JTECH-D-19-0192.1>





# Using Spectrograms from Underwater Total Pressure Sensors to Detect Passing Vessels in a Coastal Environment

MARGUS RÄTSEP, KEVIN E. PARNELL, AND TARMO SOOMERE

*Department of Cybernetics, School of Science, Tallinn University of Technology, Tallinn, Estonia*

MAARJA KRUSMAA, ASKO RISTOLAINEN, AND JEFFREY A. TUHTAN

*Centre for Biorobotics, Department of Computer Systems, School of Information Technologies, Tallinn University of Technology, Tallinn, Estonia*

(Manuscript received 25 November 2019, in final form 11 May 2020)

## ABSTRACT

Monitoring vessel traffic in coastal regions is a key element of maritime security. For this reason, additional ways of detecting moving vessels are explored by using the unique structure of their wake waves based on pressure measurements at the seabed. The experiments are performed at a distance of about 2 km from the sailing line using novel multisensor devices called “hydromasts” that track both pressure and near-bed water flow current velocities. The main tool for the analysis is a windowed Fourier transform that produces a spectrogram of the wake structure. It is shown that time series from the pressure sensors, measured at a frequency of 100 Hz, 0.2 m above the seabed are a valid source of input data for the spectrogram technique. This technique portrays the properties of both divergent and transverse waves with an accuracy and resolution that is sufficient for the evaluation of the speed and distance of the detected vessels from the measurement device. All the detected passages are matched with vessels using automatic identification system (AIS) data. The use of several time series from synchronized multisensor systems substantially suppresses noise and improves the quality of the outcome compared to one-point measurements. Additional information about variations in the water flow in wakes provides a simple and reasonably accurate tool for rapid detection of ship passages.

## 1. Introduction

The ability to detect and identify passing vessels, their properties, and sailing parameters has a number of important applications. They include maintaining control in territorial waters (Till 2013), recognizing illegal fishing (Kurekin et al. 2019), avoiding navigational accidents (Chen et al. 2018), ensuring the security of various facilities (Dugad et al. 2016; Anupriya and Sasilatha 2018), and allowing a better understanding of the impact of high speed or strongly powered ships on the coastal environment (Soomere et al. 2011).

Several techniques can be used to detect the presence of vessels and distinguish and monitor vessel movements. The most common are radar and radio surveillance (Siegert et al. 2019), satellite sensing including synthetic aperture (SAR) technology (Zilman et al. 2004; Gierull 2019; Renga et al. 2019), both airborne and local

(visual and hyperspectral) optical techniques (Park et al. 2018), various acoustic (sonar) technologies (Huang et al. 2017; Zhu et al. 2018), and classic visual observations from the coast or patrolling vessels.

Some of these techniques (e.g., several acoustic recognition systems) are only able to detect the presence of a ship in a certain region. More advanced technologies provide, similarly to the automatic identification system (AIS; self-reporting system on board of ships for vessel tracking), the location (or a sequence of locations) of vessels. However, the detection of the sailing parameters (speed and the course of the vessel) from such data sources is not always possible (Fujino et al. 2018). Also, none of these methods guarantees the reliability of detection of vessels present in a given region under every possible scenario. To address the gaps in both reliability and accuracy, additional means for the surveillance of sea areas should be studied.

A feasible way forward is to improve the accuracy of detection of disturbances that a ship creates in the

*Corresponding author:* Margus Rätsep, margus.ratsep@ttu.ee

DOI: 10.1175/JTECH-D-19-0192.1

© 2020 American Meteorological Society. For information regarding reuse of this content and general copyright information, consult the AMS Copyright Policy ([www.ametsoc.org/PUBSReuseLicenses](http://www.ametsoc.org/PUBSReuseLicenses)).

surrounding environment (Panico et al. 2017). A moving ship always generates a system of surface waves called a wake. From about three ship lengths behind every displacement vessel, a characteristic wake emerges (Newman 1977). The properties of its main components have been known for decades (Sorensen 1973; Wehausen 1973). It usually consists of the turbulent wake (seen mostly as foam behind the ship) (Zilman et al. 2004; Fang et al. 2011) and the Kelvin wave wake (Fig. 1) (Sorensen 1973; Wehausen 1973).

The Kelvin wake consists of two wave systems. The crests of longer transverse waves form a large angle with respect to the ship's track and almost follow the ship's motion. The crests of shorter divergent waves are roughly parallel to the ship's path. These waves propagate mostly out of the wave generation area (Sorensen 1973; Wehausen 1973). This characteristic triangular spatial pattern of ship wakes (Fig. 1) is implemented, e.g., in the analysis of the data from satellite photography and synthetic aperture radar, for vessel detection (Zilman et al. 2004).

Vessel wakes have also unique structure in the spectral representation of the wave elevation data (Wyatt and Hall 1988; Sheremet et al. 2013; Torsvik et al. 2015; Pethiyagoda et al. 2017, 2018). Moreover, it is possible to extract different wake components from this representation to characterize the movement of the vessel (Torsvik et al. 2015; Pethiyagoda et al. 2017).

Field experiments have used two sources of time series to characterize the ship wake. High-frequency tracking of water surface undulations created by wakes using downward-looking devices were used by Didenkulova et al. (2013) and Torsvik et al. (2015), among others. Pressure time series in the water column or on the seabed were utilized, e.g., in Sheremet et al. (2013) and Benassai et al. (2015). Both methods produced well-defined spectrograms that allowed for detailed analysis of vessel wakes (Sheremet et al. 2013; Torsvik et al. 2015). However, the spectrograms obtained from pressure recordings (Sheremet et al. 2013; Benassai et al. 2015) highlighted only the energy (or height) of ship wakes and the distribution of energy between wake components of different length, but not the properties of the transverse and divergent waves. More generally it was not possible to properly describe the wake components in the time–frequency plane in the manner that can be used for estimating vessel speed and wake traveling distance (Torsvik et al. 2015).

Both approaches have some shortcomings. The intense wind-wave background can shadow shorter components of ship wakes in the spectrogram based on water surface undulations and limit the extraction and analysis of the associated properties of ships (Torsvik et al. 2015). Also, the pressure signal of shorter waves rapidly attenuates in the water column. Therefore, the pressure readings have

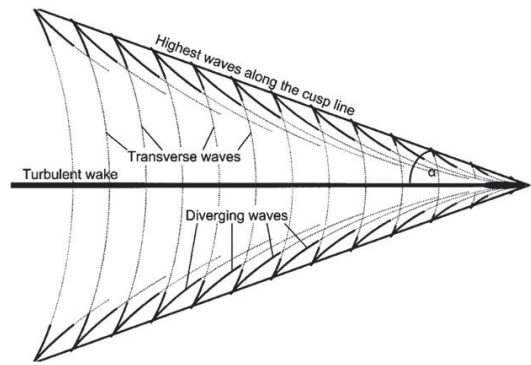


FIG. 1. The standard scheme of the classic Kelvin ship wakes; the ship is moving to the right. The half angle of the wedge is  $\alpha \approx 19.47^\circ$ .

to be corrected to compensate for the attenuation of the higher-frequency part of the wave data. As a result, some of the information about the wake may be lost (Cavaleri 1980; Kuo and Chiu 1994; Karimpour and Chen 2017).

This paper aims to extend the spectrogram-based analysis of the properties of transverse and divergent waves of vessel wakes from surface elevation recordings (Torsvik et al. 2015) to datasets recorded by pressure sensors incorporated into novel multisensor measuring devices. We start from a short discussion of the core properties of wave wakes of vessels and their reproduction in spectrograms. This is followed by a demonstration that the data collected from pressure sensors can be used to analyze the ship's movement at the same level of detail as it is done based on other types of recordings of surface elevations.

To raise the signal-to-noise ratio in wake spectrograms and improve the quality and contrast of the signatures of vessels in spectrograms, we use recordings from a gridded array of five identical pressure sensors. Finally, we discuss the potential applications and possible extensions of the presented technology for estimates of ship location, speed, and course. As ship motion always produces a wave wake, this approach could be (a part of) an automatic vessel detection system. The main message is that the pressure recordings from the seabed, even if associated with a certain loss of information, may provide a convenient prefiltered time series in which the wind-wave signal is attenuated and ship wakes are highlighted.

## 2. Methodology and experimental setup

### a. Kelvin wake

The two components of the Kelvin wake, the divergent and transverse waves, are basically linear waves.

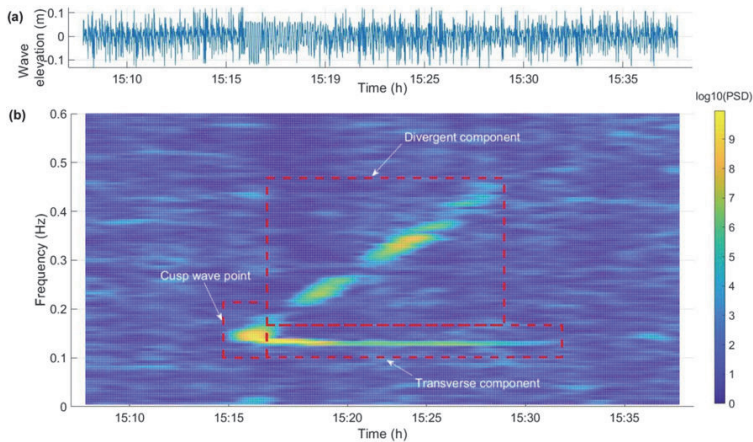


FIG. 2. (a) An example of the pressure time series of the vessel wake that is converted to water elevation data. (b) Short-time Fourier transform of the corresponding series. Wake elements are marked with red dashed rectangles.

Even though ship wakes may contain other (nonlinear) components (Soomere 2007), or have other specific features for high sailing speeds (such as features characteristic to the Mach cone; Rabaud and Moisy 2013), the divergent and transverse waves, are always present if the ship is sailing at speeds below a certain threshold called critical speed. This speed is the maximum propagation speed  $\sqrt{gh}$  of long waves for the given water depth  $h$  and the acceleration due to gravity  $g$  (Sorensen 1973). The waves fill a triangular area called the Kelvin wedge (Fig. 1). The largest wave amplitudes (cusp waves) occur along so-called cusp lines at the border of the Kelvin wedge owing to the interaction of transverse and divergent waves (Kuznetsov et al. 2002).

In deep water, the half angle of the Kelvin wedge is  $\arcsin(1/3) \approx 19.47^\circ$  (Fig. 1), the shape of this wedge does not depend on the sailing speed, and the diverging waves are short crested. The signature of such wakes in the spectrogram representation has a characteristic *L*-like shape (Fig. 2b). The upper, inclined part of this signature corresponds to shorter divergent waves. It has a frequency increasing over time (also known as a chirp signal), which is commonly observed at a fixed location at the seashore after the passage of a steadily sailing ship (Sheremet et al. 2013). The lower, mostly horizontal part of this signature represents longer transverse waves that have a constant frequency for a steadily sailing ship and is also constant for a fixed observer. The cusp waves are represented by the common point of these two parts of the signature.

If the ship sails in waters where the length of excited waves is 2 times or more the water depth, the Kelvin wedge becomes wider, a large portion of the energy of

generated waves is concentrated in a few divergent waves and the transverse waves become weaker (Sorensen 1973; Soomere 2007). The wave system becomes highly nonlinear and contains several other components at so-called near-critical speeds (Soomere 2007) when the sailing speed is  $\pm 15\%$  of the critical speed. At even higher speeds most of the wave energy is concentrated in a few long-crested divergent waves. This kind of wake may contain specific types of solitons (Soomere 2007) or resemble a Mach-type wave system (Rabaud and Moisy 2013). The described transformation makes it possible to identify some properties of sailing ships from the records of their wakes (Wyatt and Hall 1988) and to create characteristic “portraits” of the wake systems for different ships and for specific speeds (Torsvik et al. 2015; Pethiyagoda et al. 2018). In this paper, we focus on the extraction of the classic *L*-like signatures from the viewpoint of efficient (all passages detected) and reliable (no false signals) detection of ship passages.

#### b. Measurement devices

For measuring the wakes we used a device called a “hydromast” (Ristolainen et al. 2016), which is designed to sense near-bed drivers of hydrodynamic processes. Its name is inspired by the neuromast of the lateral line of the fish, which is used for sensing the flow (Bleckmann and Zelick 2009). In addition to pressure data, it incorporates the possibility of obtaining a proxy of flow speed and direction using inertial measurements of the water flow (Ristolainen et al. 2019). In this paper, we only discuss part of the functional capacity of hydromasts, namely, their pressure sensors, the option of having a proxy of flow velocities, and the ability to provide

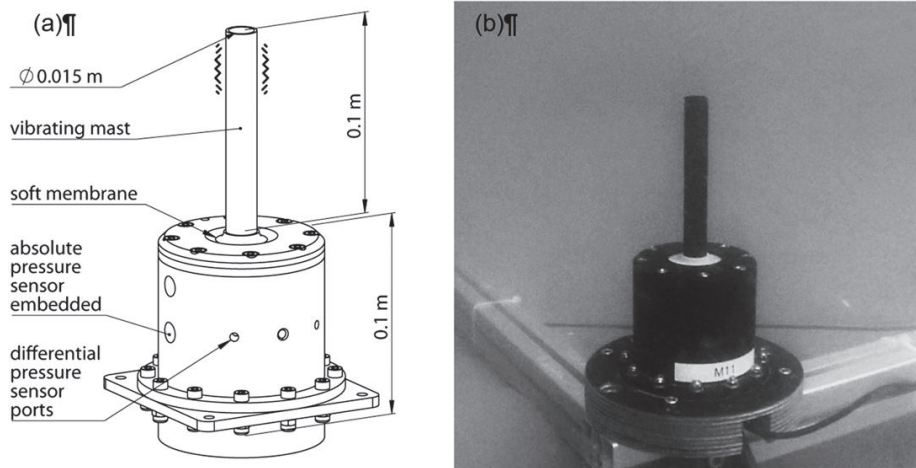


FIG. 3. (a) The components of the hydromast. (b) The working device.

synchronized pressure recordings from an array of devices.

The hydromasts used in this study (Fig. 3) encompass a vibrating stem that is fixed to a pressure-sensitive body (Ristolainen et al. 2019). Vortex induced vibrations are caused by vortex shedding from the stem. The vibrations are measured in the directions of three perpendicular axes by a micromechanical inertial measuring unit (IMU) fixed to the lower end of the stem (Fig. 3a). The device incorporates another identical, stationary, IMU, for reference and for reducing measurement noise generated by the hydromast body self-motion. The stem is made from 100 mm long, 15 mm diameter rigid hollow polyoxymethylene (POM) plastic. The aim was to have the density as close to the surrounding water as possible to reduce the restoring force caused by buoyancy. Pressure is measured using an absolute pressure sensor (MPX5100GP, NXP) for recording the water depth and two differential pressure sensors (MPXV7002, NXP) for measuring dynamic pressure relative to the stagnation point (Ristolainen et al. 2019). The output stream of the device includes inter alia a time stamp in milliseconds, the absolute and two differential pressure sensor outputs in millivolts, temperature, and calibration status.

### c. Field experiment

The results presented below are based on a dataset recorded in the nearshore of Tallinn Bay. It is a semi-closed area at the southern coast of the Gulf of Finland in the northeastern Baltic Sea, with dimensions of approximately 10 km  $\times$  20 km. This area is known for extensive traffic of strongly powered ships that sail at or close to near-critical speeds (Soomere 2005). Most of the

vessel traffic in the bay follows the traffic separation scheme for entering/departing the Port of Tallinn (Fig. 4). The typical shortest distance from the ships to the device location is about 1.5–2.5 km. Measurements were conducted from 10 to 21 July 2017 near Pikakari Beach (Fig. 4), a small accumulation feature with a sandy and gently sloping near-shore on the western shore of Tallinn Bay. No recordings exist for 15 July due to the maintenance of the devices.

Nine hydromasts were assembled into a regularly spaced rectangular array using a 5 m  $\times$  5 m aluminum frame. The time-averaged water depth at the measurement site was 3 m. The frame was anchored to the bottom using 8 mm metal bars with additional weights at the corners of the frame. The stems were at the height of 0.3 m above the seabed. The absolute and differential pressure was read at a height of 0.2 m from the bed with a frequency of 100 Hz. The data were saved as text files in 5 min blocks.

### d. Analysis of pressure data and velocity proxy

The data streams from the sensors were merged into continuous 24 h blocks starting at midnight. The outliers (values that differed more than three standard deviations from the mean value of the pressure series) were removed. The absolute pressure data were used to identify and analyze the properties of the ship wakes. The recorded data  $p^*$ , originally given in millivolts, were converted into pressure  $p$  (Pa) using the calibration relation obtained from a water tank test:

$$p = 27.1208p^* + 4475.72. \quad (1)$$

The correlation coefficient between the raw data and the linear fit to the raw data is  $R^2 > 0.9$ . As Tallinn Bay has virtually no tides (Leppäranta and Myrberg 2009) and

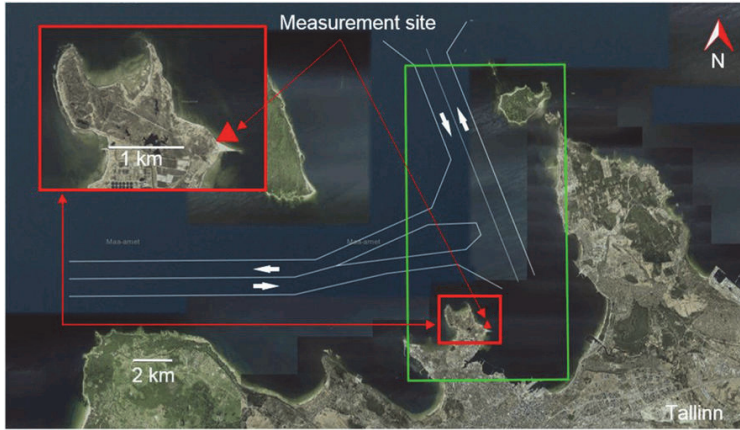


FIG. 4. The location of Tallinn Bay, traffic separation scheme (white lines), and sailing directions sailing (white arrows) along its main fairways. The measurement site is at Pikakari Beach (red triangle). The area where AIS data were retrieved is marked with a green rectangle (Estonian Maritime Administration 2019).

water level variations are just a few centimeters on calm summer days (due primarily to wind and air pressure effects), it is reasonable to assume that the water depth remained nearly constant during the fieldwork. The height of the water column above the device is the difference between the average depth  $h = 3$  m at the measurement site and the height of the sensor  $d_s = 0.2$  m above the seabed. The attenuation of the pressure signal in the water column compared to the amplitude of water surface fluctuations was corrected using the classic relationship for linear waves (Karimpour and Chen 2017):

$$P_0(z = -h_s) = P + q = \rho gh_s + \rho g \eta K_p, \quad (2)$$

where  $P_0$  is the total pressure,  $P$  is static pressure (equal to the mean water pressure),  $q$  is the dynamic pressure that represents the water fluctuations,  $h_s = h - d_s$  is the depth of the sensor,  $g$  is gravity acceleration,  $\rho$  is the water density,  $z$  is the depth of the sensor with positive values above the water level,  $\eta$  is the water surface elevation, and  $K_p$  is the dynamic pressure to the surface elevation conversion factor (Karimpour and Chen 2017):

$$K_p = \frac{\cosh k(h+z)}{\cosh(kh)} = \frac{\cosh(kd_s)}{\cosh(kh)}. \quad (3)$$

Here, the wavenumber  $k$  is a function of the wave angular frequency  $\omega = 2\pi/T$  and local water depth  $h$ , defined by the dispersion relation of surface gravity waves:

$$\omega^2 = gk \tanh(kh). \quad (4)$$

The values of the wavenumber  $k$  were evaluated using the approach proposed in (Goda 2010).

The time series of fluctuations of the water surface were sampled at a frequency of 5 Hz, which is sufficient to allow well-defined spectrograms (Torsvik et al. 2015). The short-time Fourier transform was applied to this time series with the frequency resolution of 0.005–0.6 Hz and a Hamming window with a length of 1024 data points. We employed an overlap of time windows of 178 s to obtain a good resolution with a 0.5 s step and to simultaneously reduce the likelihood of extracting false multiple signatures in close proximity of each other instead of one real signal. The resulting spectrograms were normalized to make it easier and more consistent to compare the results from different sensors.

Additionally, vibration level of a stem, measured by IMU could be used for automatic vessel wake detection as this information can be considered as a proxy of water velocity around the instrument. In our case, IMUs positioned in the hydromasts produced two datasets instead of one combined acceleration measurement: the linear acceleration information and gravity vector data. To detect the extreme positions of the vibrating stem, we used both of them for vessel wake detection.

For each of the hydromasts, the data from the casing IMU were subtracted from the stem IMU (Ristolainen et al. 2019). As we were only interested in very strong readings (in terms of the ratio between high and low values in the relevant time series), there was no need to convert the sensor output into dimensional units. Similar to the pressure signal, the outliers were removed. Also, both datasets were normalized and the root-mean-square

average of the acceleration was found from the three perpendicular axes used for measurements. High-frequency fluctuations (that cannot be part of ship wake signal) were filtered out using the ninth-order low-pass Butterworth filter with a cutoff frequency of 5 Hz. A threshold depending on the resulting average value was applied to limit the minimum time interval between ship wakes to one event within every 10 min. The resulting sets of possible ship wake events were compared with visual findings from the spectrograms derived from the absolute pressure data.

#### e. The AIS data

The signatures of wakes obtained using the pressure sensors were compared with data from the vessel AIS sourced from BigOceanData (BigOceanData 2019). The AIS data were retrieved for the entire period of fieldwork for all ships that sailed in the area marked in Fig. 4 encompassed by 59.45°–59.60°N, 24.65°–24.80°E. The AIS dataset does not necessarily contain information about all ships. For example, there were no ship AIS records in the retrieved record for 19–20 July, presumably due to technical issues.

The AIS data are recorded once in every 5 min for all vessels. The information provided is the geographical location (longitude, latitude), the time stamp, name of the vessel, International Maritime Organization (IMO) identifier, Maritime Mobile Service Identity (MMSI) number, call sign, course, speed, and status of a vessel (BigOceanData 2019). The status can be one of the following: “undefined,” “underway using engine,” “underway sailing,” “moored,” “anchor,” or “restricted maneuverability.” In total 206 unique vessels were identified using a total of 82 800 entries in the AIS dataset.

The data were grouped by vessels and separated into passings that may be detected at the measurement site. Passing is defined here as a closest AIS position to the measurement site from the series of consecutive AIS contacts or positions of a vessel. We only considered vessels that actually sailed in Tallinn Bay, that is, the vessels that reported their speed and course outside the harbors and anchoring areas. Most of these vessels were moving in the area of interest (Fig. 4). A single vessel may have several passings per day. The passings could represent either passage through the area of interest or relocating within the area. For example, the passenger ferry *Megastar* (owned and operated by Tallink) had six passings on 11 July. *Megastar* had three return journeys between Tallinn and Helsinki (about 60 km to the north of Tallinn Bay) and thus had three entries to and three departures from the Port of Tallinn. For each passing, we evaluated the closest AIS contact based on the coordinates and the closest approximate

position to the location of devices based on the trajectory of the vessel.

### 3. Results

#### a. Multiple sensors

Experience with spectrogram analysis of surface elevation data suggests that on many occasions some components of ship wakes may be severely masked by wind waves (Torsvik et al. 2015). This is a frequent problem in semiencllosed sea areas such as Tallinn Bay where even fairly moderate winds may generate waves with periods of 2–3 s (frequencies 0.3–0.5 Hz) with a wide spectrum that overlaps with vessel wakes in frequency space. While the elimination of some features such as narrowbanded swells from the recorded signal may be possible, it is usually not feasible to remove the signal of wave fields with a wide spectrum from the spectrogram. The presence of relatively strong levels of wind-wave noise does not necessarily destroy the entire approach but may modify the results significantly and may render part of the chirp-like signal of divergent waves imperceptible in spectrograms (Torsvik et al. 2015). A typical case with such a problem is illustrated in Fig. 5a.

The use of time series pressure sensors has another shortcoming. While the high-frequency part of the surface wave field is often attenuated, the near-bed pressure signal frequently contains a substantial level of low-frequency (periods > 10 s) pressure oscillations that may mask the longer components of the wake such as transverse waves or precursor solitons (e.g., near-horizontal higher energy lines up to 0.2 Hz in Fig. 5b compared to Fig. 5a). A part of this noise has typical periods > 15 s and thus is much longer than ship wake components.

This shortcoming may be mitigated using several synchronized pressure sensors located at a certain distance from each other. Such a configuration is complicated and expensive to build from downward-looking devices but easily manageable using an array of hydromasts. We used for this purpose data from the five (devices on the corners and at the center of the grid) out of nine hydromasts of the frame described above. Adding data from the additional four sensors did not increase the quality of the spectrogram in terms of better signal to noise ratio. The long wave speed at the measurement location was  $5.4 \text{ m s}^{-1}$ . The phase speed of longer vessel wake components is thus on the order of  $3\text{--}4 \text{ m s}^{-1}$ . The phase shift of single wave crests at different sensor locations is therefore much smaller than the wave period (usually > 3 s).

If the low-frequency background noise is not coherent over the distance between the sensors, it can be suppressed

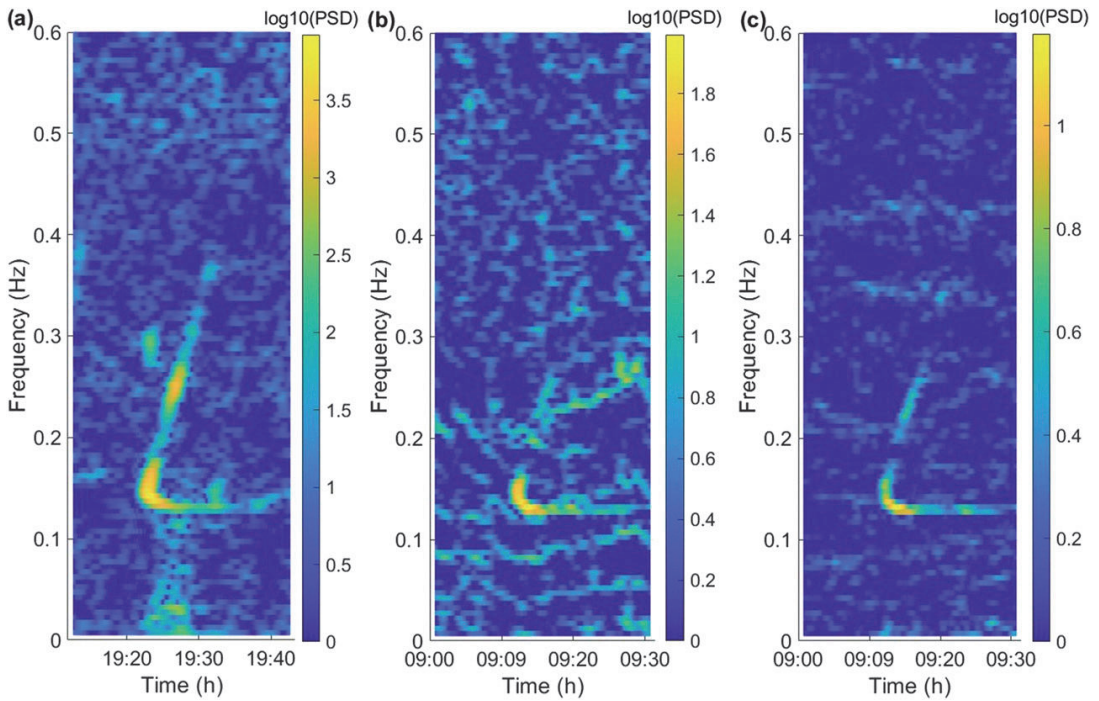


FIG. 5. (a) The signature of passenger ferry *Tallink Star* approaching the Port of Tallinn on 25 Jun 2009 with a wind-generated sea with typical periods of 2–2.5 s (Torsvik et al. 2015). The wake is measured using a one-point measurement device (a down-looking echosounder mounted on a tripod) from above the water level. (b) The signature of the same vessel approaching Port of Tallinn on 17 Jul 2017 under similar weather conditions. The wake is detected using a single pressure sensor mounted at the seabed at a depth of 3 m. The pressure sensor is at a height of 0.2 m from the seabed. (c) As in (b), but visualized using five sensors located in the center and the corners of a frame of size 5 m × 5 m. The spectrograms are normalized by frequency spectrum and overlapped.

by merging several properly synchronized spectrogram snapshots of coherent waves into one picture. This approach was realized by using ensemble averaging, which was done by averaging the normalized spectrograms from a cluster of five sensors into a single diagram. This procedure substantially improved the wake-to-background spectrum noise ratio (Fig. 5c). It greatly simplified the wake detection process, eliminated false decisions, and made it possible to evaluate some properties of ship motion.

#### b. Detection of a sequence of ship wakes

The applied three-step process of detection of single wake by (i) evaluating very large values of the velocity proxy as the potential time instance of the arrival of ship wakes, (ii) subsequent spectrogram analysis of pressure fluctuations at the locations of single sensors, and (iii) refinement of the signatures of single ships by means of merging and averaging normalized spectrograms from a cluster of sensors, leads to an overall relatively efficient and reliable recognition of ship passages (Fig. 6).

An example is given in Fig. 6. During the represented time interval, 12 ship wakes can be visually identified in the spectrogram calculated from the absolute pressure data as described above (Fig. 6c). All 12 wake signatures were matched with the corresponding passages retrieved from the AIS data. Some passages have only the signature of diverging waves, which makes automatic distinguishing complicated. However, most of the detected signatures contain the visually distinguishable divergent and transverse wave components that have been used in similar studies that use wave elevation data for estimating energy, duration and spectral composition of the wake and its components (Torsvik et al. 2015). The number of ship passages found from the overthreshold values of the gravity vector data was 12 (Fig. 6b). From these events, 10 cases matched the relevant visually identified images of ship wakes in the spectrogram. Two were false-positive signals and two ship passages (at 2240 and 2350 LT; LT = UTC + 3 h) were missed. The total number of ship passages identified in a similar manner from the linear acceleration dataset was 14 (Fig. 6a). From these events,



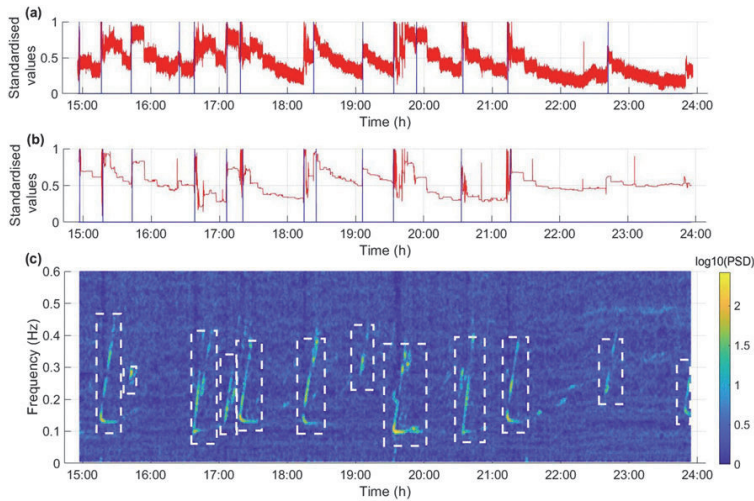


FIG. 6. The comparison of the detection results on 10 Jul 2017. (a) Time series of the linear acceleration (red) with detected events (blue vertical lines) (the number of detected events was 14), (b) time series of the gravity vector (red) with detected events (blue) (12 wakes captured), and (c) the spectrogram based on the pressure data where ship wakes are portrayed as yellow structures (outlined with white dashed rectangles; in total 12 wakes can be seen).

11 matched the ship wake images visually identified from the spectrogram. Therefore, four contacts were false-positive and one contact was missed.

Throughout the period when both the measurement data and AIS information were present, 852 events of vessels passing by the measurement site were filtered out from the AIS data and 160 wake structures were visible in the spectrograms (as in Fig. 6c). The number of wake events in the spectrograms was limited due to the speed of the ships as wakes from the vessels sailing below 15 kt (approximately  $28 \text{ km h}^{-1}$ ) were seldom visible in the spectrograms. The second factor was the location of the measurement devices, as Katariina jetty (southeast from the measurement site in Fig. 4) sheltered the measurement site from the wakes of majority of the departing vessels and the tip of Pikakari peninsula stopped wakes from the greater number of the ships operating east–west directions north from reaching the measurement site (Fig. 4). Also, on some occasions, wakes from several vessels arrived at the sensors less than 10 min apart, which resulted in reading them as one structure.

Due to these circumstances, we focused mainly on the vessels approaching the port of Tallinn at a speed of 15 kt or more. There were 144 passings (out of 852) that met these criteria. Majority of them (135) were roll-on–roll-off type ferries or passenger ships. The rest (9 vessels) were small craft (with a length less than 24 m). From those

144 events, 116 cases were matched with corresponding wakes structures in the spectrograms, 13 misses were due to small time interval (less than 10 min) between the wakes, 9 cases were small craft, and in 6 cases ferries were sailing near 15 kt.

From the 160 cases when a wake was visible in the spectrogram, 152 wakes were also detected by using the linear acceleration data and 134 by utilizing gravity vector information from the sensors. Despite the slightly better detection rate, linear acceleration information provided a higher total number of extreme events (292) compared to the gravity vector information (200).

#### 4. Discussion and conclusions

It is known that high-resolution, one-point measurements of surface fluctuations collected by instruments such as downward-looking echo sounders generated by wake waves can be used for ship detection (Torsvik et al. 2015). Such measurements often require expensive field equipment that can be difficult to deploy and are negatively affected by wind waves. The data can be evaluated to estimate the sailing regime in terms of depth Froude numbers, speed, and distance to the measurement location to be estimated (Torsvik et al. 2015; Pethiyagoda et al. 2017, 2018).

The main goal of this work was to investigate the use of time series of wake waves for vessel detection using

other technologies. We have demonstrated that information of comparable quality (i.e., suitable for the detection of properties of the ship and its sailing regime) can be produced using time series of properly located high-resolution pressure sensors. The use of such devices is on many occasions technically simpler, less expensive, and much less affected by atmospheric conditions. The spectrogram technique of windowed Fourier analysis is identical for the two approaches.

A specific feature of the use of the pressure signal is its attenuation for shorter waves in the water column. On the one hand, this feature may serve as a convenient low-pass filter to single out the ship wakes from the background of short-period wind seas. On the other hand, this feature may lead to an unacceptable level of low-frequency pressure fluctuations and/or noise in the recorded signal. We demonstrate that this shortcoming can be mitigated by using synchronized time series from an ensemble of pressure sensors in cases when the low-frequency pressure variations are incoherent. The resulting signatures of wakes in almost all cases match the corresponding references retrieved from the automatic identification system database.

The increased signal-to-noise ratio produced by overlapping spectrograms from several sensors apparently provides a simple and possibly better approach to the automatic detection of ship passages and several properties of her movement. The extended dataset, that also contains proxy information about near-bed velocities, could provide an additional basis for automatic vessel detection and may overcome some of the difficulties discussed in Torsvik et al. (2015). In particular, the use of multimodal datasets to characterize the properties of the wake has clear potential to increase the success rate of wake detection and quantification of the ship's sailing regime compared to the tracking of just one physical quantity from above the water level.

In vessel detection applications, the location, speed, and course of the vessel are the key features to be determined. The main message from the presented analysis is that spectrogram representations constructed using the pressure time series are of sufficient quality for the interpretation of the different components of ship wakes. The properties of these components (the slopes of the branches that correspond to diverging and transverse waves and the location of the intersection point of these branches) allow the quantification of several features of the vessel movement, such as the shortest distance of the sailing line to the measurement location, the location at which the first waves of the wake were produced, and the speed of the

vessel and the local depth Froude number (Torsvik et al. 2015; Pethiyagoda et al. 2018) based on the evolution of a wake in time at a fixed point.

We also demonstrated that additional information provided by multisensor flow measurement devices can serve as a useful aid for the rapid detection of ship wakes. The proxy of near-bed water velocity from the described devices known as hydromasts (Ristolainen et al. 2016) may perform nearly as well as the procedure of detecting wakes from the spectrograms. The use of such datasets requires careful calibration and additional preprocessing tools to improve the accuracy and reliability of ship detection.

The improvement in the quality of spectrogram representation of the wakes using the signals from a cluster of closely positioned sensors is a first step toward the use of multiple sensor technology. The use of such clusters may serve as a feasible way toward the quantification of the vessel's course based on the analysis of phase shifts in single crests of the approaching wake. Another standing research question is the determination of the particular vessel (or vessel type) based on its wake. They both seem feasible using synchronized information in multimodal data streams from a properly positioned cluster of measurement devices.

In conclusion, we demonstrated that datasets from near-bed pressure sensors are equivalent to data of water surface elevation collected using surface measurements when considering, in the context of spectrogram technique, the detection of vessels and their sailing regimes. The use of synchronized multisensor systems makes it possible to substantially suppress noise and improve the quality of the outcome. Water movement data, which are also collected by the hydromast sensors, provide rapid detection of ship passages with a high success rate.

*Acknowledgments.* The current work was done in the frame of the European Union's Horizon 2020 research and innovation program project LAKHsMI under Grant Agreement 635568. Also, this research was supported by the Estonian Ministry of Education and Research (Estonian Research Council, Institutional Support IUT33-3 and PUT 1690) and the European Regional Development Fund program Mobilias Plus, reg.nr 2014-2020.4.01.16-0024, and cosupported by the Flag-ERA project FuturICT2.0, Estonian Center of Excellence EXCITE, the Estonian Research Infrastructures Roadmap object Infotechnological Mobility Observatory (IMO), and Baltic Research Programme (EEA Financial Mechanisms 2014-2021) project "Solutions to current and future problems on natural and constructed shorelines, eastern Baltic Sea" (EMP480).

## REFERENCES

- Anupriya, K. R., and T. Sasilatha, 2018: Ship intrusion detection system—A review of the state of the art. *Soft Computing Systems: ICSCS 2018*, I. Zelinka et al., Eds., Communications in Computer and Information Science, Vol. 837, Springer, 147–154, [https://doi.org/10.1007/978-981-13-1936-5\\_17](https://doi.org/10.1007/978-981-13-1936-5_17).
- Benassai, G., V. Piscopo, and A. Scamardella, 2015: Spectral analysis of waves produced by HSC for coastal management. *J. Atmos. Oceanic Technol.*, **20**, 417–428, <https://doi.org/10.1007/S00773-014-0290-1>.
- BigOceanData, 2019: BigOceanData. Accessed 14 April 2019, <http://www.bigoceandata.com/>.
- Bleckmann, H., and R. Zelick, 2009: Lateral line system of fish. *Integr. Zool.*, **4**, 13–25, <https://doi.org/10.1111/j.1749-4877.2008.00131.x>.
- Cavaleri, L., 1980: Wave measurement using pressure transducer. *Oceanol. Acta*, **3**, 339–346.
- Chen, P. F., Y. M. Huang, J. M. Mou, and P. H. A. J. M. van Gelder, 2018: Ship collision candidate detection method: A velocity obstacle approach. *Ocean Eng.*, **170**, 186–198, <https://doi.org/10.1016/j.oceaneng.2018.10.023>.
- Didenkulova, I., A. Sheremet, T. Torsvik, and T. Soomere, 2013: Characteristic properties of different vessel wake signals. *J. Coastal Res.*, **65**, 213–218, <https://doi.org/10.2112/SI65-037.1>.
- Dugad, S., V. Puliyadi, H. Palod, N. Johnson, S. Rajput, and S. Johnny, 2016: Ship intrusion detection security system using HoG & SVM. *Int. J. Adv. Res. Comput. Eng. Technol.*, **5**, 2504–2507, <http://ijaracet.org/wp-content/uploads/IJAR CET-VOL-5-ISSUE-10-2504-2507.pdf>.
- Estonian Maritime Administration, 2019: Estonian Maritime Administration's web application Nutimeri. Accessed 3 May 2019, <https://gis.vta.ee/nutimeri/>.
- Fang, M. C., R. Y. Yang, and I. V. Shugan, 2011: Kelvin ship wake in the wind waves field and on the finite sea depth. *J. Mech.*, **27**, 71–77, <https://doi.org/10.1017/jmech.2011.9>.
- Fujino, I., C. Claramunt, and A.-O. Boudraa, 2018: Extracting courses of vessels from AIS data and real-time warning against off-course. *Proc. Second Int. Conf. on Big Data Research*, Weihai, China, Association for Computing Machinery, 62–69, <https://doi.org/10.1145/3291801.3291823>.
- Gierull, C. H., 2019: Demystifying the capability of sublook correlation techniques for vessel detection in SAR imagery. *IEEE Trans. Geosci. Remote Sens.*, **57**, 2031–2042, <https://doi.org/10.1109/TGRS.2018.2870716>.
- Goda, Y., 2010: Reanalysis of regular and random breaking wave statistics. *Coastal Eng. J.*, **52**, 71–106, <https://doi.org/10.1142/S0578563410002129>.
- Huang, W., D. Wang, H. Garcia, O. R. Godø, and P. Ratilal, 2017: Continental shelf-scale passive acoustic detection and characterization of diesel-electric ships using a coherent hydrophone array. *Remote Sens.*, **9**, 772, <https://doi.org/10.3390/rs9080772>.
- Karimpour, A., and Q. Chen, 2017: Wind wave analysis in depth limited water using OCEANLYZ, a MATLAB toolbox. *Comput. Geosci.*, **106**, 181–189, <https://doi.org/10.1016/j.cageo.2017.06.010>.
- Kuo, Y.-Y., and Y.-F. Chiu, 1994: Transfer function between wave height and wave pressure for progressive waves. *Coastal Eng.*, **23**, 81–93, [https://doi.org/10.1016/0378-3839\(94\)90016-7](https://doi.org/10.1016/0378-3839(94)90016-7).
- Kurekin, A. A., B. R. Loveday, O. Clements, G. D. Quartly, P. I. Miller, G. Wiafe, and K. A. Agyekum, 2019: Operational monitoring of illegal fishing in Ghana through exploitation of satellite Earth observation and AIS data. *Remote Sens.*, **11**, 293, <https://doi.org/10.3390/rs11030293>.
- Kuznetsov, N. G., V. G. Maz'ya, and B. Vainberg, 2002: *Linear Water Waves: A Mathematical Approach*. Cambridge University Press, 513 pp.
- Leppäranta, M., and K. Myrberg, 2009: *Physical Oceanography of the Baltic Sea*. Springer, 378 pp.
- Newman, J. N., 1977: *Marine Hydrodynamics*. MIT Press, 402 pp.
- Panico, A., M. D. Graziano, and A. Renga, 2017: SAR-based vessel velocity estimation from partially imaged Kelvin pattern. *IEEE Geosci. Remote Sens. Lett.*, **14**, 2067–2071, <https://doi.org/10.1109/LGRS.2017.2751083>.
- Park, J.-J., S. Oh, K.-A. Park, P.-Y. Foucher, J.-C. Jang, M. Lee, T.-S. Kim, and W.-S. Kang, 2018: The ship detection using airborne and in-situ measurements based on hyperspectral remote sensing. *J. Korean Earth Sci. Soc.*, **38**, 535–545, <https://doi.org/10.5467/JKESS.2017.38.7.535>.
- Pethiyagoda, R., S. W. McCue, and T. J. Moroney, 2017: Spectrograms of ship wakes: Identifying linear and nonlinear wave signals. *J. Fluid Mech.*, **811**, 189–209, <https://doi.org/10.1017/jfm.2016.753>.
- , T. J. Moroney, G. J. Macfarlane, J. R. Binns, and S. W. McCue, 2018: Time-frequency analysis of ship wave patterns in shallow water: Modelling and experiments. *Ocean Eng.*, **158**, 123–131, <https://doi.org/10.1016/j.oceaneng.2018.01.108>.
- Rabaud, M., and F. Moisy, 2013: Ship wakes: Kelvin or Mach angle? *Phys. Rev. Lett.*, **110**, 214503, <https://doi.org/10.1103/PhysRevLett.110.214503>.
- Renga, A., M. D. Graziano, and A. Moccia, 2019: Segmentation of marine SAR images by sublook analysis and application to sea traffic monitoring. *IEEE Trans. Geosci. Remote Sens.*, **57**, 1463–1477, <https://doi.org/10.1109/TGRS.2018.2866934>.
- Ristolainen, A., J. A. Tuhtan, A. Kuusik, and M. Kruusmaa, 2016: Hydromast: A bioinspired flow sensor with accelerometer. *Biomimetic and Biohybrid Systems*, N. Lepora et al., Eds., Lecture Notes in Computer Science, Vol. 9793, Springer, 510–517, [https://doi.org/10.1007/978-3-319-42417-0\\_55](https://doi.org/10.1007/978-3-319-42417-0_55).
- , —, and M. Kruusmaa, 2019: Continuous, near-bed current velocity estimation using pressure and inertial sensing. *IEEE Sens. J.*, **19**, 12 398–12 406, <https://doi.org/10.1109/jsen.2019.2937954>.
- Sheremet, A., U. Gravois, and M. Tian, 2013: Boat-wake statistics at Jensen Beach, Florida. *J. Waterw. Port Coastal Ocean Eng.*, **139**, 286–294, [https://doi.org/10.1061/\(ASCE\)WW.1943-5460.0000182](https://doi.org/10.1061/(ASCE)WW.1943-5460.0000182).
- Siebert, G., J. Hoth, P. Banyś, and F. Heymann, 2019: Generic framework for vessel detection and tracking based on distributed marine radar image data. *CEAS Space J.*, **11**, 65–79, <https://doi.org/10.1007/s12567-018-0208-6>.
- Soomere, T., 2005: Fast ferry traffic as a qualitatively new forcing factor of environmental processes in non-tidal sea areas: A case study in Tallinn Bay, Baltic Sea. *Environ. Fluid Mech.*, **5**, 293–323, <https://doi.org/10.1007/s10652-005-5226-1>.
- , 2007: Nonlinear components of ship wake waves. *Appl. Mech. Rev.*, **60**, 120–138, <https://doi.org/10.1115/1.2730847>.
- , K. E. Parnell, and I. Didenkulova, 2011: Water transport in wake waves from high-speed vessels. *J. Mar. Syst.*, **88**, 74–81, <https://doi.org/10.1016/j.jmarsys.2011.02.011>.
- Sorensen, R. M., 1973: Ship-generated waves. *Adv. Hydrosci.*, **9**, 49–83, <https://doi.org/10.1016/B978-0-12-021809-7.50007-9>.
- Till, G., 2013: *Seapower: A Guide for the Twenty-First Century*. Routledge, 432 pp., <https://doi.org/10.4324/9780203880487>.

- Torsvik, T., T. Soomere, I. Didenkulova, and A. Sheremet, 2015: Identification of ship wake structures by a time-frequency method. *J. Fluid Mech.*, **765**, 229–251, <https://doi.org/10.1017/jfm.2014.734>.
- Wehausen, J. V., 1973: The wave resistance of ships. *Adv. Appl. Mech.*, **13**, 93–245, [https://doi.org/10.1016/S0065-2156\(08\)70144-3](https://doi.org/10.1016/S0065-2156(08)70144-3).
- Wyatt, D. C., and R. E. Hall, 1988: Analysis of ship-generated surface waves using a method based upon the local Fourier transform. *J. Geophys. Res.*, **93**, 14 133–14 164, <https://doi.org/10.1029/JC093iC11p14133>.
- Zhu, C., H. Garcia, A. Kaplan, M. Schinault, N. O. Handegard, O. R. Godø, W. Huang, and P. Ratilal, 2018: Detection, localization and classification of multiple mechanized ocean vessels over continental-shelf scale regions with passive ocean acoustic waveguide remote sensing. *Remote Sens.*, **10**, 1699, <https://doi.org/10.3390/rs10111699>.
- Zilman, G., A. Zapolski, and M. Marom, 2004: The speed and beam of a ship from its wake's SAR images. *IEEE Trans. Geosci. Remote Sens.*, **42**, 2335–2343, <https://doi.org/10.1109/TGRS.2004.833390>.





**Publication III**

Rätsep, M., Parnell, K.E., Soomere, T., Kruusmaa, M., Ristolainen, A. and Tuhtan, J.A., 2021. Surface vessel localization from wake measurements using an array of pressure sensors in the littoral zone. *Ocean Engineering*, 233, 109156.  
<https://doi.org/10.1016/j.oceaneng.2021.109156>





Contents lists available at ScienceDirect

## Ocean Engineering

journal homepage: [www.elsevier.com/locate/oceaneng](http://www.elsevier.com/locate/oceaneng)

## Surface vessel localization from wake measurements using an array of pressure sensors in the littoral zone

Margus Rätsep<sup>a,\*</sup>, Kevin E. Parnell<sup>a</sup>, Tarmo Soomere<sup>a</sup>, Maarja Kruusmaa<sup>b</sup>, Asko Ristolainen<sup>b</sup>, Jeffrey A. Tuhtan<sup>b</sup>

<sup>a</sup> Department of Cybernetics, School of Science, Tallinn University of Technology, Tallinn, Estonia

<sup>b</sup> Centre for Biorobotics, Department of Computer Systems, School of Information Technologies, Tallinn University of Technology, Tallinn, Estonia

## ARTICLE INFO

## Keywords:

Ship wake  
Spectral analysis  
Vessel localization  
AIS data  
Pressure sensor

## ABSTRACT

Vessel detection and localization based on wake measurements have been used extensively in aerial and satellite reconnaissance. Here, a wake-based approach for vessel localization and speed estimation is developed using a grid of pressure sensors on the seabed. The sensor array consisted of 9 devices in a  $3 \times 3$  rectangular grid with 2.5 m spacing between the instruments. The array was deployed at a depth of 3 m approximately 2.5 km from the fairway. The pressure time series from all sensors were used to estimate vessel speed and the travelling distance of the wake by interpreting the geometry of its time-frequency representation. The wake direction and an estimate of the vessel course are calculated from the delays of the incoming wake between the sensor locations, equivalently, based on cross-correlations of the signal at neighbouring sensors. Results for single events are compared with data collected from the vessels self-reporting systems (AIS). It is concluded that a grid of pressure sensors can provide a reliable estimation of the vessel location and its speed. The presented technique makes it possible to locate ships, and their speed and course, as the next step towards a vessel traffic monitoring system based on wake recordings.

### 1. Introduction

The increase in the density of maritime traffic, a variety of ship types and multiple uses gradually adds to the complexity of offshore and coastal sea management (van Westrenen and Baldauf, 2020). It also generates a higher probability of accidents (Altan and Otay, 2018) and raises pressure on the marine (Claremar et al., 2017; Zanatta et al., 2020) and coastal (Delpeche-Ellmann and Soomere, 2013) environment. In particular, the introduction of unmanned Marine Autonomous Surface Ships additionally increases the related risks due to a reduced recovery capability (Thieme et al., 2018). Specifically, losing contact with a ship can severely limit the options for maintaining control in critical applications. To cope with this risk, the ability of coastal services to detect a vessel and estimate its position, speed and course are essential.

Our research is motivated by several studies which have developed vessel tracking methods. Vessel movements can be retrieved from well-known sources like radar and radio systems (Zilman et al., 2004; Gierull, 2019; Renga et al., 2019; Siegert et al., 2019), sonar technologies (Huang et al., 2017), acoustic devices and/or using direct visual

observations from other vessels and the coast (Fefilat'yev et al., 2012; Magnier and Gervaise, 2020). Some of these methods including sophisticated methods such as those described in Pradhan and Gupta (2017), Zhang et al. (2017), and Joseph et al. (2019) enable vessel detection only: determining if there are vessels present in the sea area of interest. However, before taking appropriate action, additional information such as the vessel position, speed and sailing course, are needed. The entire process of assessing these three properties (position, speed and course) is referred to as 'localization'. An adequate estimate of these parameters is a key part of composing a Recognized Maritime Picture (RMP) which represents a set of information necessary for creating situational awareness in maritime operations (NATO Standardization Agency, 2015). One possible method to achieve this, discussed in this paper, is to make use of the disturbances left by the passing vessel to the surrounding water (Panico et al., 2017; Zhang and Jiang, 2020).

One of the core sources of information about the location, properties and sailing parameters of the ship is its wave wake (Newman, 1991; Tuck et al., 1971; Wu and Meadows, 1991). This problem, essentially an inverse ship-wave problem (Newman, 1991), does not necessarily have

\* Corresponding author.

E-mail address: [margus.ratsep@ttu.ee](mailto:margus.ratsep@ttu.ee) (M. Rätsep).



a unique solution for all desired parameters. Technically, one of the simplest properties to determine from recordings of a wake is speed. A ship's speed  $U$ , wave propagation direction with respect to the sailing line  $\theta$ , and wave number  $k$  (or length)  $L = 2\pi/k$  are rigorously related:

$$k(\theta) = \frac{g}{U^2 \cos^2 \theta} \quad (1)$$

where  $g$  is the acceleration due to gravity (Newman, 1977; Wu, 1991). Therefore, one only needs the wave number  $k$  and the wake propagation angle  $\theta$  of any part of the wake to determine the ship's speed (Wu, 1991). The wave number can be retrieved from the dispersion relation based on wave period or frequency. This almost naive approach works well if the ship is following, for example, traffic separation regulations (Torsvik et al., 2015), and can be used at any distance from the sailing line provided the wake is distinguishable. However, without *a priori* information about the sailing line, these quantities need to be evaluated simultaneously.

A straightforward solution to the problem of determining a ship's speed and direction can be obtained from the entire two-dimensional (2D) pattern of ship-generated waves (Wu, 1991; Wu and Meadows, 1991) by evaluation of the relevant 2D wave spectrum. This approach was discussed by Tuck et al. (1971) and justified in detail by Wu (1991). A limited solution can also be obtained from the one-dimensional (1D) time series of the wave system.

This approach requires high-resolution images of the water surface that are capable of resolving single wave crests. Synthetic aperture radar (SAR) images of this quality and the appropriate techniques for extraction of wave patterns have become available only since the turn of the century (e.g. Chaillan and Courmontagne, 2006; Courmontagne, 2005) and have been relatively recently extended to situations with substantial wind wave background (Yu and Wu, 2014; Zilman et al., 2015). Alternatively, applications based on scanning laser and image processing have been used in towing tanks and confined environments (e.g. Gomit et al., 2015, 2013). These developments have made it possible to produce highly accurate 2D spectra of ship waves (Gomit et al., 2014).

The applications of these techniques have been described in a number of studies estimating parameters of ship characteristics and their motion based on spectral analysis. Arnold-Bos et al. (2007) present a method for estimates of ship speed and sailing direction based on the entire pattern of its Kelvin wake. They use the generalized Radon transform followed by stochastic matched filtering to reliably detect the loci of the wake signature in the 2D spectrum of the image. Several methods such as the fractional Fourier transform (Chen et al., 2020) or convolutional neural networks (Kang and Kim, 2019) have been developed to derive the ship's speed from the SAR imagery of its wake. This approach has provided a thorough description of linear, nonlinear and evanescent modes of the wave wake in spectral space (Sun et al., 2018) and allows for the derivation of several ship motion parameters from these representations (Fan et al., 2019).

The 2D or 1D patterns of wakes with the necessary resolution are rarely available to use for the localization of vessels. Also, the described spectral methods are relatively sensitive to noise and missing information about part of the wake. If the quality of snapshots of the wake pattern is too low, the locus will remain undefined in the spectral space. Moreover, in conflict situations, it is likely to be impossible to obtain the required data with the necessary quality.

Some localization and surveillance methods that are valuable on the open sea may not be suitable for use in the littoral zone due to the presence of a rigid coastline, which can create false positive contacts for vessel detection (Aiello et al., 2019) and requires extensive resources for on-site observation. This creates a clear need for additional research to improve the detection and localization of vessels that operate near the shore or in confined waters.

For this reason, we revert to more robust and less demanding (albeit at times less exact) methods for ship localization and the specification of motion parameters. Namely, we rely on the decomposition of one-point

recordings of far-field wake signals into time-frequency representations (3D compositions of time, frequency and power, here referred to as spectrograms) by utilizing Short-Time Fourier Transform instead of 1D and 2D Fast Fourier Transform as used in cases referred to above.

Recent research into vessel wakes has shown that ship wakes have a content-rich structure in the time-frequency representation (Sheremet et al., 2012). On many occasions, this structure can be extracted from one-point recordings of water surface fluctuations measured from above (Torsvik et al., 2015) or from pressure recordings from the seabed (Sheremet et al., 2012). Moreover, using the relations between different components highlighted in the spectrograms, a ship's sailing characteristics including the speed and minimum distance of the sailing line from the measurement site (Torsvik et al., 2015) or changes in the vessel movement such as course and speed alterations (Pethiyagoda et al., 2017) can be calculated.

The main benefit of this approach is that the loci of single wave components are represented as straight lines – asymptotes of the relevant linear dispersion relation – at some distance from the point that corresponds to the border of the Kelvin wedge (Pethiyagoda et al., 2017). This property makes it possible to reconstruct the location and orientation of these lines on the spectrogram even if there are only a few recorded wave crests that present diverging and transverse waves. The crossing point of these two lines (transverse and divergent waves) is directly related to the point that represents waves at the border of the Kelvin wedge. It is therefore possible to reduce the problem of determination of a ship's speed to a certain analysis of geometric features in the spectrogram. Moreover, this method is much less sensitive to the presence of other waves. In particular, background waves with frequencies clearly different from the wake components at the edge of the Kelvin wedge can be eliminated by a suitable spectral filter. This reflects the general perception that it is easier to detect the presence of a ship sailing using waves portrayed in the spectral domain than from the spatial pattern of its wake.

Motivated by these findings and confirmation that results based on the spectrogram methods developed by Torsvik et al. (2015) coincide with actual ship sailing data derived from their self-reporting systems (Rätsep et al., 2020a), the question is whether it is possible to develop a simple remote vessel detection and localization system based on the wake recordings that would contribute additional information to the RMP building process. This process usually consists of five steps. The first three are generally instrument or sensor-based (NATO Standardization Agency, 2015). These are (i) vessel detection (whether a particular vessel is in the area of interest), (ii) localization and (iii) recognition (providing additional information that would help to recognize either a particular ship or a ship type) (NATO Standardization Agency, 2015).

It has been already demonstrated that vessel detection based on the wake readings is possible using multimodal pressure and inertial sensors located on the seabed (Rätsep et al., 2020b). Careful merging of data from several underwater pressure sensors led to spectrograms with a quality comparable to those derived from readings collected using downward-looking echo sounders (Rätsep et al., 2020a; Torsvik et al., 2015), while keeping the sensors concealed (Rätsep et al., 2020b).

Based on these results we address in this paper a further step towards vessel localization – the second step of the RMP building process. The procedure is divided into two major parts. First, we use specific features of the geometry of the wake signatures retrieved from spectrograms (Rätsep et al., 2020b) to estimate the speed and the distance of the passing vessels by further developing methods suggested by Torsvik et al. (2015) and developed by Pethiyagoda et al. (2017) towards utilisation of geometric properties of the loci of ship wakes in spectrograms. Secondly, by applying beamforming theory to the sensor grid (here referred to as the phase-shift technique), we determine the direction of the incoming wake. The core idea is to use the time of arrival difference between single wave crests at different locations under the assumption that the crests are locally straight. A similar concept has been widely used to quantify wind-wave propagation direction

(Borgman, 1969; Panicker and Borgman, 1970) and associated along-shore sediment transport (Seymour and Higgins, 1978) in previous wave research at a time when directional wave sensors were not yet available (see also, e.g., Dean and Dalrymple, 1991, Section 7.4). By combining these two methods, we show that it is possible to determine the vessel position with its speed and an estimate of its sailing course at the moment in time when the wake was generated.

The structure of the paper is as follows. The paper is divided into 5 sections. Section 2 provides the mathematical background to the properties of vessel waves in the Kelvin wake and geometry needed for the current work. Also, it describes the measurement site, sensors, data sets and methods used in the analysis process. Section 3 gives an overview of the results by comparing our calculated vessel locations, sailing speeds and courses with the values derived from AIS data. The limitations, challenges and areas of the potential use of the proposed techniques are discussed in Section 4. Section 5 summarizes the main results.

## 2. Methodology and experimental setup

### 2.1. Kelvin wake

A moving vessel inevitably leaves behind a system of surface waves. A displacement vessel yields a distinctive pattern of surface waves, known as the Kelvin wake. Its properties are described in detail in many overviews (Sorensen, 1973; Wehausen, 1973; Newman, 1977; Soomere, 2007; Fang et al., 2011). The description in this section follows these sources. If the ship sails steadily, the pattern of generated waves is stationary in the coordinate system attached to the ship. The geometry of this pattern can be established provided the dispersion relation of the relevant wave class is known. It is sufficient to recognize that (i) the constant phase curves (also the wave crests and troughs) are always perpendicular to the wave vector, and that (ii) the local phase velocity (celerity)  $c_f$  of stationary waves is equal to the projection of the velocity of the ship onto the direction of the wave vector (Yih and Zhu, 1989a, 1989b, 1989b).

Therefore, a wave component that travels steadily at an angle  $\theta$  with respect to the sailing line has the phase velocity

$$c_f = \frac{\omega}{k} = U \sin \theta \quad (2)$$

where  $\omega = \omega(k)$  is the dispersion relation for the produced waves. If the ship sails from X to O (Fig. 1), travelling the distance  $U\Delta t$  in time where  $\Delta t = t_1 - t_0$ , the steady waves only fill a certain circle (for example, circle (1) or circle (2) in Fig. 1) during  $t$ . The radius of this circle is a

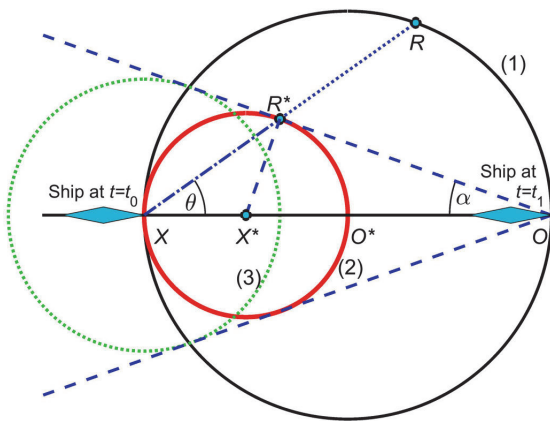


Fig. 1. Scheme of the location of wave energy in ship waves. Circle (3) indicates the area filled by waves created by a paddle located at X during  $\Delta t$ .

function of the time and the ratio of the phase speed and group speed  $c_g = \partial\omega/\partial k$ . If the group speed is smaller than the phase speed (which is the typical case for water waves), the energy released at X covers the distance  $c_g\Delta t < c_f\Delta t$  and reaches, e.g., in the sailing direction only until a certain point  $O^*$  between X and O. The generated waves thus fill circle (2) with a diameter  $Vtc_g c_f^{-1}$  and centred at  $X^* = X + \frac{1}{2} Vtc_g c_f^{-1}$ .

Consequently, steady ship waves only can exist within a triangular area (called the Kelvin wedge) that contains all circles (2), and that is limited by their common tangents going through O. The relevant half-angle of the apex  $\alpha$  of the wedge is defined from the purely geometrical condition

$$\sin \alpha = \frac{\frac{1}{2} Vtc_g c_f^{-1}}{Vt - \frac{1}{2} Vtc_g c_f^{-1}} = \frac{1}{2c_g c_f^{-1} - 1} \quad (3)$$

A vessel moving in a deep water regime, where  $\omega = \sqrt{gk}$ , produces the Kelvin wedge with its half-angle being  $\arcsin(1/3) \approx 19^\circ 28'$ , independent of the vessel speed. Transverse waves travel along the vessel sailing line (Fig. 2), and divergent waves move away from it (Fig. 2). The two wave systems interact on the borders of the Kelvin wedge due to which the cusp waves are generated (Fig. 2). The amplitude of cusp waves, which notably exceeds the amplitudes of transverse and divergent waves, decays slowly (as  $r^{-1/3}$ ) with the distance  $r$  from the vessel (Kuznetsov et al., 2002). The cusp waves propagate at an angle of  $\arccos(\sqrt{2/3}) \approx 35^\circ 16'$  from the sailing line, while transverse components travel at smaller angles, reaching  $0^\circ$  at the sailing line. The divergent components move at higher angles than cusp waves.

The properties of this wave system for a vessel sailing in waters of finite depth are governed by the general dispersion relation of water waves  $\omega = \sqrt{gk \tanh kh}$  that additionally depends on the water depth  $H$ . For this situation

$$2c_g = c_f (1 + 2kH \sinh^{-1} 2kH) \quad (4)$$

and Eq. (3) has a somewhat more complicated form:

$$\sin \alpha = \frac{1 + 2kH \sinh^{-1} 2kH}{3 - 2kH \sinh^{-1} 2kH} \text{ or } \cos^2 \alpha = 8 \frac{1 - 2kH \sinh^{-1} 2kH}{[3 - 2kH \sinh^{-1} 2kH]^2} \quad (5)$$

The properties of steady waves located at the border of the Kelvin wedge on circle (2) can be easily found from Eq. (1) and the dispersion relation for divergent waves for this case. The triangle  $OX^*R^*$  is obviously right-angled and the angle  $OX^*R^*$  is  $\pi/2 - \alpha$ . The triangle  $XR^*X^*$  is equilateral; therefore the angle  $R^*X^*X^*$  is  $\theta = [\pi - (\pi/2 + \alpha)]/2 = \pi/4 -$

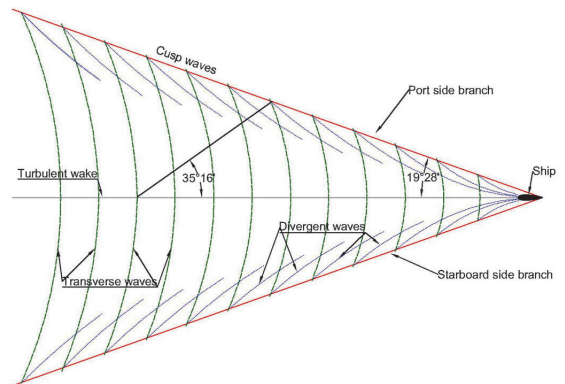


Fig. 2. An example of the Kelvin wake generated by surface vessel motion. The half-angle of the Kelvin wake is  $19^\circ 28'$  and the travelling angle of the cusp waves is  $35^\circ 16'$  to the sailing line. The ship is moving to the right. (Newman, 1977; Torsvik et al., 2015).

$\alpha/2$ .

Similarly, Eq. (1) becomes much more complicated:

$$gk \tanh kH = \frac{2k^2 U^2}{3 - 2kH \sinh^{-1} 2kH} \quad (6)$$

Eq. (6) for the wave number  $k$  at the border of the Kelvin wedge can be interpreted as the following transcendental equation for with respect to  $kH$  (Sorensen, 1973):

$$\frac{gk \tanh kH}{2kH} (3 - 2kH \sinh^{-1} 2kH) = \left( \frac{U}{\sqrt{gH}} \right)^2 \quad (7)$$

Eq. (7) is just another way of saying that the basic geometric properties of the Kelvin wave system depend on the depth Froude number:

$$F_H = \frac{U}{\sqrt{gH}} \quad (8)$$

where  $U$  is the speed of the vessel and  $g$  is the acceleration due to gravity. For ships sailing at subcritical speeds,  $F_H < 1$  (this is the case for most ships), Eq. (6) has a real solution and the Kelvin wake consists of two systems of waves. The deviation of the properties of the Kelvin wave from the situation in deep water (when  $F_H \ll 1$ ) can thus be characterised using the variations of the angles  $\alpha$  and  $\theta$  (Fig. 3).

For relatively fast vessels in shallow waters ( $0.6 < F_H < 1$ ) the wake is affected by the water depth  $H$  and the overall appearance of the Kelvin wedge depends on the particular value of  $F_H$ .

The changes to the half-angle of the Kelvin wedge and the angle of cusp wave propagation  $\theta$  are relatively modest (less than  $0.05^\circ$ ) until  $F_H$  reaches a value of about 0.6. For larger values of  $F_H$ , the apex angle of the Kelvin wedge starts to increase and  $\theta$  to decrease. The deviation of  $\theta$  from its deep-water value reaches  $1^\circ$  at  $F_H = 0.767$ . The wave generation process for transcritical speeds  $F_H \sim 1$  is strongly nonlinear and cannot be described in terms of the classic depth Froude number (Soomere, 2007). When  $F_H > 1$ , a further increase in  $F_H$  leads to a decrease in the half-angle of the Kelvin wedge from its formal limiting value  $90^\circ$  at  $F_H \rightarrow 1$ . The wave system will consist solely of divergent waves (Wehausen, 1973; Pethiyagoda et al., 2015) and may even obtain a shape characteristic of a Mach stem (Rabaud and Moisy, 2013). We do not consider this case in our study as parts of the methodology rely on the presence of divergent waves.

The method for the identification of properties for the evaluation of the ship's location and speed is based on the spectrogram representation of one-point recordings of the wake. Pethiyagoda et al. (2017) showed that in this representation the wake signal is concentrated around the curve that they call the linear dispersion curve (Fig. 4). This curve is described as

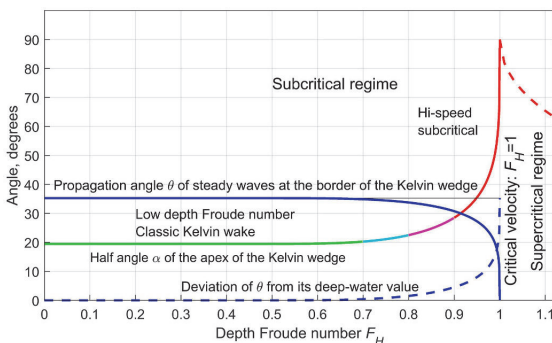


Fig. 3. The dependence of the half-angle of the Kelvin wedge on the depth Froude number  $F_H$ . The changes are minor for  $F_H \leq 0.7$  and become noticeable for  $0.7 \leq F_H \leq 0.8$ .

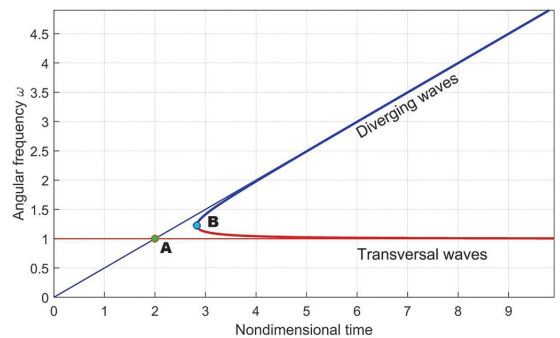


Fig. 4. Nondimensional linear dispersion curve of ship waves (Pethiyagoda et al., 2017). The edge of the Kelvin wedge (marker ‘A’) is associated with the location of the crossing points of the asymptotes of the branches for transverse and divergent waves.

$$2\sqrt{2}\omega_{\pm} = \sqrt{T^2 + 4 \pm T\sqrt{T^2 - 8}} \quad (9)$$

where  $\omega_{\pm}$  is the dimensionless angular frequency of the waves, “+” corresponds to diverging waves and “-”, to transverse waves, and  $T = t/y$  is dimensionless time. These two branches meet at the point  $T = \sqrt{8}$ ,  $\omega = \sqrt{3/2}$  (Fig. 4). Both branches approach rapidly to straight lines when  $T$  increases. The branch for the divergent waves has an asymptote  $\omega = T/2$  whereas the branch for the transverse waves approaches the horizontal line  $\omega = 1$ .

The point where the two branches meet corresponds to the edge of the Kelvin waves, therefore, to cusp waves that are the highest of the far-field wake and thus the easiest to detect. However, from Fig. 4 it becomes clear that the determination of the coordinates of this point in the spectrogram representation is a complicated task as it is located at the vertical section of the dispersion curve. Therefore, even small errors in the evaluation of the properties of cusp waves may lead to large errors in the estimated frequency of waves and thus to large errors in the estimated ship speed.

To a first (linear) approximation, the point that represents the edge of the Kelvin wedge in this representation is always directly related to the crossing point  $T = 2$ ,  $\omega = 1$  of these two asymptotes (marker ‘A’ in Fig. 4). This relationship is invariant with respect to the ship’s speed and also with respect to the relevant depth Froude number (Pethiyagoda et al., 2017). Consequently, the aim is to specify this point and not the meeting point of the two branches of the linear dispersion curve.

The existence of the two asymptotes makes it possible to identify the instant of arrival of the wake in the spectrogram even when only a few components of the wake are detectable (e.g., distinguishable from a relatively high wind wave field). As this linear dispersion curve is invariant to the Froude number, the method itself is insensitive to the variations in this parameter. However, the performance of the method does depend on the depth Froude number as the ratio of the energy of transverse and divergent waves and the extension of the identifiable parts of the two branches varies with the variation in the Froude number (Pethiyagoda et al., 2017). An intrinsic limitation is that both branches must be present in the spectrogram. Therefore, the method as described here cannot be used for supercritical speeds when steady transverse waves cannot exist.

## 2.2. Measurement site and devices

The measurements were conducted on the nearshore of Tallinn Bay in July 2017. Tallinn Bay is a semi-enclosed area of approximately  $10 \times 20$  km in size. It is located on the south-eastern coast of the Gulf of

Finland in the north-eastern Baltic Sea (Fig. 5). It is open to the central part of the Gulf of Finland to the north and the north-west. The two entrances to the bay (from the north and west) are regulated by a local vessel traffic separation scheme (Fig. 5).

To retrieve steady wake signatures (that would not be affected by the speed and course alternations), we focused on vessels approaching the port of Tallinn from the north. We chose to deploy our measurement devices near the shore of the Pikakari peninsula (Fig. 5). Katariina jetty to the south-east of the measurement site and the tip of Pikakari peninsula to the north-west shelter the measurement location from waves approaching from the west and south, respectively. Their presence shelters the measurement location from waves generated by the predominant wind and also means that wakes from the vessels sailing out of the port of Tallinn or approaching from the west are negligible at the sensor location. The sailing direction of vessels that approach the port from the north-north-west was approximately 159° (clockwise from north). The deviation of courses from this, estimated from ship self-reporting systems, was typically less than  $\pm 10^\circ$ .

The water depth in part of the traffic separation scheme where the wakes of the approaching vessels could have originated (Fig. 5) ranges from 40 to 70 m. Passenger vessels entering to port were travelling at 15 to 30 knots<sup>1</sup> in the mentioned area, and therefore they are sailing at subcritical speeds. Even though the depth Froude number for such speeds may reach values about 0.7, on average it was below 0.5. For these Froude numbers, the deviation of the geometry of the Kelvin wedge from the deep-water geometry is insignificant (Fig. 3).

The data were collected with multimodal pressure and inertial sensors called hydromasts (Fig. 5) (Ristolainen et al., 2019). In total, 9 sensors were mounted with an equal horizontal spacing of 2.5 m on an aluminium frame (S1 to S9 in Fig. 5). The frame was deployed at a depth of 3 m on the seabed with an orientation of 22.5° north to properly catch the single wake wave crests of the incoming vessels. The frame was secured to the seabed with 8 mm metal bars and additional weights on the corners.

The hydromasts recorded the absolute pressure of the water column (absolute pressure sensor in Fig. 5) and an estimate of the near-bed water velocities using a calibrated relationship with the linear acceleration of the vibrating mast at the top of the device (Fig. 5). This dataset has also been used for automatic vessel wake detection (Rätsep et al., 2020b). Here, however, we only use the pressure data. The pressure sensors were located near the bottom of the instrument and therefore the readings were obtained at 0.2 m above the seabed. The measurement frequency for all the sensors was 100 Hz.

### 2.3. Data conversion

The spectrogram technique involved the conversion of the pressure data into water level elevation and subsequent implementation of the short-time Fourier transform. The main focus was on the retrieval of the ship wake components from the frequency spectrum of the wave data, therefore we did not concentrate on actual wave height values, power values on the time-frequency representation of the pressure data and the sensitivity caused by external sources to the data. This technique is based on the process described by Rätsep et al. (2020b) and is presented here only in summary form, to provide a complete overview of the procedure. The starting point is the geometry of the wake structure retrieved from the corresponding spectrogram based on (Torsvik et al., 2015) and it essentially uses the existence of two asymptotes of the linear dispersion curve of ship waves.

As a first step, outliers (values that differed by more than three standard deviations from the mean pressure value) were removed from the absolute pressure data. An example of input data is given in Fig. 6a. The data stream, originally measured in mV, was converted into

pressure  $P_0$  (Pa) by a calibration relation established in a test tank:

$$P_0 = 27.1208 * p + 4475.72 \quad (10)$$

with  $R^2 > 0.9$ . The height of the water column was calculated considering the average depth at the measurement site as  $h = 3$  m and the height of the sensor  $d_s = 0.2$  m above the seabed. As this area is microtidal, with typical tidal amplitudes a few cm (Leppäranta and Myrberg, 2009), tide-driven changes to the water depth are ignored. The attenuation of water surface fluctuations in the water column was estimated using the relation (Dean and Dalrymple, 1991; Karimpour and Chen, 2017):

$$P_0(z = -h_s) = P + q = \rho g h_s + \rho g \eta K_p \quad (11)$$

where  $P_0$  is total pressure,  $P$  is the mean water pressure,  $q$  represents the water surface fluctuations,  $h_s$  is the depth of the sensor,  $g$  is gravity acceleration,  $\rho$  is the water density,  $z$  is the depth of the sensor with positive values above the water level,  $\eta$  is the water surface elevation, and  $K_p$  is the dynamic pressure to the surface elevation conversion factor (Dean and Dalrymple, 1991; Karimpour and Chen, 2017):

$$K_p = \frac{\cosh k(h+z)}{\cosh(kh)} = \frac{\cosh(kd_s)}{\cosh(kh)} \quad (12)$$

Here, the wavenumber  $k$  was calculated following the method proposed by Goda (2010). This procedure of reconstruction of wave heights is not essential for our method and we only included it in order to keep the compatibility of our research with other studies that have tracked the water surface. The frequency of pressure fluctuations in surface waves exactly matches the frequency of waves. Therefore, possible errors of the conversion of measured data series into wave time series may only affect the wave heights but does not distort the location of high-energy fluctuations on the linear dispersion curve.

Wave data were downsampled to the frequency of 5 Hz. A short-time Fourier transform was applied in the frequency range of 0.005–0.6 Hz (periods from 5/3 to 200 s) with a step size of 0.005 Hz on a uniform scale, using a Hamming window function of 1024 data points (with a length of 204.8 s or about 3–4 min) and overlap of 1014 points (203.8 s) with a 2 s step. Each application of the Fourier transform produces a discrete representation of the frequencies of identified waves. The maximum mismatch of the frequency of the relevant high-energy point from the corresponding point of the linear dispersion curve depends on the retrieved frequency and decreases with the increase in this frequency. This feature suggests that the asymptotes of the linear dispersion curve are better represented in the time-frequency representation (Fig. 4). Finally, the spectrograms from different sensors were normalised and merged, following the idea of using ensemble averaging of the output of different sensors to increase the wake-to-background-noise ratio (Rätsep et al., 2020b). The Fourier transform does not introduce any systematic bias in the frequency of the retrieved high-energy fluctuations. However, as all sensors are recording the same wave, the process of merging the data from 9 sensors does not decrease the typical error in frequency retrieved from a single sensor.

### 2.4. Spectrogram analysis: speed of the vessel and the distance travelled by the wake

Vessel localization requires knowledge of the position, speed and course. We approached the first part of this problem by determining the propagation direction and the distance travelled by its wake to the measurement location under the assumption that a ship sailed more or less with a steady speed and course. The two other parameters (speed and course) were assessed during the analysis process. We employed two different and independent techniques: a spectrogram technique for finding the speed and the distance that the wake had travelled from its point of origin to the measurement site, and a phase-shift technique based on the time delays of the incoming wake at the pressure sensors in

<sup>1</sup> 1 knot is 1.852 km per hour.

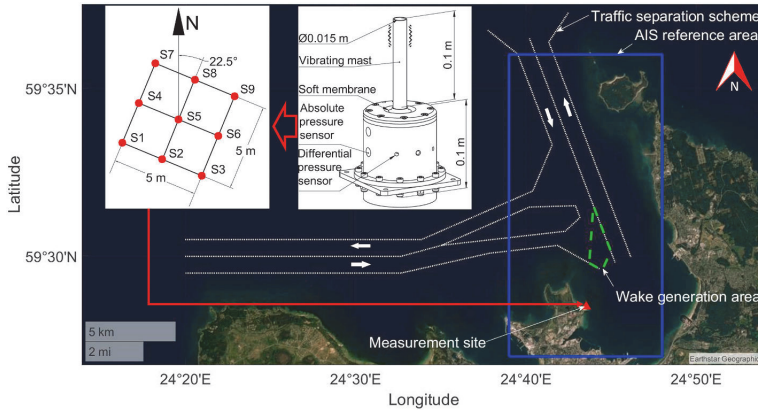


Fig. 5. The traffic separation scheme in Tallinn Bay (Estonian Maritime Administration, 2017). Arrows show the sailing direction. The geometry of the grid and the details of sensors are indicated in the upper left corner.

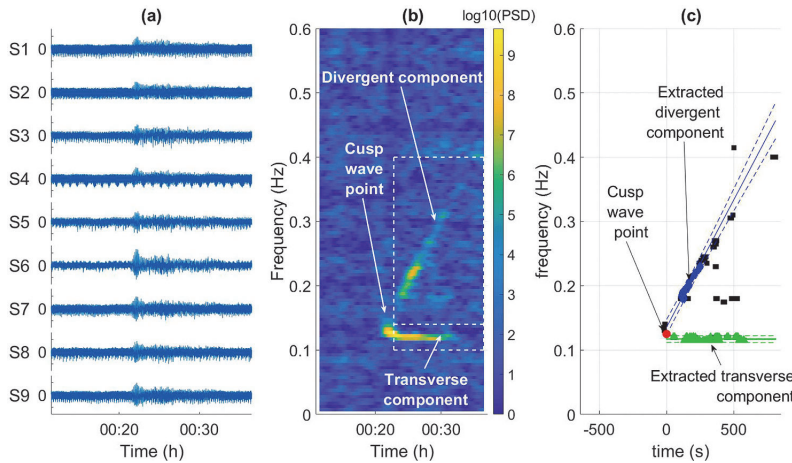


Fig. 6. Wake readings from the M/V Megastar. (a) Pressure data output from sensors S1–S9 (grid position is indicated in Fig. 5) after the removal of outliers and normalization. (b) An example of time-frequency representation (spectrogram) of a ship wake. (c) The peaks of this wake are extracted from the background noise and linearly fitted. The time moment ‘0’ marks the cusp wave point (as the maximum spectrogram value (Torsvik et al., 2015)). It is evident that direct estimates of frequency of cusp waves using a few points in its vicinity contain large uncertainty. Fits to the datasets are shown with solid lines and error bars with 95% of confidence are marked as dashed lines. Black squares represent extracted time-frequency points for which the energy value was lower than the average of the extracted wake components.

the grid for estimating the direction of the incoming wake. From this information, we derive a possible course on which the vessel sails.

Ship wake signatures (Fig. 6b) were extracted from the spectrograms using peak detection analysis (Fig. 6c) and divided into the divergent and transverse components. The speed of the ship and the distance travelled by the wake were determined using relations developed by Torsvik et al. (2015) and actually stemming from Wu (1991). The main wake components used in this process were transverse waves (Pethiyagoda et al., 2018) represented by the almost horizontal branch of an L-like signature (Fig. 6b). The divergent waves are represented by an inclined branch in this signature. In other words, the frequency of transverse waves changes insignificantly after the cusp waves have arrived, however, the frequency of divergent waves varies substantially (and almost linearly in this representation) for the fixed observation location (Fig. 4). Such signals are often referred to as chirp signals or ‘chirps’ (Sheremet et al., 2012). The cusp waves were associated with the intersection of the two branches of the spectrogram (Figs. 4 and 6b). The width of these branches depends on the scale of the image that was tuned manually to achieve optimal extraction. This width was also taken into account when estimating the possible errors of estimates of vessel speed and distance. Finally, the features on spectrograms that reflect

transverse and divergent components were fitted with straight lines (Fig. 6c).

Torsvik et al. (2015) applied three approaches for determining the speed  $U$  of the vessel from the spectrogram. They all rely on the speed  $f$  of certain components of ship waves. If the starting point of the branch for the diverging waves is well defined, the ship’s speed is (Torsvik et al., 2015):

$$U = \sqrt{\frac{3}{2}} \frac{g}{2\pi f_{cusp}} \tag{13}$$

where  $f_{cusp}$  is the frequency of cusp waves (marker ‘B’ in Fig. 4). This frequency matches the meeting point of the signatures of diverging and transverse waves that corresponds to the non-dimensional frequency  $\omega = \sqrt{3}/2$  in Fig. 4. Alternatively, it is possible to use the asymptotic value  $\omega = 1$  of the signature of the transverse component of the ship wake. If we denote the relevant frequency by  $f_{\infty}$ , the ship’s speed is (Torsvik et al., 2015):

$$U = \frac{g}{2\pi f_{\infty}} \tag{14}$$

Expressions (13) and (14), theoretically, lead to the same results.

Their applicability is, however, greatly different because of the sensitivity of the accuracy of the specification of the relevant frequency. As the frequency of cusp speed corresponds to the vertical section of the linear dispersion curve, even small errors in the estimates of cusp wave timing may lead to large errors in  $f_{cusp}$ . The estimates of  $f_{\infty}$  are evidently much more stable. Consistent with the described features, the approach based on the signature of the transverse component generally leads to a better match of the estimates of the speed of the vessels compared to the AIS information (Rätsep et al., 2020a). This conjecture is not unexpected as the location of the meeting point of the two branches is much more complicated to identify compared to the frequency of transverse waves. For this reason, only results obtained using Eq. (14) are considered in this study.

The distance from the point of origin of the wake to the sensor was estimated using the ship's speed  $U$  and the time interval  $\Delta t$  during which the frequency of the divergent component reached from the cusp wave frequency  $f_{cusp}$  to  $\sqrt{2}$  times higher value  $\sqrt{2}f_{cusp}$  (Torsvik et al., 2015). To find  $\Delta t$ , a linear fit was built for the divergent component. The distance  $L$  to the measurement site from the point of origin of the vessel wake is (Torsvik et al., 2015) estimated as:

$$L = \sqrt{6}U\Delta t \quad (15)$$

### 2.5. Detection of wakes

To compare our results with actual sailing parameters from passing ships, we used data from the vessel self-reporting systems (Automatic Identification System, AIS) collected from the area marked in Fig. 5 ("VesselFinder," 2020). The AIS data were recorded on average with 5-min intervals for the majority of the vessels. The data included the geographical location retrieved from a GPS device, timestamp, name, International Maritime Organisation number, call sign, course and speed ("VesselFinder," 2020). In total, 249 different vessels were identified with 101,275 AIS readings. The accuracy of the estimates of the vessel speed depends therefore mostly on the accuracy of timestamps. These are normally provided with an accuracy of a few seconds and thus the AIS-based estimates of speed apparently have errors below 1%.

Due to the relatively intense traffic (wakes from several vessels often arriving at the measurement site less than 30 min apart) we focused on single strong (transverse and divergent component visible and extractable from spectrogram as shown in Fig. 6) wake events. This approach means that we filtered out signals of wakes originating from departing vessels, and multiple vessel cases. Therefore, the cases were to some extent 'hand-picked'.

The AIS data were sorted into single ship passing events. A 'passing' is defined here as a series of consecutive data points indicating the sailing trajectory and time stamps of a ship that passes the measurement site. For each position in the passing, a corresponding wake origin point was calculated based on the vessel course at that point. The ship's position that had the smallest perimeter of a triangle with vertices at the measurement site, the AIS position, and estimated wake origin was chosen as the reference of that particular passing. Those positions were matched with wake readings. We focused on situations where there was only a single vessel within 3.7 km (2 nmi<sup>2</sup>) of the measurement site and travelling faster than 15 knots in a time window of  $\pm 15$  min from the wake event, as the closest AIS location to the wake origin point on the vessel track may have been before reaching it or after passing it. Wakes from the vessels sailing below 15 knots were not detected mostly because they were indistinguishable from the background wind waves.

Examples of weak wakes, overlapping wakes and single detectable wakes are given in Fig. 7. Fig. 7a and d correspond to M/S Seawind slowing down from its transit speed of 15 knots as it approached the port of Tallinn (change from solid line to dashed line in Fig. 7a.). Even though

it was a single vessel passing the measurement site in the 30-min window (Fig. 7a.), the wake structure was not extractable from the spectrogram without additional filtering (Fig. 7d), due to the low signal to noise ratio (SNR). Therefore this and similar cases were discarded.

The second case depicts a "rush hour" near the measurement site. Two vessels M/V HSC Express from Helsinki (from the north) and MV Victoria I from Mariehamn (from the north-west) were entering port more or less at the same time (Fig. 7b: two solid lines passing the measurement site). This results in two wake structures visible in the spectrogram (Fig. 7e). As the determination of the branches of the relevant wave systems, and therefore also sailing characteristics of a particular vessel, from this pair are complicated without further analysis, cases like this were excluded from our analysis.

The last pair (Fig. 7c and f) shows an example of events selected for this study. A single vessel (M/V Megastar at 25 knots) approached the port of Tallinn (solid line in Fig. 7c). AIS data indicate that this time window contains also two other vessels: a patrol boat operated by the Estonian Police and a Border Guard Board entering the harbour and passing the measurement site with speed less than 15 knots and a yacht sailing up north outside the 2 nmi area. Despite this additional traffic, the spectrogram (Fig. 7f) contained only a single discernible wake event with divergent and transverse component visible for extraction.

These constraints left 70 passings for analysis. These vessels were passenger craft (RO-RO ferries such as M/V Star and M/V Superstar, and high-speed craft like M/S HSC Express and M/S Supercat) entering the port of Tallinn.

### 2.6. The direction of the incoming wake and the travelling course of the vessel

The direction of the incoming wake was estimated using the same pressure data but utilized a somewhat different approach. Outliers were removed in the same manner as described previously. Instead of down-sampling and correcting the data, fluctuations were filtered out using a 9th order Butterworth filter to ease the estimation of the time delays. Due to high noise levels and small time-shifts of the approach of the wake at different sensors (a maximum of 1.6 s at S1 and S9 in Fig. 5) a relatively large time window (15 min) was used to achieve reliable values of the cross-correlation. This duration matches the typical length of the wake signal (Fig. 6 and 7).

To reduce the effect of noise, delays were calculated between all possible sensor pairs (in total 36 pairs using sensors S1 to S9 from the instrument grid in Fig. 5). For each pair, two possible directions were found using the time delay and the distance between the sensors, based on the positions of each pair and wake wave speed of 4.3 m/s. This phase speed corresponds to transverse waves with a typical period of 7 s in 3 m deep water. This resulted maximum of 72 possible combinations for 36 sensor pairs (as an example in Fig. 8). As 36 directions from the 72 were misleading (X2 to X15 in Fig. 8a) and around half (16–18) of the sensor pairs were positioned perpendicular to the wavefront (for example sensor pairs S1–S4, S4–S7, S1–S7 if the source was X1 in Fig. 8a), which produced high alterations of the found direction, then only 18 to 20 directions (from the sensor pairs that were more or less parallel to the wavefront, for example, S1–S2, S2–S3, S1–S3 in Fig. 8a) out of 72 could be considered when finding the actual wake direction. For these reasons, we applied a histogram analysis (Carlotto, 1987) to determine the "population" of the angles that could be used to find the wake direction. An example is shown in Fig. 8 as "selected bin". The actual direction of the incoming wake was calculated as an average of that population, with a standard deviation multiplied by 2 indicating the level of uncertainty at 95% (indicated with black solid and dashed lines in Fig. 8).

As the location of the devices was chosen in a coastal segment that had an orientation more or less parallel to most of the approaching crests of ship waves, shallow-water refraction of waves is not taken into account. The relevant correction for situations when waves approach the shoreline under larger angles is straightforward (but not done here)

<sup>2</sup> nmi is denoted as nautical mile: 1 nmi is 1.852 km.

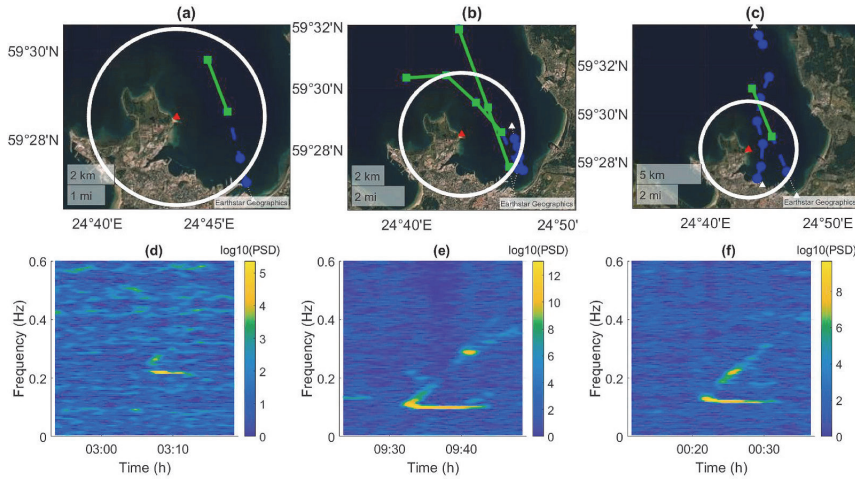


**Fig. 7.** An example of the selection process of detectable ship wakes. The top row (a–c) represents the vessel traffic up to 5 nmi from the measurement site within  $\pm 15$  min from the wake event, which time-frequency representations are shown in the bottom row (d–f). White circles in the top row (a–c) indicate the 2 nmi radius around the measurement device (Fig. 5). Squares connected by solid lines indicate parts of sailing trajectories where the travelling speed was  $\geq 15$  knots, dots connected by dashed lines correspond to speed  $< 15$  knots. A white triangle with a dotted line describes the vessel location for the next 5 min.

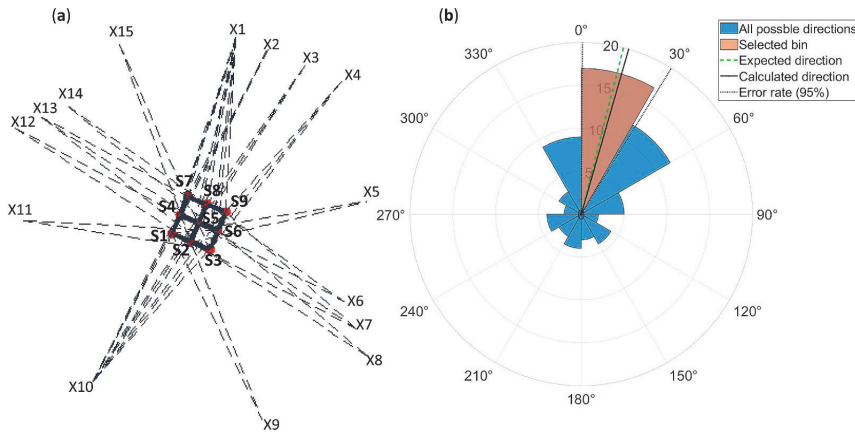


**Fig. 8.** (a) Distribution of 72 directions from 36 sensor pairs (all pairs from sensors S1 to S9). One direction (depicted as a solid straight line) from every sensor pair leads to expected X1 (in total 36), the second direction contributes to X2 to X15, which are regarded as misleading (b) An example of the distribution of all the possible directions between 36 sensor pairs from the M/V Megastar approach (Fig. 7c and f). The selected bin represents the population of directions that were used to calculate the wake direction. The expected direction of the incoming wake is around  $14.3^\circ$ , calculated based on the default course of the traffic separation scheme ( $159^\circ$ ) and the travelling angle of the cusp wave point ( $35^\circ 16'$ ).

because the intensity of refraction only depends on the wave period. Finally, the courses of the vessels were calculated based on the assumption that vessels were sailing in the deep-water regime with a travelling angle of the cusp waves of  $35^\circ 16'$  to the calculated direction of propagation of the incoming wake waves. This resulted in two different courses, one based on the starboard side branch of the vessel wake and another on the port side branch (Fig. 2). As the presented approach for vessel localization based on its wake is confined to a single point on the sailing path, one-point wake readings do not provide information to decide which of the two proposed courses is the right one. This situation is characteristic for various methods of detection of wave propagation direction that define the line along which waves propagate but leave  $\pm 180^\circ$  degree ambiguity of the direction (Engen and Johnsen, 1995). A possible way forward is to use two clusters of sensors similar to the idea of using two subsequent synthetic aperture radar images to determine the wave propagation direction (Ouchi et al., 1999). The flow-chart of the entire analysis process for vessel localization is presented in Fig. 9. The comparison positions (Fig. 9) used the wake source locations from the AIS data (as discussed in Section 2.5) and calculated positions using the distance from the spectrogram analysis

(Section 2.4) and the direction of the incoming wake (Section 2.6). The comparison of the vessel sailing speed (Fig. 9) involves the speed from the AIS position from the wake source point was derived and the speed value from the spectrogram analysis (Section 2.4). Comparison of the vessel courses (Fig. 9) incorporates differences between the course of the AIS position from the wake source point was found and the course derived from the phase shift analysis (Section 2.6).

### 3. Results

#### 3.1. Vessel positions

We start from the comparison of calculated wake source points with vessel positions derived from the AIS data. An example of the position calculations is given in Fig. 10, where M/S Megastar is approaching the port of Tallinn along the track marked by the AIS data (30 min of AIS track is also shown in Fig. 7c, the spectrogram is presented in Figs. 6b and 7f, initial data in Fig. 6a and direction estimation in Fig. 8b). The dashed line in Fig. 10 indicates the track and the dots show the instantaneous vessel positions. The square indicates the wake source point on the vessel's path with a circle around it indicating a possible area of

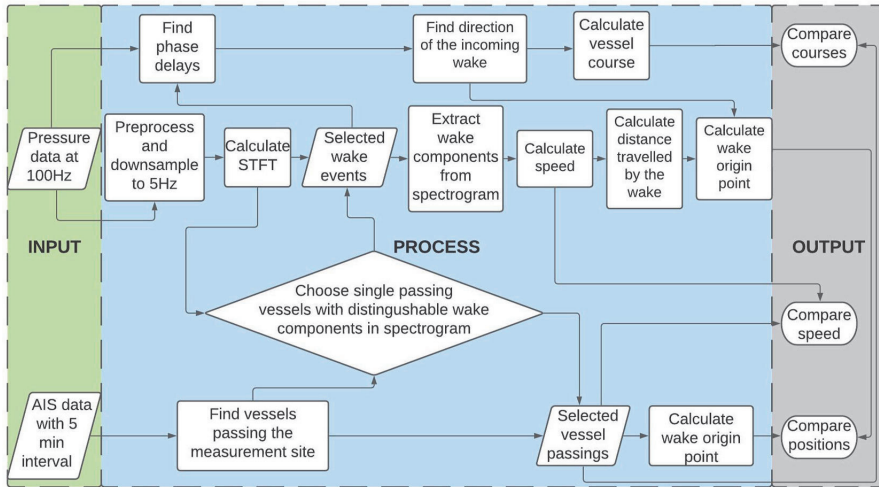


Fig. 9. The flowchart of the analysis process. Created in Lucidchart ([www.lucidchart.com](http://www.lucidchart.com)).

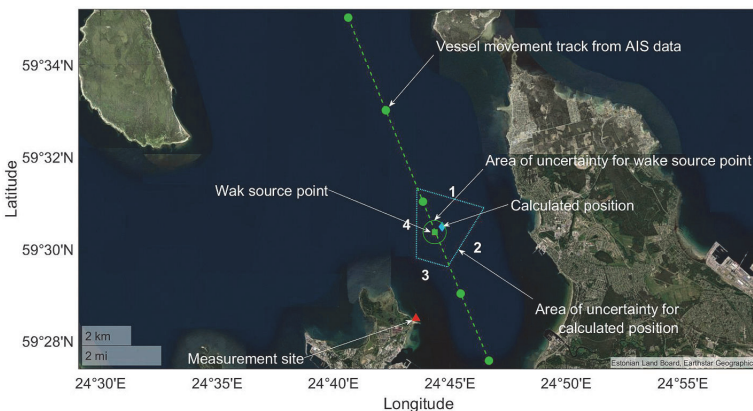


Fig. 10. An example of the results of an evaluation of the position and sailing line of M/S Megastar approaching the port of Tallinn (marked as a 'Vessel movement track from AIS data', dots indicate actual vessel AIS locations) on July 13, 2017. The wake source point was calculated using the AIS positions. Circle around the wake source point indicates possible course ( $\pm 5^\circ$ ) and speed ( $\pm 2$  knots) alterations. The vessel location at this instant found from the wake readings is indicated by the 'Calculated position'. The area of uncertainty (error estimations for the distance and direction) is shown as the dotted polygon within 95% error bars.

uncertainty based on speed and course alterations. In this case, they are less than 2.7 km apart as calculated from the location closer to the port. The distance between the vessel position at the time of wake generation and the closest AIS position varied from 5 m to 3 km, depending on the availability of the AIS data and the sailing speed of the ship. The typical interval between the AIS positions was around 5 min.

The calculated vessel position based only on the measurement data (a rhombus in Fig. 10) is estimated to be at 3.9 km from the measurement device. The difference between the estimated wake source point and the associated AIS position is about 400 m. In 49 cases (out of 70 in this study as indicated in Fig. 11), the estimated ship position was less than 1.4 km from the calculated wake origin point. In most of these cases (48) the points were closer than 1 km and on 35 occasions, less than 600 m. Location comparison between calculated results and the wake source points retrieved from AIS data for all the applicable cases (49) is shown in Fig. 12. The bias between longitudinal coordinates was 59 m with a standard deviation (SD) of 237 m and the SD between the latitudinal coordinates was 490 m (with a bias of 4 m). The average distance between calculated locations and the measurement site was on average 3.2 km with a standard deviation of 0.5 km.

From the viewpoint of vessel localization, the presented technique

failed to estimate the position if the difference between the estimated wake source point and the associated AIS position was larger than 1.4 km. This criterion is somewhat arbitrary and is based on the perception that errors larger than this value may locate the ship either to dry land (Mazaheri et al., 2014). The proportion of failures (21 out of 70) was less than 1/3 of the entire set of events. From these, in 11 cases the direction was not properly resolved from the phase-shift technique. On 6 occasions the interpretation of wake components in spectrograms was problematic and on 4 occasions problems occurred with both aspects of the presented techniques (actual numbers of successful attempts are shown in Fig. 11).

The accuracy of the proposed method was evaluated in terms of an 'area of uncertainty' (a dotted line around the rhombus in Fig. 10) using the spread of data points used by both methods (as discussed in 2.4 and 2.6). The length of this area from the line "1" to "3" in Fig. 10 represents the uncertainty of the distance estimation. Its width reflects the uncertainty of estimates of the wake components extracted from the spectrogram (Fig. 6c). In particular, the width (from the line "2" to "4" in Fig. 10) comes from the sensor pair selection process (determination of the principal direction) for finding the propagation direction of the incoming wake (as illustrated in Fig. 8). The area depicted in Fig. 10 is



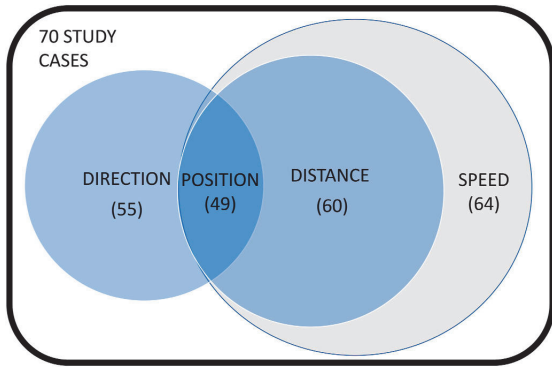


Fig. 11. The distribution of the results. The speed and distance (which depends on speed as described by Eq. (15)) calculation rely on methods described in section 2.4, the estimations of directions are based on the analysis process from section 2.6. The number in brackets indicates the successful attempts out of the 70 study cases.

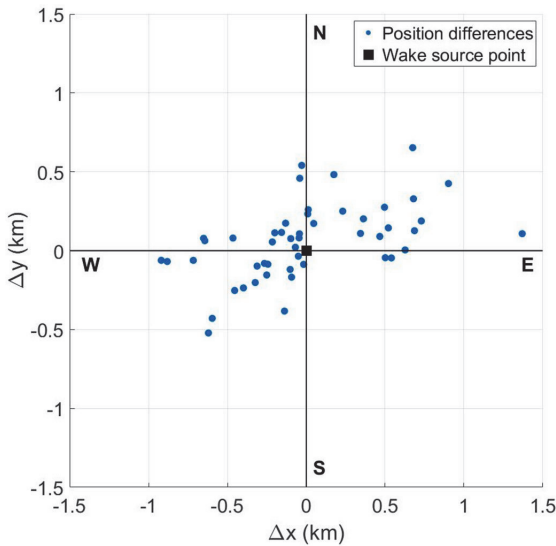


Fig. 12. Differences of wake origin points found from AIS data (the black rectangle in the centre for all 49 cases) and calculated wake points from pressure data plotted in cardinal directions (N: North, E: East, S: South, W: West). The measurement site is situated to the SW.

2.8 km long (uncertainty of distance estimation: from the line “1” to “3” in Figs. 10) and 2 km wide (uncertainty of the computation of the direction: from the line “2” to “4” in Fig. 10). This size of the uncertainty area is typical for most of the 49 successful cases. The average area of uncertainty was 1.7 km (distance) long with SD of 0.85 km and 1.9 km (direction) wide with SD of 0.46 km. The wake direction fluctuations were usually within (width of the area)  $\pm 16^\circ$ . The distance (length of the area) was estimated as varying by an average of  $\pm 0.86$  km from the spread of the data points that contributed to the analysis process.

### 3.2. Speed and course of the vessels

Vessel localization requires estimates of the speed and course of the vessel. The results of estimates are depicted in Fig. 13 and Fig. 14. The

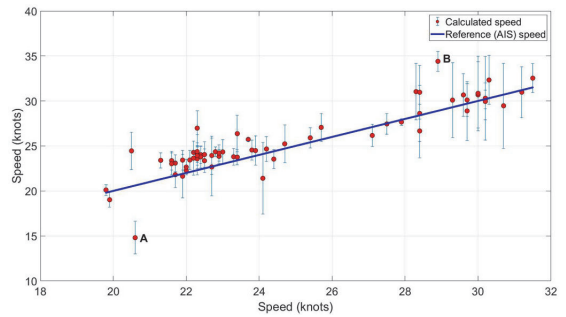


Fig. 13. A comparison between the AIS speed and the calculated speed for the 64 successful (out of 70) cases in which the transverse component was extracted adequately. Two extreme cases (difference more than 5 knots) are marked with letters A and B. Error bars represent the 95% confidence level which is illustrated in Fig. 6.

speed estimation was performed successfully in 64 cases (Fig. 11) for which the spectrogram technique was applicable using Eq. (14). Six cases were removed due to a high level of noise, which resulted in difficulties when extracting the transverse component automatically. The results match vessel speed well at the closest position from the AIS data ( $R^2 \approx 0.81$ ) whereas standard deviation between the reference (AIS) values and calculated speed was 1.60 knots and bias 0.833 knots.

Consistent with the results in Rätsep et al. (2020a), the speed calculations based on an approximation of the transverse component generally produced adequate results. It only occasionally underestimated or overestimated the AIS-based speed. An example of underestimation is point ‘A’ in Fig. 13. The M/V Viking Xpress approached at 20.6 knots, but our method provided an estimate of the speed of 14.8 knots. Other methods analyzed in Torsvik et al. (2015) gave 22.5 knots (using the highest energy value as the cusp wave point) and 21.5 knots (taking the beginning of the divergent wave component for the cusp wave point). The most severe overestimation (point ‘B’ in Fig. 13) occurred when M/S Supercat was approaching the port at 28.9 knots. Our approach resulted in an estimate of 34.4 knots whereas the two other methods gave 35.4 knots and 32.2 knots, respectively.

The possible vessel courses were computed by applying the travelling angle of the cusp wave to the opposite direction of the incoming wake. As discussed above, in the current setup, we did not have methods available to estimate which of the two branches (port or the starboard side as depicted in Fig. 2) of the wake reached the measurement site. For this reason, we calculated possible courses for both situations.

The orientation of the vessel sailing line was calculated using the 55 cases (Fig. 11) when the wake direction was successfully estimated based on the known angle between the propagation direction of the wake and the sailing line (Fig. 2). The vessel courses from the AIS were around  $159^\circ \pm 10^\circ$ . One set of these orientations (‘Set 1’ in Fig. 14) matched well (usually within  $\pm 10^\circ$ , standard deviation from the differences was  $3.28^\circ$  and bias  $0.846^\circ$ ) the vessel courses evaluated from the AIS data. This corresponds to the actual situation as the vessels approaching port were north-north-east from the measurement site when the wake was generated meaning that the measurement site received the starboard branches of their wakes.

The alternative orientations obtained from the wake direction (‘Set 2’ in Fig. 14) which correspond to a port side branch of the wake are about  $70^\circ$  (two times of the cusp wave travelling angle of  $35^\circ 16'$ , with a standard deviation of  $3.28^\circ$  and bias of  $71.4^\circ$ ) from the actual vessel course. In our case, this set could be ruled out due to two arguments. Firstly, the general orientation of the traffic separation scheme near the measurement site is  $159^\circ/339^\circ$ , whereas set 2 proposes courses around  $230^\circ$ . Secondly, the Pikakari peninsula lies to the west of Tallinn Bay which means that if the vessel had approached at a course determined by

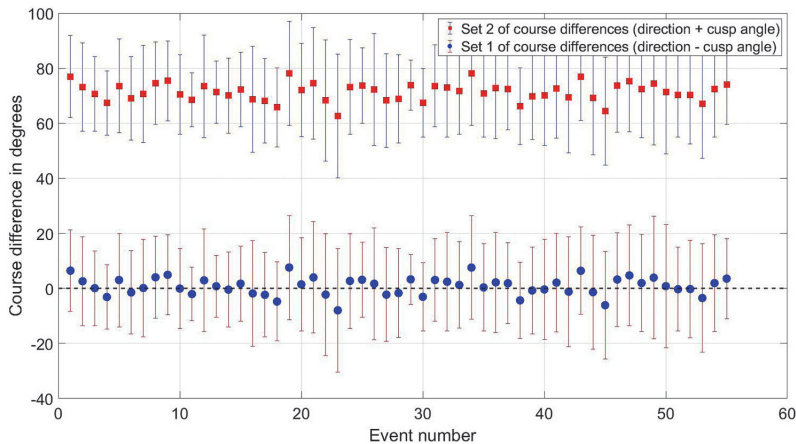


Fig. 14. Course difference between the AIS references and direction obtained using 1) starboard branch of the wake 2) port branch of the wake (black dashed line indicates the 0 value). Error bars represent the 95% confidence level shown in Fig. 8.

set 2, then it would have passed a peninsula either dangerously close (without considering course changes) or grounded near it. More generally, the magnitude of the offset ( $70^\circ$ ) between the two possible orientations of the sailing line apparently makes it often possible to select the true course in most nearshore applications simply because the other orientation is not feasible.

#### 4. Discussion

Since the first application of the spectrogram technique for the interpretation of ship wake measurements (Sheremet et al., 2012), there have been several developments to determine sailing characteristics (speed and distance from the measurement location) along with the sailing regime (Torsvik et al., 2015; Pethiyagoda et al., 2017, 2018). All these studies rely on the fundamental properties of the ship wave system that are invariant to the distance from the sailing line and the speed of the ship unless the depth Froude number exceeds the value of about 0.75. The set of such properties is particularly simple in the spectrogram representation where the two branches of the wake signal rapidly approach well-defined asymptotes. The adequacy of the retrieved properties therefore basically depends on the capacity of the wake recording systems to extract at least a small set of wave components that allow the reconstruction of these asymptotes.

In this work, we evaluated if a vessel could be positioned and its sailing parameters determined, based on one-point information that does not include any information on the vessel movement along its course. We combined the spectrogram technique to estimate the speed and distance of the passing vessels (Torsvik et al., 2015), extended to the use of pressure data in the nearshore (Rätsep et al., 2020b), with a phase-shift (cross-correlation) technique to determine the direction of the incoming wake to estimate the vessel's position and course. We demonstrated that this approach produced results comparable with the actual data derived from the vessel self-reporting systems.

The techniques used here were highly sensitive to background noise. Even though some parts of the techniques, including the construction of spectrograms, is robust, it was difficult to obtain suitable wake structures from spectrograms when the vessel was travelling at less than 15 knots (Rätsep et al., 2020a) and thus produced very low waves. It is also natural to expect that the technique will fail when wind wave background with a substantial proportion of energy in the frequency range of ship wakes masks the wave signal. Therefore, additional means such as convolution techniques should be implemented to extend the developed technique to slower and/or smaller vessels that produce relatively small

waves and for situations that involve strong wind seas. It is likely that the spectrogram technique will still work well in strong swells or short-period wind seas where the ship waves have periods different from background periods. However, as the height of cusp waves decreases as  $r^{-1/3}$  with distance from the fairway, even the signal of very large ship waves will be untraceable at very large distances.

Another intrinsic limitation of the presented technique is that substantially relies on the properties of transverse waves. As the wake of very fast vessels in shallow waters (supercritical wake) contain only diverging waves, the entire approach is not applicable for the evaluation of vessel distance, speed or course for vessels travelling at supercritical speeds. As such wakes contain a large proportion of nonlinear waves, their wake structure is much more complicated in the spectrogram representation (Pethiyagoda et al., 2017).

The developed technique is only directly applicable for single wakes (only one wake structure present in the 30-min window). However, in high-traffic regions wakes from several ships sailing with different speed and course, may arrive at the measurement devices at the same time, as seen on multiple occasions in the Tallinn Bay experiments. This makes the extraction and use of the wake structures in the spectrograms questionable, compounded by the effects of interference when applying the phase-shift analysis to determine wake direction. However, a feasible way forward is to use convolution techniques implemented in routines for acoustic localization of multiple ships (Byun et al., 2019).

Most of the relevant experiments have been conducted in relatively shallow water areas to detect highly powered passenger vessels and analyze the effects of their wakes on the coastal environment (Torsvik et al., 2015). Our approach can be even more useful for security and surveillance operations to raise situational awareness in coastal regions where using usual means of vessel detection and localization is too resource-demanding (Aiello et al., 2019) or is challenged by intentionally removed localization instrumentation (Dumitriu et al., 2018). We only note that the presented method needs to be modified for shallow regions to incorporate information about wave refraction. This change is technically complicated as it must involve ray tracing for each ship wave component but conceptually it is straightforward as refraction intensity only depends on the wave period and water depth.

However, we have also identified a range of problems. The maximum possible detection/localization distance remains unknown. We were able to position a large proportion of passing vessels by their wakes at an average distance of 3.2 km because of two favourable features. Firstly, the local traffic separation scheme guarantees that vessels sail along a prescribed waterway. Secondly, the experiment recorded only passenger

ships entering the port. To test further distances, we need to test this method in an area which is much wider than the approach to the port of Tallinn.

In addition to these problems, the developed technique can be complemented by introducing methods for determining the speed and course alterations (Pethiyagoda et al., 2017, 2018, 2018). Another natural extension would be to determine whether ship recognition, the third step of the picture building process (NATO Standardization Agency, 2015), based on their wakes is possible at large scales. However, the main message of this study is that a vessel monitoring system solely based on the wake information in the wave recordings is practically possible. This message is important due to several developments, such as the growing number of unmanned Marine Autonomous Surface Ships operating in coastal regions or (e.g., refugee) vessels which intentionally remove on-board localization instrumentation (Dumitriu et al., 2018).

We are optimistic as these first results show that vessel localization based on the wake measurements is technically feasible. An exciting improvement to the technique used here is that it can be combined with automatic wake detection (Rätsep et al., 2020b). These are the first two steps of the picture building process (NATO Standardization Agency, 2015) needed to improve the situational awareness of naval operations. What makes this method preferable for traffic monitoring is that the sensing array can be easily concealed. In our case it was set near the beach at a depth around 3 m, therefore no special equipment (ship or boat) were required.

## 5. Conclusion

The objective of this work was to determine whether vessel localization (position, speed and course of a ship) may be achieved by using wake measurements from a closely-spaced array of underwater pressure sensors. A grid of 9 sensors was deployed with a horizontal offset of 2.5 m at the depth of 3 m. Single ship wakes were manually selected from the continuous recording using 30-min windows. The properties of the ship movements were matched to AIS vessel data. A spectrogram technique was implemented for calculating the speed of the passing ship and the distance travelled by the wake.

The core new developments are the systematic use of the concept of asymptotes of the linear dispersion relation to determine some parameters of the vessel motion and the demonstration that phase shift (cross-correlation) analysis can retrieve the possible courses on which a vessel could be sailing from the direction of the incoming wake. We showed that wake data from pressure sensors can be used for surface vessel localization, with a positioning error less than 600 m in 50% of the cases.

## CRedit authorship contribution statement

**Margus Rätsep:** Conceptualization, Methodology, Formal analysis, Writing – original draft, Writing – review & editing. **Kevin E. Parnell:** Conceptualization, Writing – original draft, Writing – review & editing. **Tarmo Soomere:** Conceptualization, Methodology, Writing – original draft, Writing – review & editing. **Maarja Kruusmaa:** Conceptualization, Investigation, Writing – original draft. **Asko Ristolainen:** Resources, Investigation, Writing – original draft. **Jeffrey A. Tuhtan:** Resources, Investigation, Writing – original draft, Writing – review & editing.

## Declaration of competing interest

The authors declare that they have no known competing financial interests or personal relationships that could have appeared to influence the work reported in this paper.

## Acknowledgements

This research was supported by the Estonian Ministry of Education

and Research (Estonian Research Council, grants PRG1129 and PUT 1690) and the European Regional Development Fund program Mobilias Pluss, reg. nr 2014-2020.4.01.16-0024, project MOBTT72, and co-supported by the Estonian Center of Excellence EXCITE, the Estonian Research Infrastructures Roadmap object “Infotechnological Mobility Observatory” (IMO) and the European Economic Area (EEA) Financial Mechanism 2014–2021 Baltic Research Programme project EMP480 “Solutions to current and future problems on natural and constructed shorelines, eastern Baltic Sea”.

## References

- VesselFinder [WWW Document], 2020. accessed. <https://www.vesselfinder.com/>.
- Aiello, M., Vezzoli, R., Giannetto, M., 2019. Object-based image analysis approach for vessel detection on optical and radar images. *J. Appl. Remote Sens.* 13 (1), 014502. <https://doi.org/10.1117/1.jrs.13.01.4502>.
- Altan, Y.C., Otay, E.N., 2018. Spatial mapping of encounter probability in congested waterways using AIS. *Ocean Eng.* 164, 263–271. <https://doi.org/10.1016/j.oceaneng.2018.06.049>.
- Arnold-Bos, A., Martin, A., Khenchaf, A., 2007. Obtaining a ship's speed and direction from its Kelvin wake spectrum using stochastic matched filtering. In: 2007 IEEE International Geoscience and Remote Sensing Symposium, pp. 1106–1109. <https://doi.org/10.1109/IGARSS.2007.4422995>.
- Borgman, L.E., 1969. Directional spectra models for design use. *Offshore Technol. Conf.* <https://doi.org/10.4043/1069-MS>.
- Byun, G., Song, H.C., Byun, S.-H., 2019. Localization of multiple ships using a vertical array in shallow water. *J. Acoust. Soc. Am.* 145, EL528–EL533. <https://doi.org/10.1121/1.5111773>.
- Carlotto, M.J., 1987. Histogram analysis using a scale-space approach. *IEEE Trans. Pattern Anal. Mach. Intell.* PAMI-9, 121–129. <https://doi.org/10.1109/TPAMI.1987.4767877>.
- Chaillan, F., Courmontagne, P., 2006. On the use of the stochastic matched filter for ship wake detection in SAR images. *OCEANS 2006, Oceans 2006 Conference. OCEANS-IEEE*, Boston, MA, pp. 521–526. <https://doi.org/10.1109/OCEANS.2006.3071122>.
- Chen, C., Li, Y., Huang, K., Long, Y., Zhang, L., Ouyang, K., 2020. Ship velocity estimation in airborne along-track interferometric SAR imagery based on the fractional fourier transform. *Int. J. Antenn. Propag.* 2020, 5835620. <https://doi.org/10.1155/2020/5835620>.
- Claremar, B., Haglund, K., Rutgersson, A., 2017. Ship emissions and the use of current air cleaning technology: contributions to air pollution and acidification in the Baltic Sea. *Earth Syst. Dyn.* 8, 901–919. <https://doi.org/10.5194/esd-8-901-2017>.
- Courmontagne, P., 2005. An improvement of ship wake detection based on the radon transform. *Signal Process.* 85, 1634–1654. <https://doi.org/10.1016/j.sigpro.2005-02-013>.
- Dean, R.G., Dalrymple, R.A., 1991. *Water Wave Mechanics for Engineers and Scientists*. World Scientific, New Jersey.
- Delpeche-Ellmann, N.C., Soomere, T., 2013. Investigating the Marine Protected Areas most at risk of current-driven pollution in the Gulf of Finland, the Baltic Sea, using a Lagrangian transport model. *Mar. Pollut. Bull.* 67, 121–129. <https://doi.org/10.1016/j.marpolbul.2012.11.025>.
- Dumitriu, A., Miceli, G.E., Schito, S., Vertuani, D., Cecchetto, P., Placco, L., Callegaro, G., Marazzato, L., Accattino, F., Bettio, A., Conte, E., Golfetto, T., Cagnato, E., Scamparin, A., Roncato, R., Rossi, L., Lombardo, G., Lucrezia, M., Fontanot, F., Bettanini, C., 2018. OCEANS-18: monitoring undetected vessels in high risk maritime areas. 5th IEEE Int. Work. Metrol. AeroSpace, Metroaerosp. 2018 - Proc 669–674. <https://doi.org/10.1109/MetroAeroSpace.2018.8453531>.
- Engen, G., Johnsen, H., 1995. SAR-ocean wave inversion using image cross spectra. *IEEE Trans. Geosci. Rem. Sens.* 33, 1047–1056. <https://doi.org/10.1109/36.406690>.
- Fan, K., Zhang, H., Liang, J., Chen, P., Xu, B., Zhang, M., 2019. Analysis of ship wake features and extraction of ship motion parameters from SAR images in the Yellow Sea. *Front. Earth Sci.* 13, 588–595. <https://doi.org/10.1007/s11707-018-0743-7>.
- Fang, M.C., Yang, R.Y., Shugan, L.V., 2011. Kelvin ship wake in the wind waves field and on the finite sea depth. *J. Mech.* 27, 71–77. <https://doi.org/10.1017/jmech.2011.9>.
- Fefilatyev, S., Goldgof, D., Shreve, M., Lembke, C., 2012. Detection and tracking of ships in open sea with rapidly moving buoy-mounted camera system. *Ocean Eng.* 54, 1–12. <https://doi.org/10.1016/j.oceaneng.2012.06.028>.
- Gierull, C.H., 2019. Demystifying the capability of sublook correlation techniques for vessel detection in SAR imagery. *IEEE Trans. Geosci. Rem. Sens.* 57, 2031–2042. <https://doi.org/10.1109/TGRS.2018.2870716>.
- Goda, Y., 2010. Reanalysis of regular and random breaking wave statistics. *Coast Eng. J.* 52, 71–106. <https://doi.org/10.1142/S0578563410002129>.
- Gomit, G., Chatellier, L., Calluau, D., David, L., 2013. Free surface measurement by stereo-refraction. *Exp. Fluids* 54, 1540. <https://doi.org/10.1007/s00348-013-1540-4>.
- Gomit, G., Rousseaux, G., Chatellier, L., Calluau, D., David, L., 2014. Spectral analysis of ship waves in deep water from accurate measurements of the free surface elevation by optical methods. *Phys. Fluids* 26, 122101. <https://doi.org/10.1063/1.4902415>.
- Gomit, G., Chatellier, L., Calluau, D., David, L., Fréchet, D., Boucheron, R., Perelman, O., Hubert, C., 2015. Large-scale free surface measurement for the analysis of ship waves in a towing tank. *Exp. Fluids* 56, 184. <https://doi.org/10.1007/s00348-015-2054-z>.

- Huang, W., Wang, D., Garcia, H., Godó, O.R., Ratilal, P., 2017. Continental shelf-scale passive acoustic detection and characterization of diesel-electric ships using a coherent hydrophone array. *Rem. Sens.* 9, 772. <https://doi.org/10.3390/rs9080772>.
- Joseph, S.I.T.J., Sasikala, J., Juliet, D.S., 2019. Optimized vessel detection in marine environment using hybrid adaptive cuckoo search algorithm. *Comput. Electr. Eng.* 78, 482–492. <https://doi.org/10.1016/j.compeleceng.2019.08.009>.
- Kang, K., Kim, D., 2019. Ship velocity estimation from ship wakes detected using convolutional neural networks. *IEEE J. Sel. Top. Appl. Earth Obs. Remote Sens.* 12, 4379–4388. <https://doi.org/10.1109/JSTARS.2019.2949006>.
- Karimpour, A., Chen, Q., 2017. Wind wave analysis in depth limited water using OCEANLYZ, A MATLAB toolbox. *Comput. Geosci.* 106, 181–189. <https://doi.org/10.1016/j.cageo.2017.06.010>.
- Kuznetsov, N.G., Maz'ya, V.G., Vainberg, B., 2002. *Linear Water Waves: A Mathematical Approach*. Cambridge University Press, Cambridge, UK.
- Leppäranta, M., Myrberg, K., 2009. *Physical Oceanography of the Baltic Sea*. Springer.
- Magnier, C., Gervaise, C., 2020. Acoustic and photographic monitoring of coastal maritime traffic: influence on the soundscape. *J. Acoust. Soc. Am.* 147, 3749–3757. <https://doi.org/10.1121/10.0001321>.
- Maritime Administration, Estonian, 2017. accessed. <https://gis.vta.ee/nutimeri/>.
- Mazaheri, A., Montewka, J., Kujala, P., 2014. Modeling the risk of ship grounding—a literature review from a risk management perspective. *WMU J. Marit. Aff.* 13, 269–297. <https://doi.org/10.1007/s13437-013-0056-3>.
- NATO Standardization Agency, 2015. Mtp-01 , Volume I Multinational Maritime Tactical Instructions and Procedures.
- Newman, J.N., 1977. *Marine Hydrodynamics*. Massachusetts Institute of Technology, Cambridge, Massachusetts.
- Newman, J.N., 1991. The inverse ship-wave problem. *The Sixth International Workshop on Water Waves and Floating Bodies*. MIT, Cambridge, Massachusetts, pp. 193–197.
- Ouchi, K., Maedoi, S., Mitsuyasu, H., 1999. Determination of ocean wave propagation direction by split-look processing using JERS-1 SAR data. *IEEE Trans. Geosci. Rem. Sens.* 37, 849–855. <https://doi.org/10.1109/36.752202>.
- Panicker, N.N., Borgman, L.E., 1970. Directional spectra from wave-gage arrays. *Coast. Eng.* 117–136. <https://doi.org/10.1061/9780872620285.008>, 1970.
- Panico, A., Graziano, M.D., Renga, A., 2017. SAR-based vessel velocity estimation from partially imaged Kelvin pattern. *Geosci. Rem. Sens. Lett. IEEE* 14, 2067–2071. <https://doi.org/10.1109/LGRS.2017.2751083>.
- Pethiyagoda, R., McCue, S.W., Moroney, T.J., 2015. Wake angle for surface gravity waves on a finite depth fluid. *Phys. Fluids* 27, 1–7. <https://doi.org/10.1063/1.4921918>.
- Pethiyagoda, R., McCue, S.W., Moroney, T.J., 2017. Spectrograms of ship wakes: identifying linear and nonlinear wave signals. *J. Fluid Mech.* 811, 189–209. <https://doi.org/10.1017/jfm.2016.753>.
- Pethiyagoda, R., Moroney, T.J., Macfarlane, G.J., Binns, J.R., McCue, S.W., 2018. Time-frequency analysis of ship wave patterns in shallow water: modelling and experiments. *Ocean. Eng.* 158, 123–131. <https://doi.org/10.1016/j.oceaneng.2018.01.108>.
- Pradhan, C., Gupta, A., 2017. Ship detection using Neyman-Pearson criterion in marine environment. *Ocean. Eng.* 143, 106–112. <https://doi.org/10.1016/j.oceaneng.2017.03.008>.
- Rabaud, M., Moisy, F., 2013. Ship wakes: Kelvin or mach angle? *Phys. Rev. Lett.* 110, 214503. <https://doi.org/10.1103/PhysRevLett.110.214503>.
- Rätsep, M., Parnell, K.E., Soomere, T., 2020a. Detecting ship wakes for the study of coastal processes. *J. Coast. Res. Special Issue* 95, 1258–1262. <https://doi.org/10.2112/SI95-243.1>.
- Rätsep, M., Parnell, K.E., Soomere, T., Kruusmaa, M., Ristolainen, A., Tuhtan, J.A., 2020b. Using spectrograms from underwater total pressure sensors to detect passing vessels in a coastal environment. *J. Atmos. Ocean. Technol.* 37, 1353–1363. <https://doi.org/10.1175/jtech-d-19-0192.1>.
- Renga, A., Graziano, M.D., Moccia, A., 2019. Segmentation of marine SAR images by sublook analysis and application to sea traffic monitoring. *IEEE Trans. Geosci. Rem. Sens.* 57, 1463–1477. <https://doi.org/10.1109/TGRS.2018.2866934>.
- Ristolainen, A., Tuhtan, J.A., Kruusmaa, M., 2019. Continuous, near-bed current velocity estimation using pressure and inertial sensing. *IEEE Sensor. J.* 19 (24), 12398–12406. <https://doi.org/10.1109/JSEN.2019.2937954>.
- Seymour, R.J., Higgins, A.L., 1978. Continuous estimation of longshore sand transport. *Symposium on Tech. Environmental, Socioeconomic and Regulatory Aspects of Coastal Zone Management*, San Francisco, CA, pp. 2308–2318.
- Sheremet, A., Gravois, U., Tian, M., 2012. Boat-wake statistics at jensen beach, Florida. *J. Waterw. Port. Coast. Ocean Eng.* 139, 286–294. [https://doi.org/10.1061/\(asce\)ww.1943-5460.0000182](https://doi.org/10.1061/(asce)ww.1943-5460.0000182).
- Siebert, G., Hoth, J., Banyš, P., Heymann, F., 2019. Generic framework for vessel detection and tracking based on distributed marine radar image data. *CEAS Sp. J.* 11, 65–79. <https://doi.org/10.1007/s12567-018-0208-6>.
- Soomere, T., 2007. Nonlinear components of ship wake waves. *Appl. Mech. Rev.* 60, 120–138. <https://doi.org/10.1115/1.2730847>.
- Sorensen, R.M., 1973. Ship-generated waves. *Adv. Hydrosci.* 9, 49–83.
- Sun, Y., Liu, P., Jin, Y., 2018. Ship wake components: isolation, reconstruction, and characteristics analysis in spectral, spatial, and TerraSAR-X image domains. *IEEE Trans. Geosci. Rem. Sens.* 56, 4209–4224. <https://doi.org/10.1109/TGRS.2018.2828833>.
- Thieme, C.A., Utne, I.B., Haugen, S., 2018. Assessing ship risk model applicability to marine autonomous surface ships. *Ocean. Eng.* 165, 140–154. <https://doi.org/10.1016/j.oceaneng.2018.07.040>.
- Torsvik, T., Soomere, T., Didenkulova, I., Sheremet, A., 2015. Identification of ship wake structures by a time-frequency method. *J. Fluid Mech.* 765, 229–251. <https://doi.org/10.1017/jfm.2014.734>.
- Tuck, E.O., Collins, J.L., Wells, W.H., 1971. On ship wave patterns and their spectra. *J. Ship Res.* 15, 11–21. <https://doi.org/10.5957/jsr.1971.15.1.11>.
- Wehausen, J.V., 1973. The wave resistance of ships. *Adv. Appl. Mech.* 13, 93–245.
- van Westrenen, F., Baldauf, M., 2020. Improving conflicts detection in maritime traffic: case studies on the effect of traffic complexity on ship collisions. *Proc. Inst. Mech. Eng. Part M J. Eng. Marit. Environ.* 234, 209–222. <https://doi.org/10.1177/1475090219845975>.
- Technical Report 91-1 Wu, Z., dissertation, Ph.D., 1991. On the estimation of a moving ship's velocity and hull geometry information from its wave spectra. The University of Michigan.
- Wu, Z., Meadows, G.A., 1991. A remote sensing technique for the estimation of a moving ship's velocity and length from its wave spectra. *OCEANS 91: Ocean Technologies and Opportunities in the Pacific for the 90s*. IEEE, Ocean Engineering Society, Honolulu, HI, pp. 810–817. <https://doi.org/10.1109/OCEANS.1991.627954>.
- Yih, C.-S., Zhu, S., 1989a. Patterns of ship waves. *Q. Appl. Math.* 47, 17–33.
- Yih, C.-S., Zhu, S., 1989b. Patterns of ship waves II, gravity-capillary waves. *Q. Appl. Math.* 47, 35–44.
- Yu, L., Wu, Z.-Y., 2014. Ship detection from big wave regions in optical remote sensing image. *International Conference on Computer, Network Security and Communication Engineering (CNSCE 2014)*, Shenzhen, Peoples Republic China, pp. 69–75.
- Zanatta, M., Bozem, H., Köllner, F., Schneider, J., Kunkel, D., Hoor, P., de Faria, J., Petzold, A., Bundke, U., Hayden, K., Staebler, R.M., Schulz, H., Herber, A.B., 2020. Airborne survey of trace gases and aerosols over the Southern Baltic Sea: from clean marine boundary layer to shipping corridor effect. *Tellus Ser. B Chem. Phys. Meteorol.* 72, 1–24. <https://doi.org/10.1080/16000889.2019.1695349>.
- Zhang, Y., Jiang, L., 2020. A novel data-driven scheme for the ship wake identification on the 2-D dynamic sea surface. *IEEE Access* 8, 69593–69600. <https://doi.org/10.1109/ACCESS.2020.2986499>.
- Zhang, Y., Li, Q.Z., Zang, F.N., 2017. Ship detection for visual maritime surveillance from non-stationary platforms. *Ocean. Eng.* 141, 53–63. <https://doi.org/10.1016/j.oceaneng.2017.06.022>.
- Zilman, G., Zapolski, A., Marom, M., 2004. The speed and beam of a ship from its wake's SAR images. *IEEE Trans. Geosci. Rem. Sens.* 42, 2335–2343. <https://doi.org/10.1109/TGRS.2004.833390>.
- Zilman, G., Zapolski, A., Marom, M., 2015. On detectability of a ship's Kelvin wake in simulated SAR images of rough sea surface. *IEEE Trans. Geosci. Rem. Sens.* 53, 609–619. <https://doi.org/10.1109/TGRS.2014.2326519>.

# Curriculum vitae

## Personal data

Name: Margus Rätsep  
Date of birth: 21.03.1988  
Place of birth: Estonia  
Citizenship: Estonian

## Contact data

E-mail: margus.ratsep@taltech.ee

## Education

2019–2025 Tallinn University of Technology, PhD  
2016–2018 Tallinn University of Technology, MSc  
2007–2010 Tallinn University of Technology, BSc

## Language competence

Estonian: Mother tongue  
English: Fluent

## Special courses and further training

August 2019 Summer school “Climate of the Baltic Sea Region”, Askö, Sweden

## Professional employment

2018–2021 Tallinn University of Technology, School of Science,  
Department of Cybernetics, Engineer

## Research activity

### *Articles indexed by the Web of Science database (1.1):*

Salupere, A., **Rätsep, M.**, 2019. On solitonic solutions for the hyperelastic rod equation. *Wave Motion*, 91, 102404. <https://doi.org/10.1016/j.wavemoti.2019.102404>

**Rätsep, M.**, Parnell, K.E., Soomere, T., 2020. Detecting ship wakes for the study of coastal processes. *Journal of Coastal Research*, Special Issue No. 95, 1258–1262. <https://doi.org/10.2112/SI95-243.1>

**Rätsep, M.**, Parnell, K.E., Soomere, T., Kruusmaa, M., Ristolainen, A., Tuhtan, J.A., 2020. Using spectrograms from underwater total pressure sensors to detect passing vessels in a coastal environment. *Journal of Atmospheric and Oceanic Technology*, 37(8), 1353–1363. <https://doi.org/10.1175/JTECH-D-19-0192.1>

**Rätsep, M.**, Parnell, K.E., Soomere, T., Kruusmaa, M., Ristolainen, A., Tuhtan, J.A., 2021. Surface vessel localization from wake measurements using an array of pressure sensors in the littoral zone. *Ocean Engineering*, 233, 109156. <https://doi.org/10.1016/j.oceaneng.2021.109156>

Delpeche-Ellmann, N., Giudici, A., **Rätsep, M.**, Soomere, T., 2021. Observations of surface drift and the effects induced by wind and waves in the Baltic Sea for the period 2011–2018. *Estuarine, Coastal and Shelf Science*, 249, 107071. <https://doi.org/10.1016/j.ecss.2020.107071>.

### *Abstracts of conference presentations (5.2):*

**Rätsep, M.**, Kruusmaa, M., Parnell, K., Ristolainen, A., Soomere, T., 2019. Ship wake analysis using an array of nearbed sensors, in: Humborg, C. (Ed.), *Baltic Sea Science Congress 2019*, 19–23 August 2019, Stockholm, Sweden. Abstracts. Stockholm University, p.292.

## Elulookirjeldus

### Isikuandmed

Nimi: Margus Rätsep  
Sünniaeg: 21.03.1988  
Sünnikoht: Eesti  
Kodakondsus: Eesti

### Kontaktandmed

E-post: margus.ratsep@taltech.ee

### Hariduskäik

2019–2025 Tallinna Tehnikaülikool, PhD  
2016–2018 Tallinna Tehnikaülikool, MSc  
2007–2010 Tallinna Tehnikaülikool, BSc

### Keelteoskus

Eesti keel Emakeel  
Inglise keel Kesktase

### Täiendõpe

August 2019 Läänemere kliima, rahvusvaheline suvekool, Askö, Rootsi

### Teenistuskäik

2018–2021 Tallinna Tehnikaülikool, loodusteaduskonna küberneetika instituut, insener

### Teadustegevus

Avaldatud teadusartiklite ja peetud konverentsiettekannete loetelu on toodud ingliskeelse elulookirjelduse juures.

ISSN 2585-6901 (PDF)  
ISBN 978-9916-80-253-3 (PDF)